

# **Membrane module development for water recovery from humid gas**

A thesis submitted in fulfilment of the requirements for the degree Magister Scientia in Chemical Science

By  
Francois Matthee  
Student number: 3238946

Supervisor: Prof Bernard Jan Bladergroen

University of the Western Cape  
2019

Research supported and funded by the Water Research Commission



### Declaration

I, Francois Matthee, declare that the contents of this thesis represent my own work, and that it has not previously been submitted for academic examination towards any qualification. Furthermore, all resources I have used or quoted have been fully referenced. It represents my own opinions and not necessarily those of either University of the Western Cape or South African Institute of Advanced Materials Chemistry.

Signed  Date 10 - 12 - 2019

## **ACKNOWLEDGEMENTS**

---

First and foremost, I would like to thank Prof B.J. Bladergroen for all of his advice, expertise, guidance and patience throughout the writing process. Without his help and continued support, this thesis would not have been possible.

I would like to thank the WRC for funding the research project. I would also like to thank WAKE engineering, for assistance with technical issues throughout the project.

I would also like to thank every person who was part of the project team, or who assisted in any means. Specifically, thanks to Ms. Marine Loirette, Mr. Maxime Bihannic and Mr. Bongi Hlabano-moyo. Your inputs in the project greatly helped.

Special thanks to Denise Davids and Olivier Kasikala, for always being willing to listen about any challenges I might have faced, and giving me advice when I needed it.

Thank you to my brother, Christie Matthee, my mother, Lizette Matthee and father Francois Matthee. I sincerely value your support throughout my studies, especially when I was faced with some of my hardest times.

## **ABSTRACT**

---

Over the past 5 years, South Africa has been experiencing a severe drought. This has caused industrial and agricultural processes, to compete for a limited supply of water. Since the economy relies mostly on agricultural activities, water consumption by industrial processes is taking its toll. One of these processes is the introduction of wet flue gas desulphurization (FGD) treatment at Eskom coal fired power stations.

This dissertation explores the possibility of using membrane technology as a means of water recovery after the coal combustion flue gas has been treated with wet FGD. A lab-scale permeance testing system was specially built and modified to have complete thermal control of the environment inside the system. The permeance testing system produced a gas, similar to that of a wet FGD treated flue gas, which was then tested.

A tubular lab-scale membrane module was designed and produced for the permeance testing system. The permeance figures of both Nitrogen gas and water vapour were determined for the membrane used in module production. These figures coincided with figures provided by the supplier, which warranted successful permeance testing. After success of the lab-scale testing, the data was used to design and develop a pilot-scale membrane module. This module was designed to meet pre-determined requirements as set forth by the project team. Producing lab-scale membrane modules helped identify and address possible problems in pilot-scale module design. This lead to the successful design and construction of a pilot-scale membrane module that could be used to recover the water that is needed to run the wet FGD process.

## CONTENTS

---

<b>CHAPTER 1: Introduction.....</b>	<b>12</b>
1.1 BACKGROUND .....	12
1.2 WATER RECOVERY FROM HUMID FLUE GAS .....	15
1.3 WATER RECOVERY THROUGH COMPETING TECHNOLOGIES.....	15
1.4 WATER RECOVERY THROUGH MEMBRANE TECHNOLOGY .....	16
1.4.1 Background on Humidity.....	16
1.5 RESEARCH AIMS AND OBJECTIVES .....	17
1.6 RESEARH QUESTION.....	17
<b>CHAPTER 2: Literature Review.....</b>	<b>18</b>
2.1 PREFACE .....	18
2.1.1 Membrane.....	18
2.1.2 Membrane Support structure .....	19
2.1.3 Seal.....	20
2.2 MEMBRANE MODULE DESIGNS AND CONFIGURATIONS .....	21
2.2.1 Plate & Frame modules .....	21
2.2.2 Spiral wound modules.....	22
2.2.3 Hollow fibre membrane modules .....	23
2.3 GAS SEPARATION MODULE DESIGNS .....	24
2.4 MODULE DESIGN & PROCESS CONSIDERATIONS FOR FLUE GAS DEHUMIDIFICATION .....	25
2.4.1 Process conditions and target recovery parameters .....	25
2.4.2 Membrane properties in the context of module design.....	26
2.4.3 Trans-membrane pressure difference in application .....	26
2.4.4 Feed channel pressure drop.....	28
2.5 SUMMARY FROM LITERATURE REVIEW .....	30
<b>CHAPTER 3: Experimental Work.....</b>	<b>31</b>
3.1 LAB-SCALE TESTING SYSTEM.....	31
3.1.1 Pump calibration .....	32
3.1.2 Relative humidity control.....	32
3.1.3 Temperature measurement and control .....	33
3.1.4 Humidity measurement and control .....	33
3.2 MINI MODULE DEVELOPMENT.....	33
3.2.1 Lab-scale mini module .....	35
3.2.2 Curtain type Lab-scale membrane module.....	40
3.3 PILOT-SCALE MEMBRANE MODULE DESIGN .....	42
3.3.1 Process conditions and target recovery parameters .....	42
3.3.2 Membrane selection, potting and support material.....	43
3.3.3 Trans-membrane pressure difference in application .....	43
3.3.4 Feed channel pressure drop and module configuration .....	45
3.4 PILOT-SCALE MEMBRANE MODULE PRODUCTION.....	49
3.4.1 Production of components .....	49
3.4.2 Building of the module .....	50
3.4.3 Potting and cutting of module .....	50
3.5 PROPOSED PILOT-SCALE FLUE GAS TREATMENT SYSTEM .....	50

<b>CHAPTER 4: Results and Discussion .....</b>	<b>52</b>
4.1    LAB-SCALE TESTING SYSTEM.....	52
4.1.1 Pump calibration .....	52
4.1.2 Gas flow-rate control.....	53
4.1.3 Temperature control.....	54
4.1.4 Humidity control .....	57
4.2    LAB-SCALE MEMBRANE MODULE DEVELOPMENT AND EVALUATION.....	59
4.2.1 Membrane fibre.....	59
4.2.2 Tubular lab-scale membrane module production .....	61
4.2.3 Membrane module leak test.....	62
4.2.4 Water recovery experiments.....	64
4.2.5 Lab-scale curtain-type membrane module production.....	71
4.3    PILOT CURTAIN-TYPE MEMBRANE MODULE DESIGN AND DEVELOPMENT.....	73
4.3.1 Required membrane area based on fixed process parameters .....	73
4.3.2 Amount of fibre per module.....	74
4.3.3 Potting of pilot-scale membrane module .....	75
4.3.4 Completed pilot-scale membrane module .....	76
<b>CHAPTER 5: Conclusions, Recommendations and Outputs .....</b>	<b>77</b>
5.1    LAB-SCALE MEMBRANE MODULE TESTING STATION.....	77
5.2    LAB-SCALE MEMBRANE MODULE .....	77
5.3    PILOT-SCALE MEMBRANE MODULE .....	78
5.4    RECOMMENDATIONS.....	78
<b>References .....</b>	<b>79</b>
<b>Appendix A.....</b>	<b>83</b>
<b>Appendix B.....</b>	<b>88</b>
<b>Appendix C.....</b>	<b>92</b>
<b>Appendix D.....</b>	<b>94</b>

**LIST OF FIGURES**

---

Figure 1.1: Graph adapted from (Ritchie & Roser, 2019) depicting the global primary energy consumption in (TWh) per year from 1800 – 2017 .....	12
Figure 1.2: Power station schematic with potential for water recovery from post-wet FGD process .....	14
Figure 1.3: Water recovery from flue gas through membrane technology (Sijbesma, et al., 2008).....	16
Figure 2.1: A typical example of a plate and frame module provided by (Günther, et al., 1996) .....	22
Figure 2.2: A schematic of a spiral wound module showing the flow directions, feed and permeate channels including spacers (Schwinge, et al., 2004) .....	22
Figure 2.3: Tube-side feed configuration for membrane module (Li, et al., 2004) .....	23
Figure 2.4: Shell-side feed configuration for membrane module (Li, et al., 2004) .....	24
Figure 3.1: Lab-scale testing system .....	31
Figure 3.2: Differential representation of the pressure and flowrate along a membrane .....	34
Figure 3.3: Differential model for water vapour pressure along the length of the membrane module .....	35
Figure 3.4: A schematic diagram of a designed Lab-scale membrane module (Water Research Commission, 2019) .....	36
Figure 3.5: Lab-scale curtain-type module design .....	40
Figure 3.6: The Teflon mould design used for potting the curtain-type mini module. ....	42
Figure 3.7: Intersect of a 8-layered hollow fibre membrane module; 1) Membrane intersect, 2) Membrane module frame, 3) Narrow slice of the membrane module which represents the system, 4) Distance between windings, 5) Distance between layers (Water Research Commission, 2019). ....	47
Figure 3.8: Pressure drop as function of module configuration and exhaust flow rate (Water Research Commission, 2019) .....	48
Figure 3.9: Process flow diagram for pilot-scale membrane module manufacture .....	49
Figure 3.10: Process flow diagram of proposed pilot-scale water recovery system .....	51
Figure 4.1: Watson Marlow 120U/DV calibration curve.....	53
Figure 4.2: Nitrogen gas flow rate over time.....	54
Figure 4.3: Phase 2 enclosure modification: 1) RH1, 2) T1, 3) RH2, 4) T2, 5) Fan, 6) Lomacor resistance elements, 7) Membrane module, 8) Copper coil, 9) TE .....	55
Figure 4.4: Enclosure Temperature profile as a function of time .....	56
Figure 4.5: Feed gas temperature profile as function of time.....	57
Figure 4.6: Excel spreadsheet used to calculate the required water flow rate needed to humidify a desired gas flow rate to a desired RH at a desired temperature.....	58
Figure 4.7: Relative Humidity measurement as function of time .....	58
Figure 4.8: SEM image of hollow fibre membrane (100 $\mu\text{m}$ scale) .....	59
Figure 4.9: SEM image of hollow fibre membrane (10 $\mu\text{m}$ scale) .....	60
Figure 4.10: SEM image of hollow fibre membrane focused on the membrane layer thickness .....	60
Figure 4.11: Completed laboratory membrane modules .....	61

Membrane Module Development For Water Recovery From Gas

-----

Figure 4.12: Membrane leak at increasing positive pressures .....	62
Figure 4.13: Membrane module leak testing at negative pressure .....	63
Figure 4.14: Mass of accumulated feed water and feed water flow rate .....	64
Figure 4.15: Water recovery experiment with a shell-side configuration.....	66
Figure 4.16: Water recovery experiment with a tube-side configuration .....	67
Figure 4.17: Percentage water recovery at decreasing feed gas flow rates .....	70
Figure 4.18: Lab-scale curtain-type membrane module showing creep effects of resin on membranes.....	71
Figure 4.19: Design for pilot plant curtain-type membrane module .....	75
Figure A.1: Piping and instrumentation diagram for leak testing of a membrane module (P = Pressure, I= Indicator, R= Regulator, MFC= Mass flow controller, MM=Membrane Module, HV = Hand Valve).....	87
Figure B.1: Solid works® drawing, provided by TFD, illustrating the humidity controlled laboratory-scale testing system (Front view).....	88
Figure B.2: Solid works® drawing, provided by TFD, illustrating the humidity controlled laboratory-scale testing system (Interior view) .....	89
Figure B.3: Piping and instrumentation diagram for the laboratory-scale testing system .....	89
Figure B.4: Humidity-Temperature-Relative Humidity relation of the H <sub>2</sub> O-N <sub>2</sub> system.....	91
Figure D.1: Complete Pilot-scale membrane module.....	95



## LIST OF TABLES

---

Table 1.1: Updated air quality regulations adapted from (Sonjica, 2010) .....	13
Table 2.1: Gas separation membrane modules and their applications/working conditions (Water Research Commission, 2019) .....	25
Table 2.2: Post wet-FGD flue gas composition, pressure and temperature limits (Daal, et al., 2013) .....	26
Table 3.1: List of equipment/components employed in the production of the mini curtain type membrane module.....	41
Table 4.1: Temperature and mass-flow controllers .....	52
Table 4.2: Measurements for membrane thickness .....	61
Table 4.3: Nitrogen permeance data obtained from leak test .....	63
Table 4.4: Percentage error obtained from mass balance (membrane is bypassed) .....	65
Table 4.5: Summary of shell-side water recovery .....	66
Table 4.6: Summary of tube-side water recovery.....	68
Table 4.7: Establishment of the membrane permeance using experimental lab-scale testing process parameters and the calculations as explained in 3.2.1.3.....	69
Table 4.8: Water recovery at different feed flow rates.....	70
Table 4.9: Module cutting attempts using various cutting techniques .....	72
Table 4.10: Calculated values for selected process parameters .....	73
Table 4.11: Hardness of potting material with different ratios (per unit volume) of resin compared to hardener at different curing times.....	76
Table A.1: Equipment and materials needed for production of a laboratory-scale membrane module .....	83
Table A.2: Preparation of the membrane module housing.....	84
Table A.3: Membrane fibre cutting and potting procedure .....	85
Table A.4: Manual for conducting a leak test on a laboratory-scale membrane module .....	86
Table A.5: Production and potting procedure for a mini curtain-type membrane module.....	87
Table B.1: List of equipment and components used in development of the lab scale testing system .....	90
Table C.1: Design of the 3D printed module spacers for every different layer of membrane .....	92
Table C.2: Module spacer assembly and frame.....	93
Table D.1: Produced Pilot-scale membrane module.....	94

**ACRONYMS & ABBREVIATIONS**

$\alpha_{AB}$	Selectivity of A over B
$\Delta P_{\text{fibre}}$	Pressure drop over membrane fibre
$\eta$	Gas viscosity
$\pi$	Pi (constant)
$\rho$	Gas density
$\Phi_{\text{exit total}}$	Total gas flow rate at membrane module exit
$\Phi_{\text{feed}}$	Flow rate of feed gas
$\Phi_{\text{H}_2\text{O feed}}$	Water vapour flow rate in feed
$\Phi_{\text{Normalized N}_2}$	Normalised Nitrogen flow rate
$\Phi_{\text{Permeate H}_2\text{O}}$	Permeating water vapour flow rate
$^{\circ}\text{C}$	Degrees Celsius
Antoine equation constant: A	8.07131
Antoine equation constant: B	1730.63
Antoine equation constant: C	233.426
atm	Atmosphere
bara	Absolute pressure
barg	Gauge pressure
CO <sub>2</sub>	Carbon Dioxide
f	Friction factor
FGD	Flue Gas Desulphurisation
$f_{\text{Laminar}}$	Friction factor for laminar flow regime
$f_{\text{Turbulent}}$	Friction factor for turbulent flow regime
GPU	Gas Permeation Units
HV	Hand valve
H <sub>2</sub>	Hydrogen gas
H <sub>2</sub> O	Water
ID	Inner diameter
ID <sub>fibre</sub>	Inner diameter of fibre
L	Length of fibre
MBR	Membrane bioreactor
MD	Membrane Distillation
Membrane permeance	Permeance of membrane fibre ( $\mu\text{mol}\cdot\text{m}^{-2}\cdot\text{s}^{-1}\cdot\text{Pa}^{-1}$ )
MFC	Mass flow controller
mmHg	Millimetres Mercury
N	Normalised
N <sub>2</sub>	Nitrogen gas
N <sub>fibres</sub>	Number of fibres in membrane module
OD	Outer diameter
OD <sub>fibre</sub>	Outer diameter of fibre
O <sub>2</sub>	Oxygen gas
P <sub>A</sub>	Permeability of A
P <sub>atmospheric</sub> = P <sub>feed</sub>	Atmospheric pressure = Feed pressure

Membrane Module Development For Water Recovery From Gas

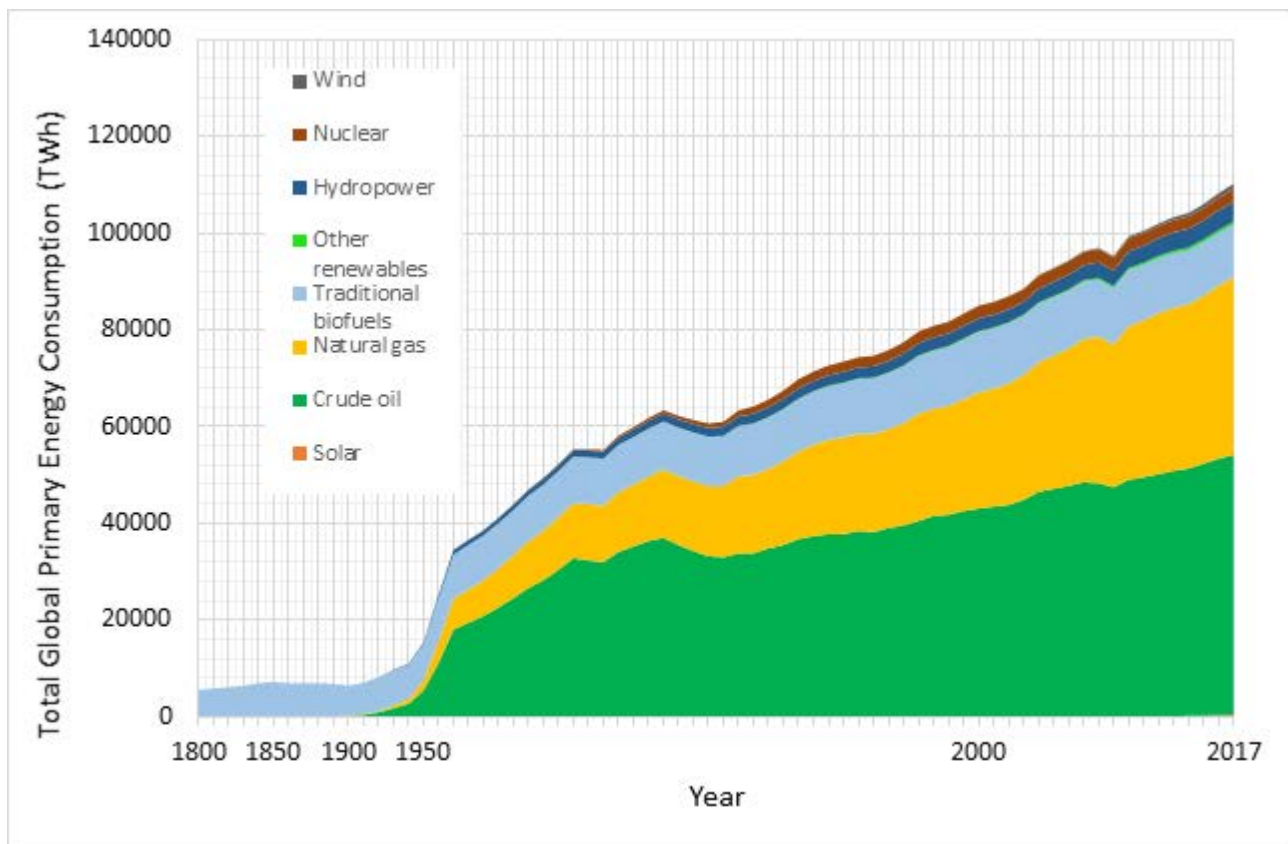
---

$P_B$	Permeability of B
$P_{H_2O \text{ exit}}$	Partial pressure of water vapour at the membrane module exit
$P_{H_2O \text{ feed}}$	Partial pressure of water vapour in feed gas
$P_{H_2O \text{ permeate}}$	Partial pressure of water vapour in permeate
$P_{H_2O \text{ reject}}$	Partial pressure of water vapour reject
PI	Pressure indicator
$P_N$	Normalised Pressure
$P_{N_2 \text{ feed}}$	Partial pressure of nitrogen in feed
PVC	Polyvinylchloride
PR	Pressure regulator
R	Universal gas constant
Re	Reynolds Number
RH	Relative Humidity
$RH_{\text{ feed}}$	Relative Humidity of feed gas
$RH_{\text{ reject}}$	Relative humidity of reject gas
RPM	Rotations per minute
SA	Surface area
$SA_{\text{fibre}}$	Cross sectional surface area of a membrane fibre
SEM	Scanning Electron Microscope
SI	Standard Index
SiC	Silicon Carbide
SO <sub>2</sub>	Sulphur Dioxide gas
SPEEK	Sulfonated poly(ether ether ketone)
STP	Standard Temperature and Pressure
T1	Temperature of feed gas
T2	Temperature of retentate gas
TFD	Thermodynamic Fluids and Design
TE	Temperature of Lab-scale system environment
$T_{\text{element}}$	Temperature of element
$T_{\text{ feed}}$	Temperature of the feed gas entering the module
Tg	Glass transition temperature
$TMP_{\text{ ave}}$	Average Trans-membrane pressure difference
$T_N$	Normalised Temperature
TWh	Terra Watt hour
UWC	University of the Western Cape
V	Gas velocity in fibre
WRC	Water Research Commission
WRR	Water Recovery Requirement

## CHAPTER 1: INTRODUCTION

### 1.1 BACKGROUND

Since the late 1800's and early 1900s, coal combustion has been an ever expanding source of energy. With the introduction and commercialization of coal power plants, use of coal sky rocketed as seen below in Figure 1.1. Coal combustion has been one of the main sources of energy since the start of the 20<sup>th</sup> century, followed by crude oil and natural gas. 'Other renewables' refers to renewable technologies such as geothermal, tidal and wave energy.



**Figure 1.1: Graph adapted from (Ritchie & Roser, 2019) depicting the global primary energy consumption in (TWh) per year from 1800 – 2017**

As time passed, the reliance on coal (Traditional biofuel in Figure 1.1) to satisfy our energy needs increased substantially. Depending on the natural resources a country possesses, a combination of the above energy sources are used to produce energy with one or more of these three non-renewable sources producing the bulk of the energy.

In 2012 global coal reserves were recorded at 897.48 billion tonnes with reserves in South Africa amounting to 7.4%, or 66.7 billion tonnes (Department of Mineral Resources, 2014). Due to this natural abundance, South Africa has come to rely on the combustion of coal as the primary source of energy production. According to

(Department of Mineral Resources, 2014), the use of coal in 2014 constituted 95% of energy production in South Africa, making South Africa the seventh largest producer of coal in the world.

During combustion of coal for energy generation, vast volumes of toxic acidic gases are released into the atmosphere unless appropriate measures are implemented. These gases may include SO<sub>2</sub>, which contributes to acid rain and human health complications (Burtraw, et al., 1998), (Franklin, et al., 1985). In 2012 the South African government attempted to reduce toxic gas emissions by passing a new air quality act 2008, which states that SO<sub>2</sub> emissions from new and existing solid fuel combustion installations are restricted to 500 mg/Nm<sup>3</sup> and 3500 mg/Nm<sup>3</sup> respectively (Molewa, 2012). Table 1.1 displays the air quality regulations for new and existing plants (Sonjica, 2010) and the time lines for implementation.

**Table 1.1: Updated air quality regulations adapted from (Sonjica, 2010)**

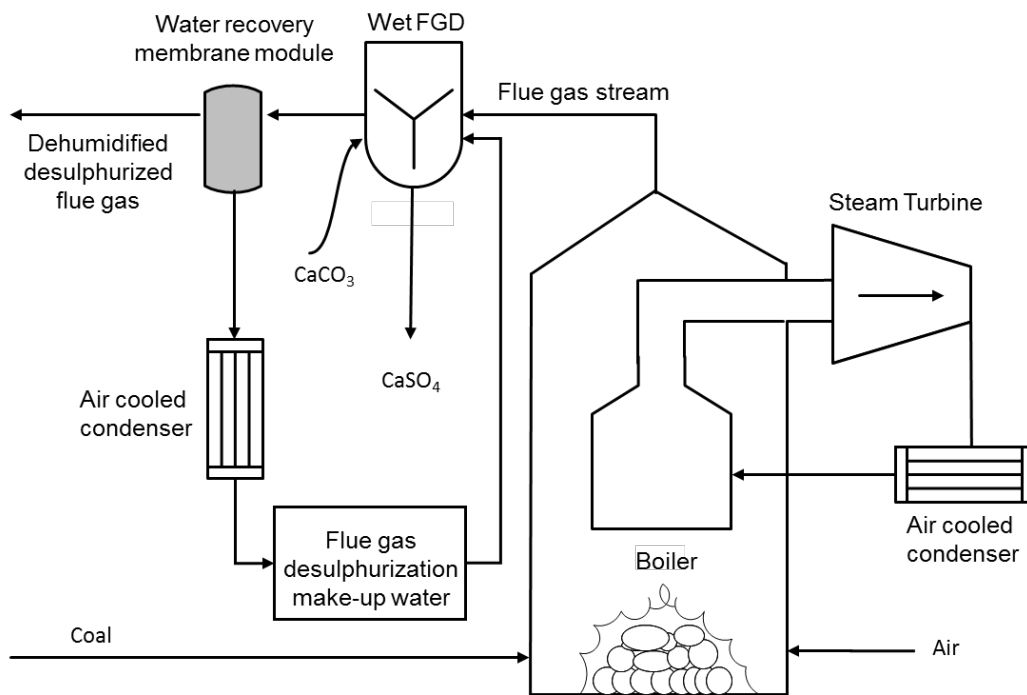
<b>Application</b>		All installations with design capacity equal to or greater than 50 MW heat input per unit, based on the lower calorific value of the fuel used.			
<b>Substance or mixture of substances</b>		<b>Plant status</b>	<b>mg/Nm<sup>3</sup> (0°C, 1 atm, 10% O<sub>2</sub>)</b>		
<b>Common name</b>	<b>Symbol</b>		<b>2010</b>	<b>2015</b>	<b>2020</b>
Particulate matter	PM	New	50	50	50
		Existing		100	50
Sulphur dioxide	SO <sub>2</sub>	New	500	500	500
		Existing		3500	500

The South African Electricity supplier (Eskom) implemented wet flue gas desulphurisation as a technique in order to comply with the new SO<sub>2</sub> emission standards at their new power plants (Medupi and Kusile) (Molewa, 2012). In order to bind the SO<sub>2</sub> to the absorbent, an intensive contact between the aqueous sorbent phase and the flue gas is required. During this contact process, flue gas is continuously saturated with water vapour before exiting the gas stack.

Over the past five years South Africa has been afflicted by an overwhelming drought, severely impacting farmers and causing severe water restrictions to be put in place. According to (Hoffman, et al., 2009) the frequency of droughts are predicted to increase, which would severely cripple the already limited water supply available in South Africa. Agricultural water usage in the Western Cape area has seen an allowed water usage cut of 60 % since 2017 (World Wildlife Fund, 2018). This is due to domestic water needs being met, with the remaining water supply being split between agricultural (including irrigation) and industrial needs. Agricultural activities in South Africa have an undeniable impact on the country's economy (World Wildlife Fund, 2018). As such, the drought has a crippling effect on the economy. For more water resources to be available to the agricultural sector, water usage by industry has to be reduced. With Eskom opting to use the wet-FGD process, the overwhelming increase in water usage is becoming unsustainable. Wet flue gas desulphurization consumes roughly 2 tons of water per MWh power produced (Mc Nemar, 2006). Thus, it is within Eskom's best interest to reduce its water footprint in South Africa.

The book *Membranes for Industrial Wastewater Recovery and Re-use* (Judd & Jefferson, 2003), mentions that coal fired power plants could be water self-sustainable if 20% of the water vapour in flue gas can be captured for re-use in the plant (Zhao, et al., 2017). This presents adequate grounds and a need to research and investigate methods for effective water recovery from flue gas in power plants. Various techniques, such as flue gas condensation, the use of a desiccant drying system and membrane technologies are available for recovery of water vapour. As discussed in Daal, et al, 2013, flue gas condensation and desiccant drying systems are the main commercially implemented methods. Membrane technology has been presented as a viable competitor to these methods and is being researched extensively.

Unlike condensation or desiccant systems, membrane technology has ability to recover water with the added benefit of separating it from the impurities that is commonly found in the two former technologies. This results in the recovered water not needing purification, which implies it can be used as make-up water for almost all industrial processes (Wang, et al., 2012). Furthermore, membrane technology is more energy efficient and has a smaller footprint compared to condensation and desiccant systems (Macedonio, et al., 2012), (Sijbesma, et al., 2008) with the absence of phase changes and moving parts, membrane technology has been labelled an energy efficient alternative to its major competitor (condensation). The generally small carbon foot print of membrane technology has been mentioned as an additional advantage. Figure 1.2 presents a conceptual diagram of a membrane module installation retrofitted into a power plant. In Figure 1.3 the membrane module concept is presented on both the macro and micro scale with the macro being supplied by Sijbesma (Sijbesma, et al., 2008) on the right and micro being on the left.



**Figure 1.2: Power station schematic with potential for water recovery from post-wet FGD process**

When coal is combusted for electricity generation, the heat is used to boil water in the boiler. This produces high pressure steam which in turn is used to drive turbines. The turbines are connected to a generator which generates electricity. As mentioned in the introduction, the combustion process generates a flue gas which needs to be treated before it can be released into the atmosphere. The use of wet FGD increases the water content of the flue gas until saturated. Applying wet-FGD on an air cooled power station effectively triples the amount of water used by the plant.

## **1.2 WATER RECOVERY FROM HUMID FLUE GAS**

Since the start of the 20<sup>th</sup> century the most notable energy production has been due to combustion of hydrocarbons. Hydrocarbons are classified as organic molecules mainly consisting of carbon and hydrogen atoms bonded in a chain-like structure. Water vapour and carbon dioxide are the by-products when combustion takes place (Wang, et al., 2012); (Levy, et al., 2008). The water vapour produced can form 12 – 16% of the product gas (Wang, et al., 2012). When the water vapour is not recovered, all the water is lost to the atmosphere in addition to underlying heat loss in the plant which in turn may lower the thermal efficiency of the power plant (Wang, et al., 2012). It has been predicted that if 40 to 60 % of the water vapour in the flue gas would be recovered, it would lead to a thermal efficiency increase in the plant of up to 5% (Wang, et al., 2012). Furthermore, water can be considered as a corrosive agent if condensation of the water vapour in the flue gas occurs in the stack. This could compromise the structural integrity of the stack internals which, together with the reduction in thermal efficiency, presents a need for dehydration of flue gas (Sijbesma, et al., 2008).

## **1.3 WATER RECOVERY THROUGH COMPETING TECHNOLOGIES**

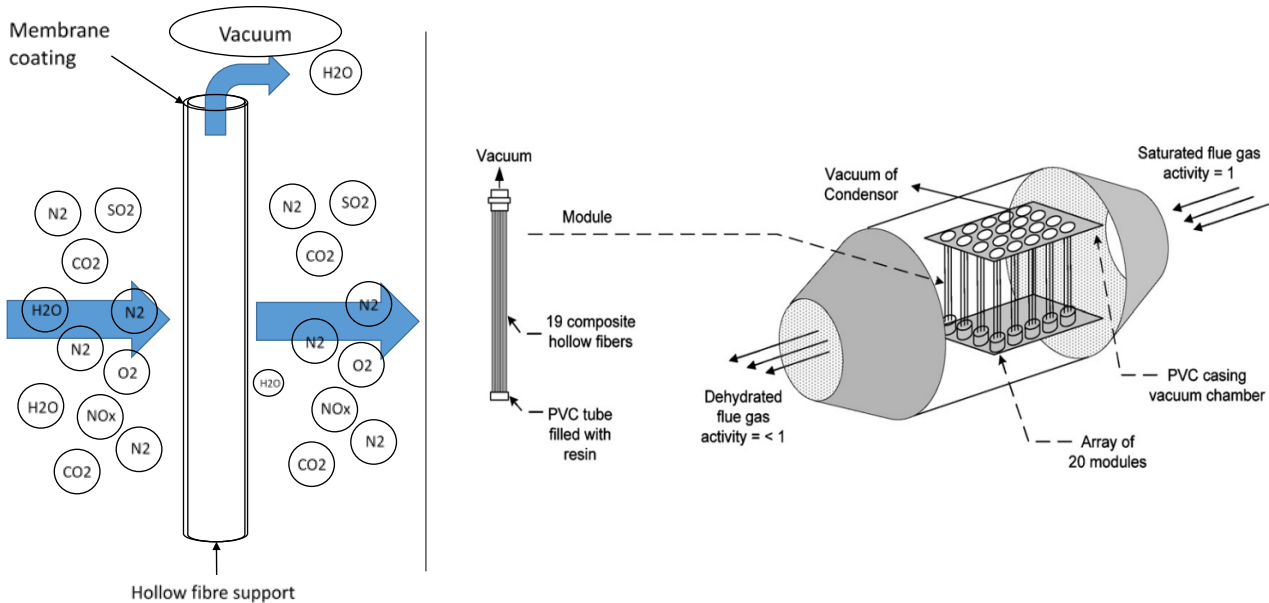
Levy conducted a pilot-scale study which revealed that multiple condensing heat exchangers, designed to recover water vapour from flue gas, resulted in water recovery efficiencies of 10 – 34 % depending on the amount of water present in the coal (Levy, et al., 2008). It should be noted that heat exchangers used to recover water from flue gas need special anti-corrosion tubing (Wang, et al., 2012). There are several challenges concerning water recovery in this manner. Firstly, this water recovery technique requires a substantial amount of cooling hardware to reduce the temperature of the flue gas stream for effective water recovery (Wang, et al., 2012). Furthermore the recovered water needs to be treated before it can be reused due to the acidity of the recovered water. The acidity poses a threat to the integrity of the cooling hardware due to the corrosive nature of acidic solutions. One possible solution to the aforementioned problem would be to install acid traps, however this would lead to extra maintenance costs.

Another method of water recovery described by Isetti (Isetti, et al., 1997) is the absorption of water by liquid desiccants. The desiccant system is a commonly used and accepted water capture technology even though it can be a highly energy intensive process to regenerate the desiccants and the water is of poor quality (Sijbesma, et al., 2008). On the other hand, if the thermal energy used to regenerate the hygroscopic solution can be obtained from other sources, the energy savings compared to the air-cooling method described above are significant (Isetti, et al., 1997), (Peng & Howell, 1984). It should be noted that in both technologies the

resultant water is of poor quality which would require treatment before reuse. This creates a need for a technology that recovers the water vapour in a flue gas without the impurities that lower the quality of the water.

## 1.4 WATER RECOVERY THROUGH MEMBRANE TECHNOLOGY

As mentioned above, membranes have several advantages over present competing technologies. Thus it is a more appealing alternative to technologies installed currently.



**Figure 1.3: Water recovery from flue gas through membrane technology (Sijbesma, et al., 2008)**

In Figure 1.3 the image on the left shows a single hollow fibre membrane illustrating the flow of a gas over the membrane while is vacuum applied inside the fibre. This causes a partial pressure gradient, a driving force for water vapour molecules to permeate through the membrane leaving the feed gas dehydrated. The permeated water molecules are removed at the fibre end. The image on the right (Sijbesma, et al., 2008) shows an array of water vapour selective membrane modules that are placed in the path of a flue gas.

### 1.4.1 Background on Humidity

Dry inert gas has a defined set capacity at which it can hold water at given temperature conditions. At high temperatures, a gas has a higher vapour holding capacity than at low temperature (National Physical Laboratory (Great Britain), 1996). Once the full vapour holding capacity has been exhausted, the gas is termed as “saturated”. Relative humidity may be defined as the partial pressure of water vapour in a gas mixture relative to the maximum possible (saturation) partial pressure at the same temperatures (Jensen, 2012). This definition is in contrast to absolute humidity which is the mass of water vapour per unit mass of dry gas at a given temperature and pressure (National Physical Laboratory and Institute of Measurement and Control, 1996).



## **1.5 RESEARCH AIMS AND OBJECTIVES**

The research conducted in this project aims to explore an alternative water recovery technology, capable of reducing the water consumption of power stations. More specifically, to address the water usage increase at ESKOM power stations after instalment of wet-FGD systems.

The main objective is the successful design and production of a lab-scale membrane module, which can be used to test the feasibility of membrane technology in addressing the increased water consumption by power stations. The success will be determined by measuring the permeance, selectivity and water recovery of the modules. Another objective is the design of an up-scaled membrane module for water recovery at pilot plant scale. However, this will only be considered once the design and production of lab-scale membrane modules are considered successful.

## **1.6 RESEARH QUESTION**

- What module configuration is suitable for the task of extracting water from un-pressurized flue gas
- What module design would comply with the pressure drop requirements prescribed by Eskom
- What are the membrane properties in terms of permeance and selectivity
- How many meters of fibre should be used to extract 33% of the water present in the feed stream (with a relative humidity of 95% at 60°C) at a given feed flow rate

In order to answer these research questions lab-scale membrane modules and a membrane module testing system needs to be constructed. Following this, the designed and produced lab-scale membrane modules will be tested. These tests will be for leak-freeness, along with permeance of the different feed gas components so as to establish permeability and selectivity of the membrane. Once a leak-free lab-scale membrane module has been produced and sufficient water vapour recovery has been achieved, design of a pilot-scale membrane module capable of recovering 33% of the total water vapour entering the module will commence.

## CHAPTER 2: LITERATURE REVIEW

---

### 2.1 PREFACE

Membranes have been on the forefront of research over the past few decades because of its promising aspects in various fields (He & Hägg, 2012). Membrane technology is generally seen as energy efficient, small in foot print and reliable for a variety of applications from petroleum refining (Asatekin & Mayes, 2009) to food and dairy (Rosenberg, 1995) to wastewater treatment (Pankhania, et al., 1994) and desalination (Yang, et al., 2009). Thousands of publications can be found on the development of membranes, however relatively few are found on the development of membrane modules.

A membrane module allows a membrane to be used for a practical application (Baker, 2004). In order to design an effective membrane module, knowledge about the desired application and process conditions are critical. The membrane module can be operated in different ways and typically consists of a membrane (see section 2.1.1) and the membrane support structure (see section 2.1.2) which includes connection points for the inlet (the feed stream) and the two outlets for the concentrate- and permeate- flows respectively. An effective seal (see section 2.1.3) is an important part of the membrane support structure, critical to achieve a functional selective module (Anon., 2018). More details on membrane modules designs will be discussed in section 2.2.

The lion share of this chapter has been adopted from the Water Research Commission report which has been co-authored by the author of this thesis (Water Research Commission, 2019).

#### 2.1.1 Membrane

A membrane forms the interphase between two phases in two distinct compartments and its selectively permeable barrier properties enable separation (Ulbricht, 2015). Selective permeability (permselectivity), is a membrane property allowing select species to permeate through the membrane wall at an exponentially greater rate compared to others. Membranes materials are characterised by their permeability towards different species, while membranes are characterised by the permeance of those species. For a membrane material to find a commercial application the material must;

- A) form an uncompromised continuous barrier, eg should be casted into a film and not display any protruding holes or cracks
- B) be processed into a layer, as thin as technology allows this to happen. These layers need to display thermal and mechanical characteristics supportive of the membranes intended use (Mottern, et al., 2008).

There are various application specific factors that need to be taken into account when selecting a membrane module (Koros & Mahajan, 2000). Besides obvious properties such module productivity and selectivity, the expected lifetime and cost are most critical to complete any economic projections. Mechanical properties,

process specific thermal and chemical compatibility and membrane surface interaction with potential foulants and cleaning agents all impact module life (Koros & Pinnau, 1994).

A wide range of membrane materials have been developed over the year and processed into defect free films of decreasing thicknesses.

For the development of a water vapour selective membrane modules designed to recovery water from saturated flue gas, dense polymeric membranes can be used as they show an efficient trade-off between high permeability and selectivity of a water vapour over any of the other constituents in flue gas (Sijbesma, et al., 2008). These membranes take advantage of the different solubility and diffusivity of gaseous components to achieve separation, which is facilitated by a vapour pressure difference between the feed and permeate side of the membrane wall (Sijbesma, et al., 2008). The gasses dissolve and diffuses along the polymer chains of the membrane in order to pass through the membrane. Once the solubility and rate of diffusion for one specie surpasses that of the others, the membrane can be considered for recovery applications. In a study by (Sijbesma, et al., 2008), sulphonated poly(ether ether ketone) SPEEK showed promising properties with a water vapour permeability of  $1.6 \mu\text{mol}\cdot\text{m}^{-2}\cdot\text{s}^{-1}\cdot\text{Pa}^{-1}$ . The water vapour/nitrogen selectivity was reported as  $1 \times 10^7$ .

### **2.1.2 Membrane Support structure**

The support structure of a membrane module can be separated into two main parts. The support structure for the membrane and the support structure for the module housing.

#### **2.1.2.1 Membrane support structure**

The primary function of the support layer is to provide mechanical stability to the membrane during operation. The support strength must be high enough to withstand the trans-membrane pressure differences, which can be as high as 100 Bar (Mottern, et al., 2008) and the pressure transferred onto the membrane by compression seals. Its thickness is usually in the order of millimetres.

#### **2.1.2.2 Module housing**

The design of a module housing which includes the choice of materials will be guided by the process conditions such as the application temperature, pressures and chemical environments. Materials commonly used in gas separation modules include glass, plastic, aluminium and stainless steel (Ismail & Kumari, 2004), (Li & Chung, 2004).

Membrane modules must also conform to specified safety regulation. The immediate mechanical requirement are determined by the design of the module (shape, size, material, thickness) and the process conditions often involving a feed pressure exceeding 5 Bar (Choi, et al., 2002). To meet the mechanical requirements throughout its intended lifetime, material compatibility with the feed medium at the required process temperature and pressure need to be considered. As the lifespan of the membranes is increased by regular

membrane cleaning (Sijbesma, et al., 2008), all exposed module components need to be compatible with these cleaning agents

### 2.1.3 Seal

A membrane module employs different types of seal mechanisms to prevent liquid or gas from leaking. There are two types of leaks (Water Research Commission, 2019);

- A) External leaks occur on locations where the feed medium exits the module other than through the outlet. To avoid any external leaks gaskets or O-rings are often used (Wood & Gifford, n.d.).
- B) Internal leaks are leaks that allow the feed medium to leak from the feed side to the permeate side in any way other than through the membrane. Tubular membranes, may use compression seals (Yacou, et al., 2012) while flat membranes may use gaskets (Croopnick, et al., 1977) often integrated with the spacer. Sufficient pressure, evenly applied will prevent the feed medium to percolate passed the seal. Sealing multiple tubular membranes with O-rings is challenging. The most popular seal for multiple tubular modules is an epoxy resin as explained in (Li, et al., 2004).

The choice of seal depends on the type of membrane along with the temperature and pressure of the application. Added to this is compatibility of the seal material with components in the feed, reject and permeate streams (Water Research Commission, 2019).

Materials that can be considered as membrane seals include polyurethanes, polyolefins, polyethylenes, polyolefin copolymers, polyamides, polystyrenes, polyvinylchlorides, silicone rubbers, epoxy resins, polyesters and polysulphides (Ismail & Kumari, 2004). Polymer hollow fibre membranes are typically embedded in epoxy (Li & Chung, 2004) and the process to achieve such seal is known as potting. These adhesives have a wide range of viscosities and hardness. When selecting an appropriate potting resin there are certain characteristics that need to be taken into account as presented by (Ismail & Kumari, 2004), (Water Research Commission, 2019);

1. A sufficiently low viscosity. This is to penetrate the interstitial regions between fibres in order to form a continuous seal.
2. Curing time should be long enough to allow proper distribution of the resin between all fibres and short enough to allow production targets to be reached.
3. The resin needs to adhere well to the embedded fibres to ensure a leak free module even when pressurized.
4. The resin curing should not involve excessive temperature peaks which could damage the fibres.
5. The resin formulation should be chemical resistant to the environment of the application.

Other characteristics important when considering a specific resin is the glass transition temperature of the resin ( $T_g$ ) and plasticisation behaviour.  $T_g$  is the temperature region where the polymer transitions from a hard glassy material to a soft rubbery material (Epotek, 2012) and has an important influence on the mechanical properties of solid polymers. Higher  $T_g$ 's correlate to an increased polymer chain stiffness, higher modulus of

elasticity and better tensile properties at elevated temperatures which would prevent swelling and shrinkage of potting resin rendering a potentially more durable membrane module.

Plasticisation is defined as the process of changing the structure of a polymer to make it easier to bend (Dictionary, 2018). Some of the feed gas components, typically CO<sub>2</sub>, may dissolve into the polymer matrix depending on their partial pressure and temperature, and cause plasticisation, an increase in chain mobility induced by dissolved gases. Plasticisation causes a decrease in T<sub>g</sub> and its modulus of elasticity.

In a study by Ismail (Ismail & Kumari, 2004), epoxy resins showed a higher resistance to CO<sub>2</sub> plasticisation than polyurethane resins. The author prescribed this to the high number of hydrogen bonds between the chains of polyurethane compared to epoxy. Pandey (Pandey, et al., 2002) hypothesised that the polar groups interact with CO<sub>2</sub> and give rise to plasticization effects. Both studies indicate that an epoxy is the preferred resin to use for potting in a gas-separation membrane module.

Polymers age with time, even at ambient conditions, and the ageing phenomenon can be aggravated with the presence of CO<sub>2</sub> gas (Ismail & Kumari, 2004). This should be taken into account when designing membrane modules operating in CO<sub>2</sub> rich environments such as flue gas.

## **2.2 MEMBRANE MODULE DESIGNS AND CONFIGURATIONS**

Various membrane module configurations are available and have an impact on system performance (Li & Chung, 2004). The three generic membrane module types; A) Plate and frame, B) Spiral wound and hollow fibre modules have their own characteristic properties such as membrane packing density and membrane surface to volume ratio (Li & Chung, 2004). Each membrane module type and their typical applications will be discussed below.

### **2.2.1 Plate & Frame modules**

Plate and frame modules formed part of the earliest membrane systems (Baker, 2004). In the plate and frame design, flat sheet membranes, porous membrane supports and spacers are clamped together, as they form a feed flow path (Strathman, 1988). These are stacked between two end plates thus forming the plate & frame configuration (Strathman, 1988). This provides the mechanical integrity needed for these modules to be stacked together in a modular way and form an integrated module system (Drioli, et al., 2002). Plate and frame modules are used in many water treatment applications and are commonly known as stacked membrane modules (Forwardosmosistech, 2014). However, Plate and frame modules are expensive when compared to alternatives on small scale. This has limited the use of this type of module. Figure 2.1 is an example of a plate and frame configuration that is still used today.

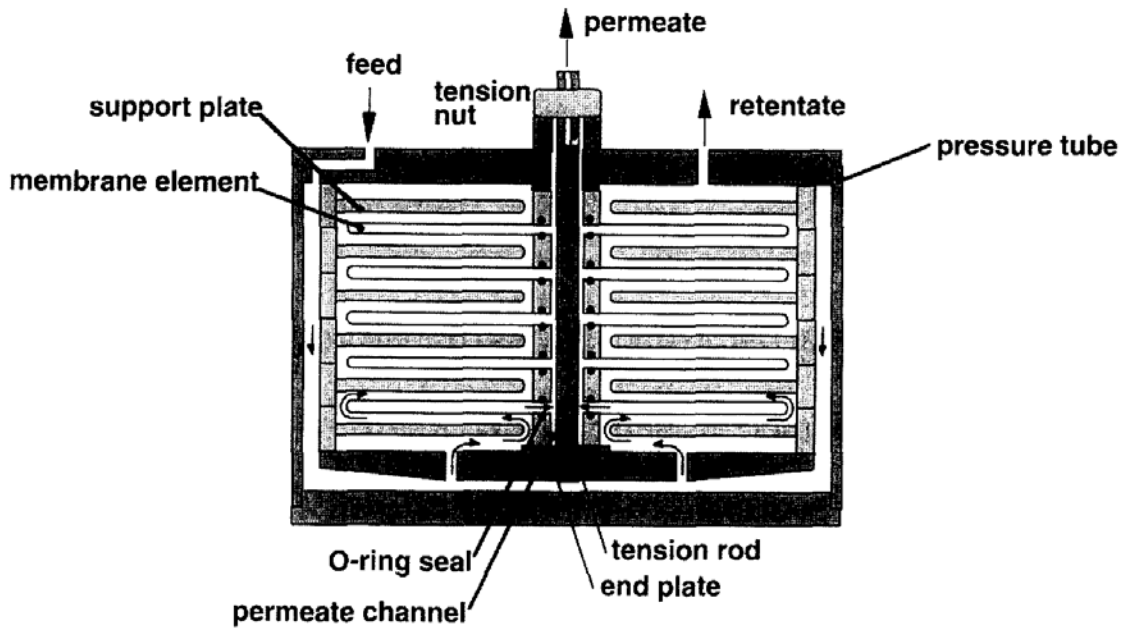


Figure 2.1: A typical example of a plate and frame module provided by (Günther, et al., 1996)

### 2.2.2 Spiral wound modules

Spiral wound modules are similar to the plate and frame configuration, but the spacer, membrane and support are made into a roll and placed in a tubular shell whose centre provides a flow channel of the permeate (Strathman, 1988). Spiral wound modules were initially designed to produce artificial kidneys. Spiral wound modules are now typically applied in seawater desalination, brackish water treatment, and drinking water treatment and are mostly associated with reverse osmosis and Nano-filtration processes (Geng, et al., 2014). In these modules, a portion of the feed permeates through the membrane into the permeate channel and spirals towards the centre where it exits through the collection tube (Baker, 2004). A schematic of a spiral wound module is presented in Figure 2.2.

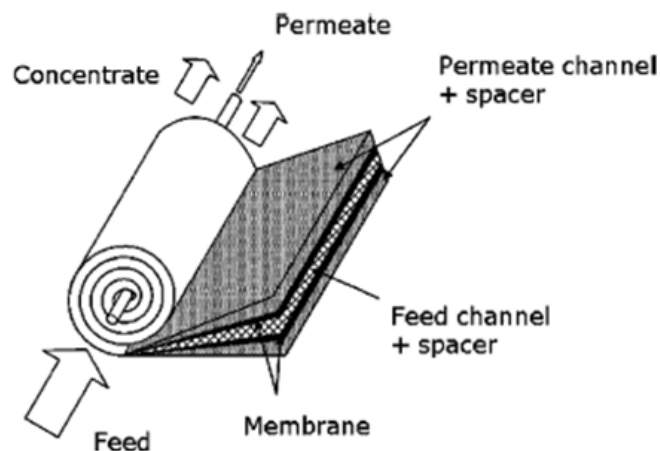


Figure 2.2: A schematic of a spiral wound module showing the flow directions, feed and permeate channels including spacers (Schwinge, et al., 2004)

The feed channel spacers make these modules sensitive to fouling, the tendency of solids to build up on the membrane surface. Depending on the application and the pre-treatment, fouling will be more or less apparent and specific pre caution is often needed to avoid it. Fouling caused by micro-organisms is referred to as bio-fouling.

### 2.2.3 Hollow fibre membrane modules

Unlike the previously discussed configurations, the hollow fibre module membrane configuration employs tubular /capillary type membranes (Strathman, 1988). The densely packed bundle of hollow fibre membranes yields a high surface to volume ratio. With a fibre diameter of 3mm, this ratio is as high as 1000 m<sup>2</sup>/m<sup>3</sup> (Liu, et al., 2003). Multitudes of bundles are positioned in steel, glass or plastic housings. The feed medium can be introduced into the bore of the fibres and as such, the permeate is collected on the shell-side. This is referred to as a tube-side configuration and is illustrated in Figure 2.3. The feed medium can also be introduced into the membrane module housing (the shell) and as such, the permeate is collected on lumen side of the fibre. Figure 2.4 shows this configuration which is referred to as the shell-side configuration.

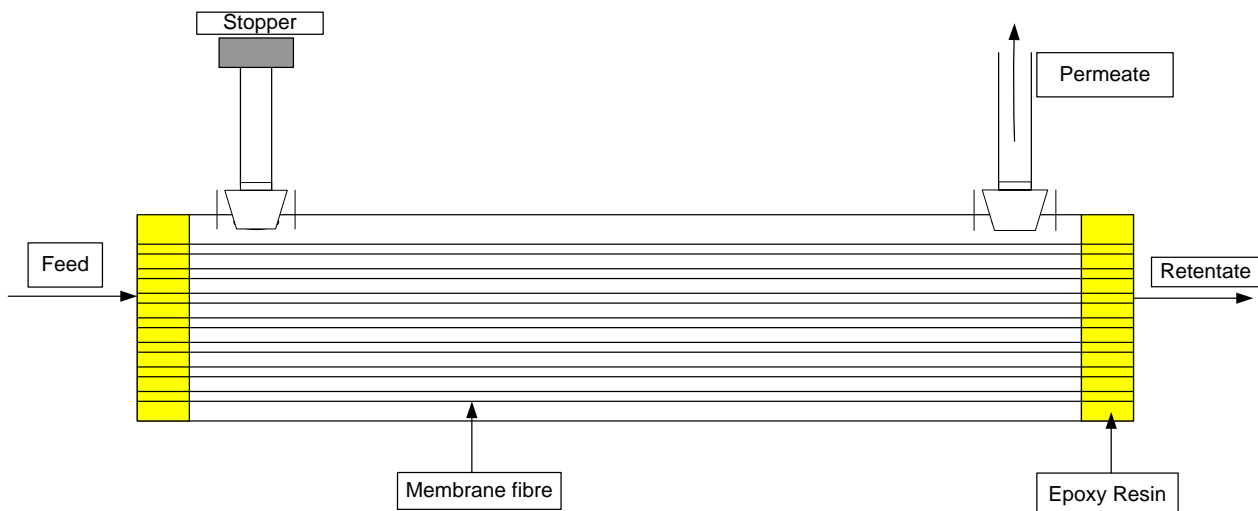
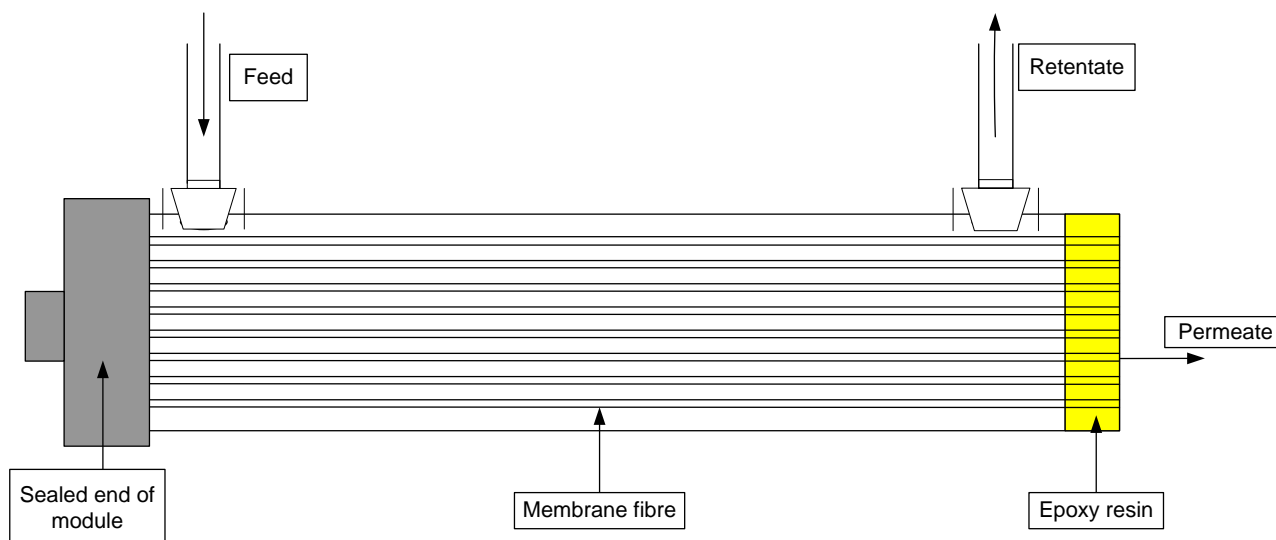


Figure 2.3: Tube-side feed configuration for membrane module (Li, et al., 2004)



**Figure 2.4: Shell-side feed configuration for membrane module (Li, et al., 2004)**

Fibres should be distributed uniformly and evenly within the housing. A 45-60% volume-based packing density is advised (Li & Chung, 2004). The overall performance of hollow fibre membrane modules is governed by the intrinsic membrane properties, coupled with fluid hydrodynamics within the module (Wan, et al., 2017).

### 2.3 GAS SEPARATION MODULE DESIGNS

Gas separation finds its application in both hollow fibre membranes modules as well as spiral wound modules (Baker, 2004). Table 2.1 contains a list of applications where membranes are applied to achieve the separation of a specific gas from a mixture of gases together with the type of module, its configuration, the trans-membrane-pressure (TMP) applied and the “feed channel pressure drop” which is defined as the reduction of pressure between the entrance and the exit of the feed stream.

Hollow fibre membrane modules for gas separation are used at various pressure ranges (Baker, 2002). For recovery of hydrogen gas in refineries, the feed gas is applied at pressures between 20 and 70 bar in a shell-side configuration (Dindore, et al., 2004). Membrane Distillation (MD) processes require membrane modules that utilize feed pressure range anywhere from 0.5 bar – 50 bar. Membrane distillation is a thermal separation process making use of the difference in vapour pressure between the feed and the permeate side. MD makes use of microporous hydrophobic membranes which reject hydrophilic media but allow vapour (hydrophobic) to permeate through the open membrane pores (Winter, 2011). However, the pressures used in a spiral wound module vary hugely depending on the membrane and the medium being used. These pressures range anywhere from 0.5 bar – 50 bar.

Membrane modules designed for dehumidification of various media are commercially available (Parker Hannifin Corp, 2018) and (PermSelect, 2017). For some applications such as the generation of dry nitrogen gas from air, the wet gas is applied on the tube side of the hollow fibres and utilises a counter-flow (Baker,



2002). Another application where a hollow fibre membrane module was used in tube feed configuration was in flue gas dehydration described by (Sijbesma, et al., 2008).

**Table 2.1: Gas separation membrane modules and their applications/working conditions (Water Research Commission, 2019)**

No	Reference	Application	Module & configuration	TMP (kPa)	Feed channel pressure drop (kPa)
1	(Koros & Vu, 2002)	CO <sub>2</sub> /H <sub>2</sub> removal	Tubular HF, tube side feed	1500-7000	NA
2	(Parker Hannifin Corporation, 2009)	N <sub>2</sub> /air	Tubular HF, tube side feed	400-700	100
3	(Way, 1993)	N <sub>2</sub> removal from ammonia	Tubular HF, tube side feed	1500	NA
4	(Parker Hannifin Corp, 2018)	H <sub>2</sub> O/air	Tubular HF, tube side feed	NA	10
5	(PermSelect - MedArray Inc., n.d.)	H <sub>2</sub> O/air	Tubular HF, shell-side feed	100	NA
6	(Houde, et al., 1995)	CO <sub>2</sub> from natural gas	Spiral wound module	3700	NA
7	(Daal, et al., 2013)	H <sub>2</sub> O from flue gas	Curtain-type HF, shell-side feed	50	NA

In a report by (Daal, et al., 2013) a “curtain” type membrane module is designed for flue gas dehydration. These membrane modules use hollow fibre membranes developed by (Sijbesma, et al., 2008). The report does not report on the feed pressure of the flue gas nor the feed channel pressure drop. Telephonic contact with the author confirmed that the inlet pressure was close to atmospheric pressure.

## 2.4 MODULE DESIGN & PROCESS CONSIDERATIONS FOR FLUE GAS DEHUMIDIFICATION

In the design phase of a membrane module, the process conditions and target recovery parameters at the location where the separation is required are considered first. The combination of the membrane properties of the available membranes, the feasible transmembrane pressure difference and an allowable feed channel pressure drop will then permit the finalization of the module design.

### 2.4.1 Process conditions and target recovery parameters

Critical to the design of a membrane module destined to recover water from flue gas, are the process conditions and their limits to which the module will be exposed to, such as flue gas temperature, relative humidity, gas composition, pressure and their variations. The process conditions for post wet-FGD flue gas are listed in Table 2.2.

**Table 2.2: Post wet-FGD flue gas composition, pressure and temperature limits (Daal, et al., 2013)**

Component	Exhaust gas partial pressure ratios	Temperature (°C)
N <sub>2</sub>	0.69	50-60
CO <sub>2</sub>	0.122	50-60
H <sub>2</sub> O	0.12	50-60
O <sub>2</sub>	0.068	50-60

### 2.4.2 Membrane properties in the context of module design

The critical membrane properties besides their cost are;

- Membrane permeability; the amount of permeating specie in mols (or units of volume), per unit of membrane area, per unit of time, per unit of pressure, times unit of membrane thickness. Some researchers prefer to express permeability in Barrer where 1 Barrer =  $3.35 \times 10^{-10} \text{ mol}\cdot\text{m}/\text{Pa}\cdot\text{s}/\text{m}^2$ . In module design, a membrane of specific thickness will be selected. The product of permeability and membrane thickness is permeance. Researchers in favour of the SI units choose  $\mu\text{mol}\cdot\text{m}^{-2}\cdot\text{s}^{-1}\cdot\text{Pa}^{-1}$  as the unit for permeance. The higher the permeance, the smaller the required surface area
- Permselectivity; used to compare the separating capacity of a membrane for 2 (or more) species (Anon., n.d.). The permselectivity of one component (A) over another component (B), is given by the ratio of their permeabilities:  $\alpha_{AB} = \frac{P_A}{P_B}$
- Stability; the conditions at which the permeance and selectivity hold. Properties of the perm selective barrier are sensitive to temperature and partial pressure of feed gas components

The membrane performance data is typically obtained with a laboratory size test module. These test modules are typically operated under optimized testing conditions to reveal the best case scenario membrane permeance and selectivity.

### 2.4.3 Trans-membrane pressure difference in application

When the trans-membrane pressure (TMP) difference is known, the minimal required membrane surface area can be calculated. Eskom concluded that the post wet-FGD flue gas will have a pressure close to atmospheric and is not likely to be re-pressurized before entering the water recovery system that houses the membrane module. Pressurizing the vast amount of flue gas would constitute an unacceptable energy penalty. Ultimately the dehumidified flue gas will be dumped into the atmosphere, which means that at the point of exit from the stack, dehumidified flue gas is at atmospheric pressure.

The driving force for water molecules to permeate through the membrane is the difference in chemical activity of the water molecules between the feed- and the permeate side. By approximation, the chemical activity difference is equal to the difference in the partial pressure of water between the feed side ( $P_{\text{H}_2\text{O feed}}$ ) and the

permeate side ( $P_{H_2O \text{ permeate}}$ ). The  $P_{H_2O \text{ feed}}$  can be calculated by using the Antoine equation multiplied by percentage of the relative humidity (RH);

**Equation 2.1**

$$P_{H_2O \text{ feed}} \left[ \frac{N}{m^2} \right] = \frac{10^{\left( A - \frac{B}{C + T_{\text{feed}} [^\circ\text{C}]} \right)} [mmHg]}{760 \left[ \frac{mmHg}{atm} \right]} 101325 \left[ \frac{N}{m^2} \right] \cdot RH$$

Whereby:

- A, B and C are empirically determined constants with their values of 8.07131, 1730.63 and 233.426 respectively
- $T_{\text{feed}}$  the temperature of the feed gas entering the membrane module
- 760 is the Hg column height in mm at 1 atm
- 101325 the number of Newton per  $m^2$  per atm

As the Antoine equation provides the pressure in the mmHg, two conversion steps are applied (see Equation 2.1) to retrieve the value of pressure in SI units, ( $N \cdot m^{-2}$ ) also known as Pascal (Pa)

Since the membrane is highly selectivity towards water, the composition of the permeate is assumed to be 100% water vapour. However, with the chance of non-condensable gasses accumulating at the permeate side over time, the  $P_{H_2O \text{ permeate}}$  is not read from the pressure gauge but derived from the temperature of the cooling element ( $T_{\text{element}}$ ) that has been placed in the pathway of the permeate gas downstream the membrane module. As the condensed water will be in equilibrium with its water vapour (100% RH), the Antoine equation can be used to calculate  $P_{H_2O \text{ permeate}}$  as follows:

**Equation 2.2**

$$P_{H_2O \text{ Permeate}} \left[ \frac{N}{m^2} \right] = \frac{10^{\left( A - \frac{B}{C + T_{\text{element}}} \right)} [mmHg]}{760 \left[ \frac{mmHg}{atm} \right]} 101325 \left[ \frac{N}{m^2} \right] \cdot 100\% RH$$

The value of the TMP at the entrance of the module ( $x=0$ ) could be determined as  $P_{H_2O \text{ feed } x=0} - P_{H_2O \text{ permeate}}$ .

While the  $P_{H_2O \text{ permeate}}$  is assumed to be constant and controlled by the temperature of the cooling element, the  $P_{H_2O \text{ feed } x}$  is changing as water is constantly removed from the feed stream as it progresses through the module.

The value of the TMP at the exit of the module ( $x=l$ ) is determined by  $P_{H_2O \text{ feed } x=l} - P_{H_2O \text{ permeate}}$ . By approximation, the average TMP ( $TMP_{\text{ave}}$ ) can be calculated as:

**Equation 2.3**

$$TMP_{\text{ave}} = \left( \frac{P_{H_2O \text{ feed } x=0} + P_{H_2O \text{ feed } x=l}}{2} \right) - P_{H_2O \text{ permeate}}$$

While there are commercial examples where water is recovered from air by condensation onto actively cooled elements (Dew Point , 2017), for the purpose of recovering water from flue gas, only convective ambient air will be considered as a cooling medium. The use of electrically driven heat pumps to remove the condensation heat will result in an unacceptable energy penalty.

#### 2.4.4 Feed channel pressure drop

For optimal membrane separation conditions the feed stream should show relative high Reynolds (Re) numbers to ensure a turbulent flow that will minimize concentration polarization. The term of concentration polarization describes the tendency of the specie rejected by the membrane to accumulate at the feed - membrane interface (Zakrzewska-Trznadel, et al., n.d.). This effectively reduces the partial pressure of the permeating specie in the feed. As a result of concentration polarization, the permeance rate of the highly permeable species will appear lower and the permeation rate of the rejected specie will appear higher. Maintaining high Re numbers to minimize the extent of concentration polarization does impose a considerable feed channel pressure drop (pressure between the feed entering the module and the reject exiting the module). This influences the total energy consumption for the separation process. For each application the impact of concentration polarization on the module's productivity needs to be in balance with the energy penalty required to keep Re numbers up. The Reynolds number in a fibre in a tube feed configuration is determined as follows;

#### Equation 2.4

$$Re = \frac{v \cdot ID \cdot \rho}{\eta}$$

Whereby

- ID = Inner Diameter of the fibre (m)
- v = gas velocity in fibre (m/s)
- $\rho$  = gas density (kg/m<sup>3</sup>)
- $\eta$  = gas viscosity (Pa·s)

The velocity of the feed gas (v) through a fibre in the module is calculated by dividing the total flow rate ( $\varphi_{\text{feed gas}}$ ) by the combined cross sectional surface area ( $SA_{\text{fibre}}$ ) of all fibres in the module;

#### Equation 2.5

$$Total SA_{fibre} = 0.25 \cdot \pi \cdot ID_{fibre}^2 \cdot N_{fibers}$$

And

**Equation 2.6**

$$v = \frac{\varphi_{feed\ gas}}{N_{fibers} \cdot SA_{fibre}} = \frac{\varphi_{feed\ gas}}{0.25 \cdot \pi \cdot ID_{fibre}^2 \cdot N_{fibers}}$$

Whereby;

- $\varphi_{feed\ gas}$  = Feed gas flow rate (m<sup>3</sup>/s)
- $N_{fibers}$  = Number of fibres in tubular module
- $SA_{fibre}$  = Cross sectional surface area of a fibre (m<sup>2</sup>)

For tube side feed hollow fibre modules, the pressure drop over each fibre can be calculated as follows;

**Equation 2.7**

$$\Delta P_{fibre} = \frac{f \cdot 2L \cdot \rho \cdot v^2}{ID_{fibre}}$$

Whereby;

- $f$  = friction factor
- $L$  = Length of fibre (m)
- $\rho$  = gas density (kg/m<sup>3</sup>)

An article by (Mc Keon, et al., 2004) studied the relation between the friction factor  $f$  and  $Re$ . It was found that for a laminar flow regime ( $Re < 2300$ ) the friction factor can be expressed as:

**Equation 2.8**

$$f_{Laminar} = \frac{16 \cdot \eta}{\rho \cdot v \cdot D} = \frac{16}{Re}$$

In a turbulent flow regime ( $Re > 100\ 000$ ) the friction factor can be expressed as:

**Equation 2.9**

$$f_{Turbulent} = 0.079 \sqrt[4]{\frac{\eta}{\rho \cdot v \cdot D}} = 0.079 \cdot \left(\frac{\eta}{\rho \cdot v \cdot D}\right)^{0.25} = 0.079 \cdot Re^{-0.25}$$

So, the first step in the determination of a pressure drop over a fibre is to calculate the  $Re$  number to know whether Equation 2.7 or Equation 2.8 should be used. When the correct friction factor is calculated, the pressure drop can be calculated.

As highlighted in the previous section, Eskom indicated that the post-FGD flue gas pressure will be close to atmospheric. As the re-pressurizing the vast amount of flue gas would constitute an unacceptable energy penalty, the project team has to design a membrane module with a low feed channel pressure drop. By lack of means to quantify this value, Eskom agreed to take 100 Pa as the allowable maximum feed channel pressure drop.

## **2.5 SUMMARY FROM LITERATURE REVIEW**

From the literature it is evident that there are key aspects that play an integral role in the successful design of a membrane module. Moreover, great diligence is necessary in the design process since there are numerous factors that could result in failure or inadequacy of the module. For a membrane module to be considered for use in dehumidification, a highly water vapour selective membrane is required. Added to this, the permeability should be high enough to accommodate the feed gas flow rate, without compromising the selectivity or requiring an unrealistic amount of membrane area. From literature, it is evident that a tubular membrane module utilising a polymeric membrane is the preferred design. When considering which membrane configuration to be implemented, the feed gas pressure drop as specified by Eskom should be taken into account. A successful design would also require the fulfilment of more basic, yet equally important criteria such as leak-freeness, suitable materials used in production and module lifetime. All of the above-mentioned criteria affects the efficiency, effectivity, and ultimately, cost of the produced membrane module.

## CHAPTER 3: EXPERIMENTAL WORK

---

### 3.1 LAB-SCALE TESTING SYSTEM

A gas mixing station, designed for another project was converted into a Lab-scale testing system to synthesize a humid gas mixture. Appendix B provides an overview of the lab-scale relative humidity system. The piping and instrumentation diagram is shown in Figure B.3. Table B.1 lists components and equipment used in its production. Figure 3.1 presents the lab-scale testing system.



**Figure 3.1: Lab-scale testing system**

Nitrogen gas is fed from the main N<sub>2</sub> gas cylinder at a pressure of 20 Bar. The gas flows from the laboratory manifold into a Tescom pressure regulator that reduces the pressure to 3 Bar, the appropriate inlet pressure for the Bronkhorst © High Tech mass flow controller with a nitrogen gas flow range of 0-1000 ml.min<sup>-1</sup>. A one directional flow is secured by stainless steel 316 ¼ " SS-4C-1 one way/check valves between the mass flow

controller and the temperature controlled enclosure. The peristaltic pump, responsible for pumping water into the gas flow, is a Watson Marlow 120 U/DV peristaltic pump. The pump is calibrated to match the system requirements and ensure a constant and accurate water flow rate. The Labview interface, provided by National Instruments, is used to control the lab-scale testing system. The testing system itself is produced by the engineering company Thermodynamic Fluids and Design (TFD). The compartment hosting the membrane module is thermally insulated and contains all the tubing necessary for production of the humidified gas. The Labview interface connected to the system controls both the flowrate of Nitrogen gas and water. Both media are introduced into a coiled copper pipe inside the system. The relative large surface area of the copper coil is deemed sufficient to evaporate the water entering the system. The resulting humidified nitrogen enters into the membrane module. Two humidity sensors, each paired with a thermocouple were placed at either side of the membrane module. Data related to relative humidity, flowrate, pump rate, temperature are processed and recorded by Labview.

### **3.1.1 Pump calibration**

A relation between the 120 U/DV peristaltic pump's revolutions per minute and the water flow rate was established. This was done firstly by measuring the mass of water pumped at the maximum revolutions per minute. Following this, a flow rate for the maximum RPM was calculated. Within the Labview interface an amperic value correlating to the maximum RPM was displayed. This was referred to as a non-scaled value. As such, the scaled values for flow rate could be calculated, since the maximum flow rate was known. This provided the values for any desired flow rate within the range of minimum to maximum. It also calibrated the program to assign an amperic value for any requested volumetric flow rate, which would then be interpreted and provided by the peristaltic pump.

### **3.1.2 Relative humidity control**

The proportions with which the two fluids were mixed were established through the temperature-relative humidity relation. This relation serves as the foundation in the Antoine thermodynamic humidity equation, which is discussed in (Coulson, et al., 1999). The system temperature and water/nitrogen flow ratios were set at values corresponding to a given relative humidity. Corresponding temperature and flow-ratio values for 7 different relative humidities were calculated by using the Antoine equation. Following this, the values were organised and plotted to produce the temperature and gas humidity-ratio graph. The 7 plotted lines depicting RH values fully covered the planned range of operation. Figure B.4 in Appendix B displays the resultant graph. In a stable and thermally controlled environment, values of the temperature and gas humidity ratio for a given RH could simply be matched with a relative humidity of your choosing by using this graph. Hence, this graph is an all-encompassing summary of the set-point combinations needed to attain a stable humidity and temperature environment.



### 3.1.3 Temperature measurement and control

As can be seen in Figure B.4 , temperature fluctuations should be avoided at any cost. Even a change of one degree Celsius has a considerable impact on the relative humidity. Considering, for example at the two temperatures 33°C and 37°C and at a (Water/Nitrogen) humidity ratio of 0.05, the RH within this temperature range would change by 20 percentage points from 80% to 100% RH. As such strict temperature control is needed for accurate RH control. Temperature control was achieved through; A) the construction of temperature controlled enclosure, B) the use of a combination of Lomacor resistance elements and Omron MY21N power relays and C) three type K thermocouple probes integrated through a custom made programmable logic controller (PLC). A feedback control mode was adopted, performing a temperature comparison between the actual temperature value and the set-point and any differences in the two values would trigger corrective action. This corrective action involved the following; if the temperature inside the system exceeded the set-point, the current supplied to the heater is cut. An adjustable opening was fixed on top of the system which was manually opened or closed. This allowed hot air inside the system to be replaced with air of ambient temperature, which subsequently cooled the air inside the system. Once the temperature inside the system dropped below the set-point, current to the heater was restored. Since the air heating system used consists of thin nickel-chrome wire wrapped around an electrical isolator with a fan passing air over the heated wire, effective heat transfer took place. This resulted in a constant temperature inside the enclosure with less than 1°C temperature oscillation. The enclosure temperature was maintained below 80°C, as the flue gas temperature downstream the wet FGD system would typically not exceed such limit.

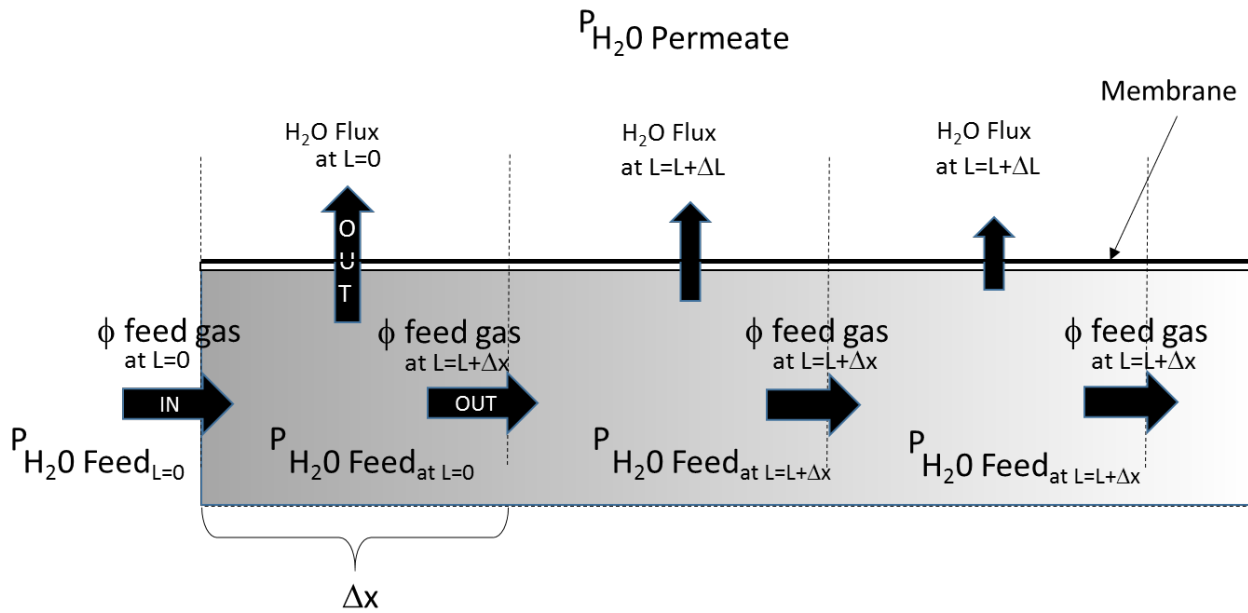
### 3.1.4 Humidity measurement and control

The humidity measurement was conducted by a capacitive type electronic hygrometer. As discussed in Section 3.1.3, the humidity was controlled by adjusting the temperature to match the aimed RH. By using the capacitance method, damage due to condensation was avoided (Water Research Commission, 2019) . This proved to be a necessary precaution owing to the condensation of water still present in the system when the system was not operational.

## 3.2 MINI MODULE DEVELOPMENT

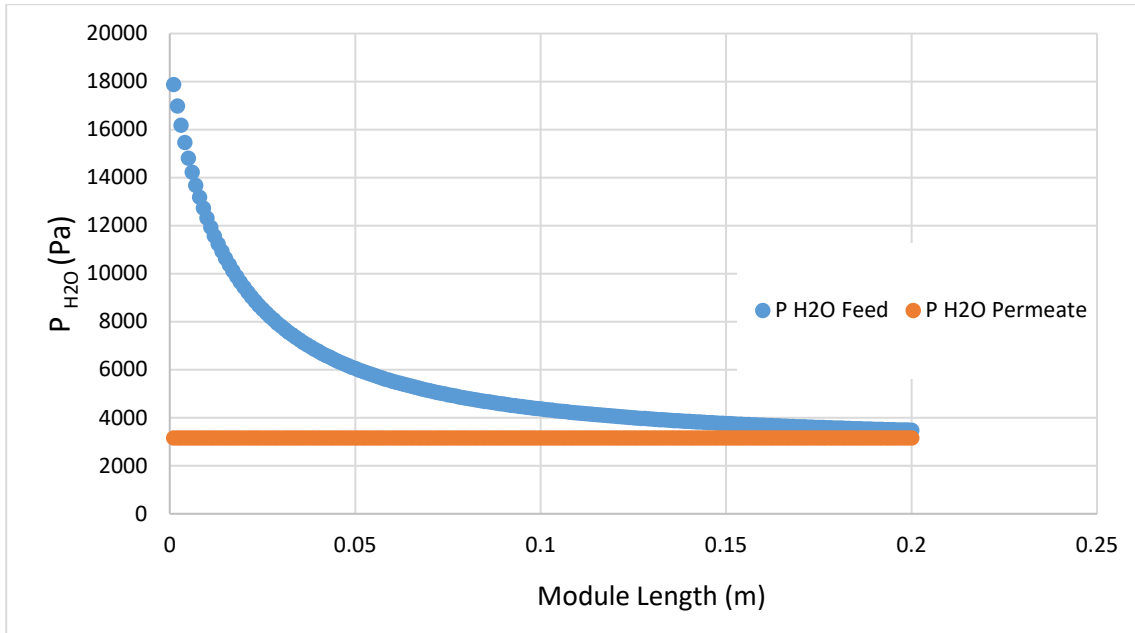
During the course of the project two types of mini modules were developed, a tubular laboratory mini module and a curtain type mini module. Analysis of both modules was essential in the development of the pilot-scale membrane module. The development of Lab-scale membrane modules started with a theoretical calculation regarding the desired amount of membrane area followed by the production of a series of “dummy” membrane modules prepared to examine and fine tune the module preparation method and ultimately conduct leak testing of the module. Leak testing conducted on dummy membrane modules produced with dense hollow fibres isolated any leakages to the influent and effluent tubing connections with the module housing. The “real” Lab-scale membrane modules designed and developed contained five 200 mm long hollow fibre membranes. The membrane selected for the research work was a PEBA<sup>®</sup>X 1074 membrane, purchased from Membrana just after its acquisition by 3M. Management of 3M has unfortunately discontinued the production of the PEBA<sup>®</sup>X 1074 membrane.

NPT ¼” quick connect Swagelok fittings, along with a 6 mm OD polyurethane Festo tube were used to provide an air tight seal on both the influent (feed) and effluent (retentate) flow tubes whilst an “O” ring aluminium fitting combination provided an air tight seal on the permeate end. Connection of the aluminium fitting to the water recovery condenser was made possible through a male ¼” NPT Swagelok fitting and more 6 mm OD polyurethane Festo tube. The designed modules presented a platform for the determination of critical hollow fibre membrane specifications that aided in up-scaling calculations.



**Figure 3.2: Differential representation of the pressure and flowrate along a membrane**

A differential mathematical calculation was completed in order to illustrate the water vapour pressure drop over the length of the membrane fibre as water vapour is recovered. The length of membrane fibre exposed to feed gas was modelled as 300 individual sections, each with a length of  $\Delta x$  ( $=1 \times 0.2\text{m} / 300$ ). Next, the initial vapour pressure difference between the permeate and feed side was calculated by using the Antoine equation. It was assumed that all water vapour molecules entering the module experienced the same initial pressure difference. The membrane water vapour permeance was assumed to be a constant as provided by the manufacturer. Finally, the pressure on the permeate side was assumed to be due solely to the recovered water vapour molecules, with these molecules having the same temperature as that of the condenser. These assumptions, together with the theoretical area of fibre being exposed to water vapour, and application of the Antoine equation, made it possible to calculate the water vapour pressure at any given length on the fibre. Since the water vapour pressure difference at length 0 m was known, the vapour pressure at length (0 m + 1 fibre section) was calculated. This value was then used as the vapour pressure difference at length (1 x 0.2m / 300). This process was repeated to obtain the vapour pressure difference at the length (2 x 0.2m / 300), which in turn, was used to calculate the vapour pressure difference at length (3 x 0.2m / 300). With every repetition, the vapour pressure difference would decrease as water vapour would theoretically be recovered whilst flowing along a length of membrane. The result of these calculations is illustrated in Figure 3.3.

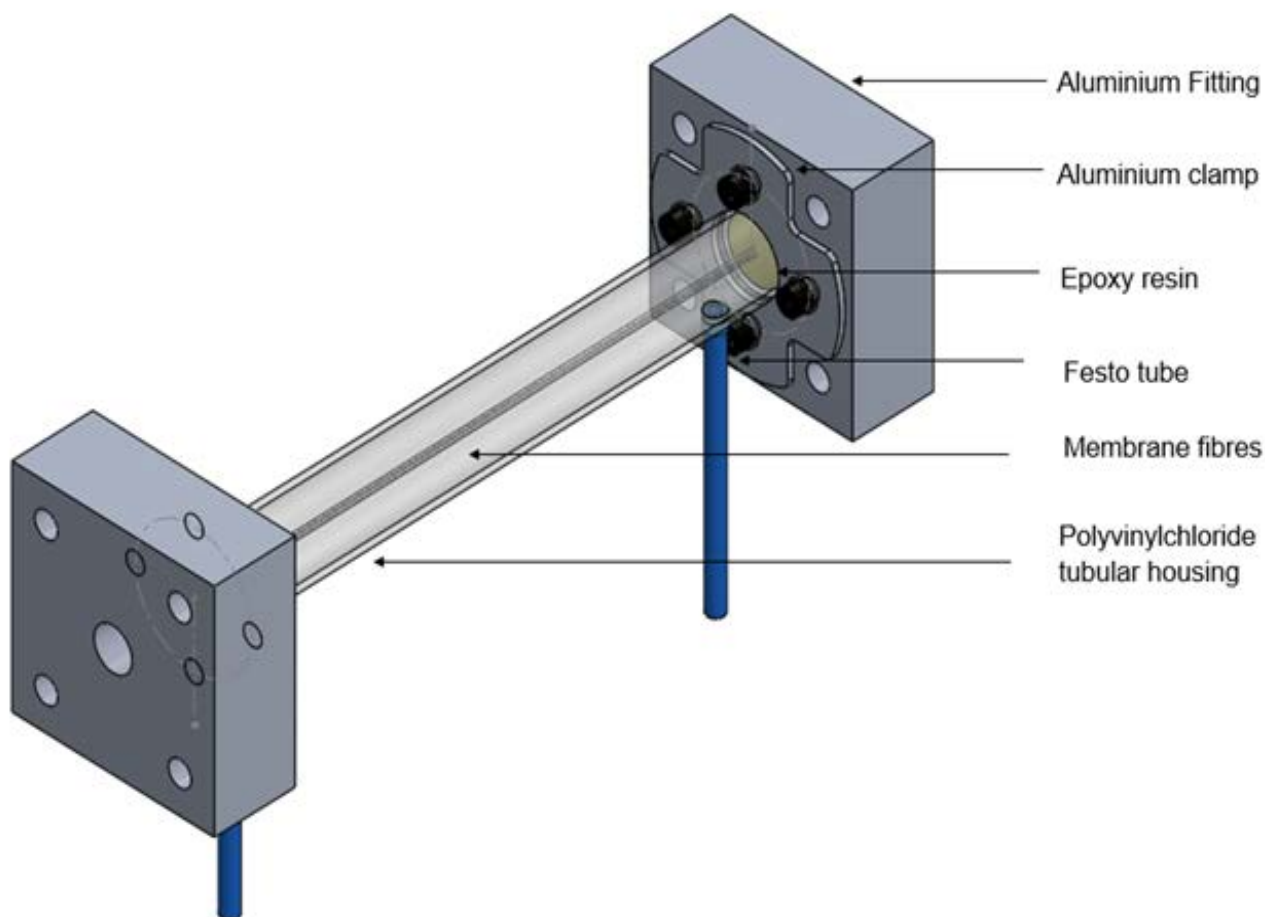


**Figure 3.3: Differential model for water vapour pressure along the length of the membrane module**

In addition to providing an estimate of the membrane area needed to achieve a desired water recovery task, this model helped with optimization of the designed membrane modules. By varying the membrane module length, the effective membrane area of the module or the condenser temperature, a range of graphs illustrating vapour pressure loss along a length of membrane would ensue. Since the driving force for water vapour permeation is the pressure difference between the feed and permeate side, the membrane module design would be inefficient if the pressure difference did not substantially decrease by the end of the module length. This would mean that not enough water vapour is permeating through the membranes. Similarly, if the vapour pressure difference decreased to a minimum value before reaching the end of the module, the module would be removing water vapour too rapidly, thereby leaving some membrane area unused and inefficient. By using the model presented in Figure 3.3, design of a membrane module, with an optimum length and membrane surface area, became a more realistic and simpler task.

### 3.2.1 Lab-scale mini module

A cylindrical Lab-scale mini module was designed for use in the establishment of essential membrane properties using the Lab-scale testing system. This lab-scale module design/development formed a key part of the mini-curtain module development process as shall be seen in Section 3.3.2. With the aid of Bongibethu Hlabano-Moyo, a Solid works® schematic image of the lab-scale mini module used in the testing of the system is presented in Figure 3.4. In conjunction with the aluminium fittings, four thread bars that are not included in Figure 3.4, were used in order to secure the lab-scale module in place. This was to prevent deformation of the module when conducting experiments at system temperatures above 40 °C.



**Figure 3.4: A schematic diagram of a designed Lab-scale membrane module (Water Research Commission, 2019)**

A detailed list of equipment and materials used in the production of a tubular laboratory-scale membrane module is presented in Table A.1 and has been added to Appendix A.

### 3.2.1.1 Potting and cutting

Potting is a procedure that seals the membranes within the PVC housing through the use of epoxy resin. A detailed description of the potting and cutting procedure is displayed in Appendix A as Table A.3. Standard Lab-scale modules are produced by embedding five PEBAX® 1074 hollow fibre membranes within a tubular PVC module housing with a resin. A guillotine was used to cut the hardened epoxy so as to expose the open ends of the fibres.

### 3.2.1.2 Leak testing of membrane module

Figure A.1 shows the piping and instrumentation diagram for the setup used in evaluating completed modules for leakages and Nitrogen permeance. Nitrogen gas was not expected to permeate through the dummy fibres, meaning any drop in pressure would be due to a leak in the module. Leaks could arise from poor adhesion between the resin and the polyvinylchloride (PVC) tubular housing, the fibre being damaged, or leaks that may develop at the contact points between the Festo tubing and the PVC. However, it was expected that N<sub>2</sub> gas

would permeate through the real membrane fibre. Thus, conducting the same test with N<sub>2</sub> permeable Nexar® membranes would result in N<sub>2</sub> permeating through the membranes. This “leak rate” could then be used to determine the N<sub>2</sub> permeance for the membranes that were used in the membrane module.

To achieve the leak testing and N<sub>2</sub> permeance testing, the effluent (retentate) tube of the membrane module was blocked using a ¼” Swagelok stopper whilst nitrogen gas was gradually fed into the module through the influent tube. Pressure was controlled by a dual pressure regulation system, the first pressure regulator (PR) reduced the 15 bar N<sub>2</sub> pressure from the gas manifold in the laboratory down to 2.5 barg, the desired inlet pressure for the Mass flow controller (MFC). The gas exited the mass flow controller at 1barg. Subsequently, the N<sub>2</sub> pressure was further reduced down to 0.5 barg using a LPR-1/4-0.7 Festo pressure regulator. When the digital pressure indicator (PI4) stabilized at 0.5 bar, the hand valve (HV2) was closed. The pressure indicator readings were monitored and logged for a minimum duration of an hour to determine the extent to which the gas pressure in the module is maintained. A leak testing setup P&ID, together with a step by step procedure is attached in Appendix A. These are presented in Table 7.3 and Table 7.4 respectively.

### 3.2.1.3 Determination of water permeance through the membranes

After establishing the N<sub>2</sub> permeance through the membrane fibre, the water vapour permeance and water recovery potential of the membranes was determined. This was achieved by using the modified Lab-scale testing system in Appendix B. A predetermined H<sub>2</sub>O / N<sub>2</sub> flow ratio was used to prepare synthetic humidified N<sub>2</sub>. This was achieved by feeding dry gas, together with Milli-Q deionised water, through a 6 mm diameter spiral wound copper pipe. The spiral wound pipe was placed vertically in the temperature controlled cabinet, with N<sub>2</sub> flowing from the bottom upwards. Water was introduced halfway up the spiral, perpendicular to the feed gas flow. This setup provided reliable and controlled production of humidified N<sub>2</sub>. Two Swagelok ¼” three way valves were fitted between RH 1 (feed) and RH 2 (retentate). Based on the process need, gas flow could be guided through the membrane module, or adjusted to bypass it. When directed through the membrane module (shell or tube configuration), gas flowed over RH1, through the membrane module, over RH2 and finally exited the system. When bypassing the module, only RH1 and RH2 were exposed to it before it exited the system. When applying a negative pressure on the module’s permeate side, RH 2 was expected to decrease while RH 1 remained constant. This would show water recovery by the module. An external refrigeration system circulated cold water and ethylene glycol mixture through a stainless steel heat exchanger, which condensed the permeated water vapour. Subsequently, the condensate was collected in a sealed glass jar. The same coolant was used to cool a glass condenser through which the retentate was directed after exiting the system. This condensed water vapour in the retentate and was collected in a round bottom flask. Recording both the mass of water fed into the system, and the mass of condensed retentate, a mass balance was created. The retentate condenser temperature was continuously logged using a TRED30-7R log tag recorder device. The volumetric flow rate was determined by using a 100 cm<sup>3</sup> soap flow meter at various intervals.

The RH value at the entrance of the module, provided by the RH 1 sensor in Figure 8.3, was used to calculate the partial pressure of water in the feed ( $P_{H_2O\text{ feed}}$ ). At a feed gas flow rate 1000ml/min, the lab-scale membrane module did not have any notable feed channel pressure drop. Following this, both the feed pressure ( $P_{\text{feed}}$ )

and the reject pressure were assumed to be equivalent to atmospheric pressure. Atmospheric pressure was measured by using a Samsung S8 smart phone with built-in barometer. The smart phone barometer provided acceptably accurate readings for use in the calculations as discussed in (Park, et al., 2019). The N<sub>2</sub> partial pressure at the entrance of the module ( $P_{N_2 \text{ feed}}$ ) was determined as follows:

**Equation 3.1**

$$P_{N_2 \text{ feed}} \left[ \frac{N}{m^2} \right] = P_{\text{feed}} - P_{H_2O \text{ feed}}$$

Since the ratio of partial pressures ( $P_{H_2O \text{ feed}} / P_{N_2}$ ) is determined by the molar ratio of H<sub>2</sub>O and N<sub>2</sub>, the flow rate of H<sub>2</sub>O at the feed is determined by the product of N<sub>2</sub> flow rate ( $\varphi_{N_2 \text{ feed}}$ ) and the ratio  $P_{H_2O \text{ feed}} / P_{N_2}$ ;

**Equation 3.2**

$$\varphi_{H_2O \text{ feed}} = \varphi_{N_2 \text{ feed}} \cdot \frac{P_{H_2O \text{ feed}}}{P_{N_2 \text{ feed}}}$$

The total feed flow rate entering the module ( $\varphi_{\text{feed}}$ ) can now be established as the sum of flow rates of N<sub>2</sub> and H<sub>2</sub>O:

**Equation 3.3**

$$\varphi_{\text{feed}} = \varphi_{N_2 \text{ feed}} + \varphi_{H_2O \text{ feed}}$$

Similar to Equation 3.2 the flow rate of H<sub>2</sub>O in the reject flow is determined as follows.

**Equation 3.4**

$$\varphi_{H_2O \text{ reject}} = \varphi_{N_2 \text{ reject}} \cdot \frac{P_{H_2O \text{ reject}}}{P_{N_2 \text{ reject}}}$$

With the permeate pressure reduced to 0.3 bara and the permeating gas exposed to the actively cooled surface of a condenser which is kept at 4°C, continuous condensation of water kept the partial pressure of water in the permeate ( $P_{H_2O \text{ permeate}}$ ) consistently lower than the partial pressure of water in the feed ( $P_{H_2O \text{ feed}}$ ), thus providing a constant driving force for water permeation.

The quantification of the permeating water required a water mol balance over the module;

**Equation 3.5**

$$H_2O_{entering\ module} - H_2O_{exiting\ module} = H_2O_{accumulation\ in\ module}$$

Since there is no accumulation of water in a membrane module with water permeating through at steady state, the mol balance simplifies to;

**Equation 3.6**

$$H_2O_{entering\ module} = H_2O_{exiting\ module}$$

Through the use of equation 3.6, the water flow rate ( $\varphi_{Permeate\ H_2O}$ ) permeating through the membrane would be,

**Equation 3.7**

$$\frac{\varphi_{feed\ H_2O} \left[ \frac{mol}{min} \right]}{60 \left[ \frac{s}{min} \right]} = \frac{\varphi_{reject\ H_2O} \left[ \frac{mol}{min} \right]}{60 \left[ \frac{s}{min} \right]} + \varphi_{Permeate\ H_2O} \left[ \frac{mol}{s} \right]$$

**Equation 3.8**

$$\varphi_{Permeate\ H_2O} \left[ \frac{mol}{s} \right] = \frac{\varphi_{feed\ H_2O} \left[ \frac{mol}{min} \right]}{60 \left[ \frac{s}{min} \right]} - \frac{\varphi_{reject\ H_2O} \left[ \frac{mol}{min} \right]}{60 \left[ \frac{s}{min} \right]}$$

Using the calculated water flow rate permeating through the membrane ( $\varphi_{Permeate\ H_2O}$ ), the surface area of the tubular module, the membrane permeance in  $mol \cdot m^{-2} \cdot s^{-1} \cdot Pa^{-1}$  was calculated as follows:

**Equation 3.9**

$$\begin{aligned} Permeance &= \frac{\varphi_{Permeate\ H_2O} \left[ \frac{mol}{s} \right]}{SA_{module} [m^2] \cdot TMP_{AVE} [Pa]} \\ &= \frac{\varphi_{Permeate\ H_2O} \left[ \frac{mol}{s} \right]}{5 \cdot \pi \cdot D_{fibre} \cdot \left( \frac{P_{H_2O\ feed\ x=0} + P_{H_2O\ feed\ x=l}}{2} \right) - P_{H_2O\ permeate} [Pa]} \end{aligned}$$

Whereby:

- TMP<sub>AVE</sub> The average Trans Membrane Pressure, the average difference between the pressure at the feed side and the permeate side
- x Indicated the position in the module, "0" begin the entrance, "L" being the exit

TMP<sub>AVE</sub> has been introduced to simplify the calculations. The driving force for water to permeate through the membrane is a function of the position in the module. The RH at the entrance of the module (x=0) is close to 100%. A portion of the water vapour permeates through the membrane, the relative humidity (and thus the partial vapour pressure) decreases as the remaining feed gas flows towards to the exit of the module. In contrast, the partial water vapour pressure at the permeate remains practically constant as due to the high membrane selectivity, the permeate only consists of water vapour. To account for the gradual reduction of the driving force, an average Trans Membrane Pressure (TMP<sub>AVE</sub>) is applied to calculate the average flow through the membrane.

### 3.2.2 Curtain type Lab-scale membrane module

The Lab-scale curtain module was produced by winding a hollow fibre membrane 35 times around a 3mm thick polypropylene frame. The frame provided mechanical support for the hollow fibres. Figure 3.5 shows the design drawing of a Lab-scale curtain type membrane module. Table 3.1 contains a detailed list of equipment and materials employed in the production of Lab-scale curtain modules.

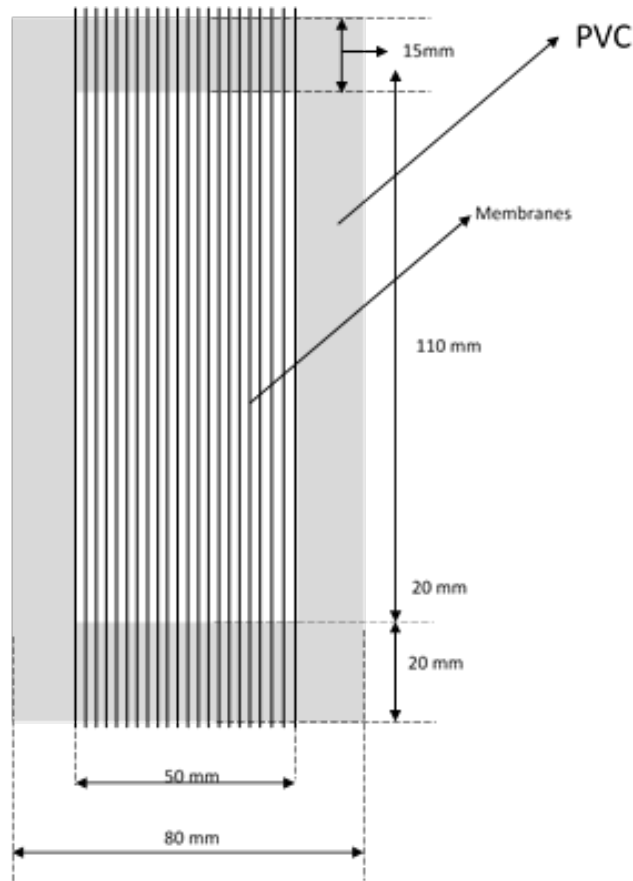


Figure 3.5: Lab-scale curtain-type module design



The membrane selected for the research work is a membrane purchased from Membrana and are referred to as PEBAX® 1074 membranes in (Sijbesma, et al., 2008).

**Table 3.1: List of equipment/components employed in the production of the mini curtain type membrane module**

Equipment/ Material	Specifications	Purpose	General
Cutter	Altendorf C90 panel saw	Module end cutting	Davidson's Discount Boards (SA)
Polyvinylchloride frame	Thickness = 3mm Width = 80 mm Middle cut-out width = 50 mm Length = 145 mm Middle cut-out length = 110 mm	Module frame	Maizey (SA)
Epoxy resin	Epothin 2™ Epoxy Resin 20-3440-128	Membrane module potting	Buehler (UK)
Epoxy hardner	Epothin™ 2 Epoxy Hardner 20-3442-064	Membrane module potting	Buehler (UK)
Membrane hollow fibres *	PEBAX® 1074 N <sub>2</sub> permeability 0.1 GPU CO <sub>2</sub> permeability 5.45 GPU Thickness 1200 µm	Separation medium for water recovery	Membrana (D)
Plastic syringes	20 ml volume	Resin filling upon potting	Laborem (SA)
Oven	Song-Ling	Acceleration of resin cure	Song-Ling
Glue gun	Stanley GR 35K	Glueing fibre end to PVC frame	Parow Bolt & Tool
Glue stick	Topline mini 7.5 x 100 mm	Glueing fibre end to PVC frame	Parow Bolt & Tool
Teflon Potting mould	Teflon 40mm x 100mm x 35mm	Potting of module	SAIAMC

### 3.2.2.1 Potting for mini curtain-type module

Once wound, one end of the PVC support frame was placed in, a potting mould. The resin would have to be removable from the mould with ease once cured. Teflon was selected for its non-stick properties. As seen in Figure 3.6, the Teflon mould was designed to be V-shaped for ease of release. A detailed potting procedure for the mini curtain type module is provided in Appendix A.

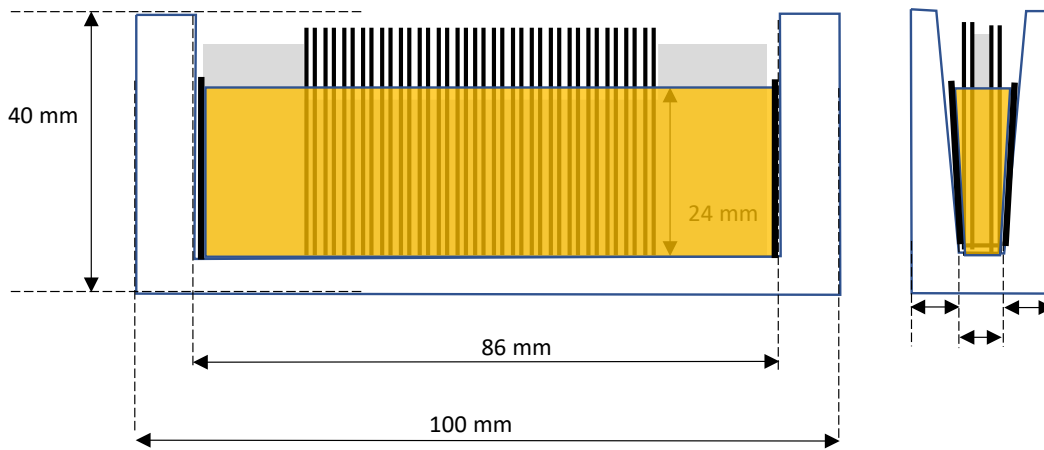


Figure 3.6: The Teflon mould design used for potting the curtain-type mini module.

### 3.3 PILOT-SCALE MEMBRANE MODULE DESIGN

For testing of a pilot-scale membrane module, a pilot-scale flue gas treatment system was proposed. The system should produce a significant volume of gas (up to 30 m<sup>3</sup>/h), with a composition similar to a flue gas of a coal fired power station after Wet Flue Gas Desulphurization (FGD).

#### 3.3.1 Process conditions and target recovery parameters

To design a pilot-scale membrane module for the proposed pilot system, the following process parameters were agreed upon;

1. Flue gas temperature; 60°C
2. Flue gas RH; 95%
3. Flow rate of simulated flue gas ( $\varphi_{\text{flue gas}}$ ); 30Nm<sup>3</sup>/h
4. The module needs to achieve a water recovery rate (WRR) of 33.3%
5. The cooling element temperature required to condensate the permeate vapour is 30°C

Parameter 1 and 2 were used to calculate the partial pressure of water in the feed gas ( $P_{\text{H}_2\text{O feed}}$ ). With the 3<sup>rd</sup> parameter fixed, the amount of water entering the module is known ( $\varphi_{\text{Feed H}_2\text{O}}$ ) and with the 4<sup>th</sup> parameter fixed, the required permeating water flow through the membrane ( $\varphi_{\text{Permeate H}_2\text{O}}$ ) is known. This results in the combined equation;

**Equation 3.10**

$$\varphi_{\text{permeate } H_2O} = \frac{WRR \cdot \varphi_{\text{flue gas}} \cdot P_{H_2O}}{R \cdot T} = \frac{WRR \cdot \varphi_{\text{flue gas}} \cdot \frac{10^{\left(A - \frac{B}{C + T_{\text{feed}}}\right)}}{760} \cdot 101325 \cdot RH_{\text{feed}}}{R \cdot (T_{\text{feed}} + 273.15)}$$

$$\varphi_{\text{permeate } H_2O} = \frac{0.333 \cdot \left(30 \cdot \frac{(273.15 + 60)}{(273.15 + 20)} \cdot \frac{(101325)}{(101224)}\right) \cdot \frac{10^{\left(8.07131 - \frac{1730.63}{233.426 + 60}\right)}}{760} \cdot 101325 \cdot 0.95}{8.314 \cdot (273.15 + 60)}$$

$$\varphi_{\text{permeate } H_2O} = 73.58 \left[ \frac{\text{mol}}{\text{h}} \right]$$

The required membrane area per module was calculated based on:

- the required permeating water flow through the membrane ( $\varphi_{\text{Permeate } H_2O}$ ) (=73.58 mol/h, see Equation 3.9)
- the membrane permeance value (see Section 4.2.3)
- the average Trans Membrane Pressure difference ( $\text{TMP}_{\text{ave}}$ ) (see Section 3.3.3)

### 3.3.2 Membrane selection, potting and support material

A semi-commercial Nexar ® hollow fibre membrane ( $\text{OD}_{\text{fibre}} = 0.0012\text{m}$ ,  $\text{ID}_{\text{fibre}} = 0.0008\text{m}$ ) was selected and purchased from Membrana. With regards to the choice of potting resin, the same Epoxy resin used for the Lab-scale membrane modules was deemed suitable. It was suggested that stainless steel sheet material of 2 mm thick be used in the production of the supporting frame for the curtain type module.

### 3.3.3 Trans-membrane pressure difference in application

Equation 2.3 showed that the  $\text{TMP}_{\text{ave}}$  can be estimated based on the values of the partial pressure in the feed, the reject and the permeate ( $P_{H_2O \text{ feed}}$ ,  $P_{H_2O \text{ exit}}$  and  $P_{H_2O \text{ permeate}}$ ).

As mentioned already, process parameter 1 and 2 can be used to calculate  $P_{H_2O \text{ feed}}$  using Equation 2.1. With the 5<sup>th</sup> process parameter fixed ( $T_{\text{element}}$  required to condensate the permeate vapour is 30°C), the partial pressure of water at the permeate ( $P_{H_2O \text{ permeate}}$ ) was calculated using Equation 2.2.  $P_{H_2O \text{ exit}}$  can be derived using the following mol balances;

**Equation 3.11**

$$\varphi_{\text{feed total}} = \varphi_{\text{exit total}} + \varphi_{\text{permeate total}}$$

And

**Equation 3.12**

$$\varphi_{feed\ H_2O} = \varphi_{exit\ H_2O} + \varphi_{permeate\ H_2O}$$

As a result of process parameter 4, the following is valid:

**Equation 3.13**

$$\frac{\varphi_{permeate\ H_2O}}{0.333} = \varphi_{feed\ H_2O}$$

By substitution of 3.14 into 3.12 and with  $\varphi_{Permeate\ H_2O}$  being 73.58mol/h,  $\varphi_{exit\ H_2O}$  is calculated:

**Equation 3.14**

$$\varphi_{exit\ H_2O} = \left( \frac{1}{0.333} - 1 \right) \cdot \varphi_{permeate\ H_2O}$$

$$\varphi_{exit\ H_2O} = \left( \frac{1}{0.333} - 1 \right) \cdot 73.58 \left[ \frac{mol}{h} \right] = 147.16 \left[ \frac{mol}{h} \right]$$

Since the membrane selectivity towards water is >100, by approximation Equation 3.11 becomes:

**Equation 3.15**

$$\varphi_{feed\ total} = \varphi_{exit\ total} + \varphi_{permeate\ H_2O}$$

**Equation 3.16**

$$\varphi_{exit\ total} = \frac{\varphi_{Normalised\ feed\ total} \cdot \frac{(273.15 + T_{feed})}{(273.15 + T_N)} \cdot \frac{(P_N)}{(P_{Feed})} \cdot P}{R \cdot (273.15 + T_{feed})} - 73.58 \left[ \frac{mol}{h} \right]$$

$$\varphi_{exit\ total} = \frac{30 \left[ \frac{m^3}{h} \right] \cdot \left( \frac{(273.15 + 61)}{(273.15 + 20)} \cdot \frac{(101325)}{(101224)} \right) \cdot 101224 \left[ \frac{N}{m^2} \right]}{8.314 \left[ \frac{Nm}{molK} \right] \cdot (273.15 + 60)[K]} - 73.58 \left[ \frac{mol}{h} \right]$$

$$= 1173.63 \left[ \frac{mol}{h} \right]$$

Similar to Equation 3.3 and filling in  $\varphi_{\text{exit H}_2\text{O}}$  and  $\varphi_{\text{exit}}$

$$\varphi_{\text{H}_2\text{O exit}} = \varphi_{\text{exit total}} \cdot \frac{P_{\text{H}_2\text{O exit}}}{P_{\text{exit total}}}$$

$$P_{\text{H}_2\text{O exit}} = \frac{\varphi_{\text{H}_2\text{O exit}}}{\varphi_{\text{exit}}} \cdot P_{\text{exit total}}$$

$$P_{\text{H}_2\text{O exit}} = \frac{147.16 \left[ \frac{\text{mol}}{\text{h}} \right]}{1173.63 \left[ \frac{\text{mol}}{\text{h}} \right]} \cdot 101224 \left[ \frac{\text{N}}{\text{m}^2} \right] = 12692 \left[ \frac{\text{N}}{\text{m}^2} \right]$$

Completing Equation 2.3 provides  $\text{TMP}_{\text{ave}}$ :

### Equation 3.17

$$\begin{aligned} \text{TMP}_{\text{ave}} &= \left( \frac{P_{\text{H}_2\text{O feed}} + P_{\text{H}_2\text{O exit}}}{2} \right) - P_{\text{H}_2\text{O permeate}} \\ &= \left( \frac{\frac{10^{\left( A - \frac{B}{C+T_{\text{feed}}} \right)}}{760} \cdot 101224 \cdot RH_{\text{feed}} + 12692.05}{2} \right) - \frac{10^{\left( A - \frac{B}{C+T_{\text{element}}} \right)}}{760} \cdot 101224 \\ &= \left( \frac{18857.83 + 13418.55}{2} \right) - 4231.7 = 15775 \left[ \frac{\text{N}}{\text{m}^2} \right] \end{aligned}$$

### 3.3.4 Feed channel pressure drop and module configuration

Equations to calculate the feed channel pressure drop in straight channels such as the tube side feed module configuration are readily available. An example calculation is presented below.

#### 3.3.4.1 Example calculation for the feed channel pressure drop

Consider a module with 1000 fibres, each 35cm long, is used to treat 30m<sup>3</sup>/h of gas in a tube side feed membrane module configuration. The calculation of the feed channel pressure drop starts by establishing Re:

$$Re = \frac{v \cdot ID \cdot \rho}{\eta} = \frac{\left( \frac{\varphi_{feed\ gas}}{0.25 \cdot \pi \cdot ID^2 \cdot N_{fibres}} \right) \cdot ID \cdot \rho}{\eta} =$$

$$\frac{\left( \frac{30 \left[ \frac{m^3}{h} \right]}{3600 \left[ \frac{s}{h} \right]} \right)}{0.25 \cdot \pi \cdot 0.0008^2 [m^2] \cdot 1000} \cdot 0.0008 [m] \cdot 1.1887 \left[ \frac{kg}{m^3} \right]}{7.6036 \times 10^{-9} \left[ \frac{N}{m^2 \cdot s} \right]} = 2073442$$

With such high Re number the flow regime will be turbulent (Chen, 1979) which requires the use of Equation 2.9 to determine the friction factor f in Equation 2.7:

**Equation 3.18**

$$\Delta P_{fibre} = \frac{f \cdot 2L \cdot \rho \cdot v^2}{ID} = \frac{0.079 \cdot Re^{-0.25} \cdot 2L \cdot \rho \cdot \left( \frac{\varphi_{feed\ gas}}{0.25 \cdot \pi \cdot ID^2 \cdot N_{fibres}} \right)^2}{D}$$

$$= \frac{0.079 \cdot Re^{-0.25} \cdot 2L \cdot \rho \cdot \varphi_{feed\ gas}^2}{ID \left( \frac{1}{16} \cdot \pi^2 \cdot ID^4 \cdot N_{fibres}^2 \right)}$$

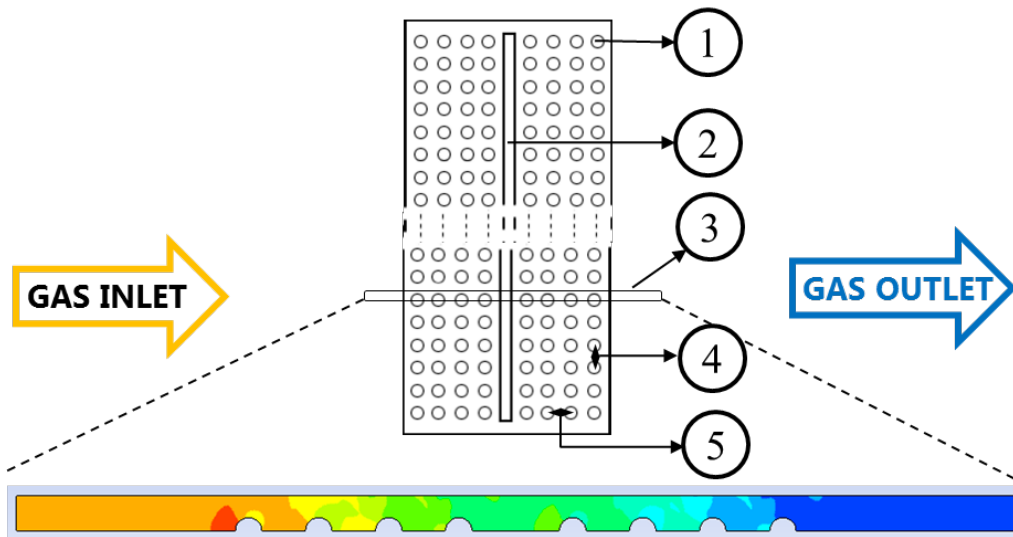
$$= \frac{0.079 \cdot 2073442^{-0.25} \cdot 2 \cdot 0.35 [m] \cdot 1.1887 \left[ \frac{kg}{m^3} \right] \cdot \frac{30^2 \left[ \frac{m^6}{h^2} \right]}{3600^2 \left[ \frac{s^2}{h^2} \right]}}{\frac{1}{16} \cdot 3.14159^2 \cdot 0.0008^5 [m^5] \cdot 1000^2}$$

$$= 595 \frac{\left[ \frac{kg \cdot m}{s^2} \right]}{m^2} = 595 \left[ \frac{N}{m^2} \right]$$

This example calculation shows that the tube side feed module configuration is unlikely to fulfil the feed channel pressure drop requirements as mentioned in Section 2.4.4. From this it appears that the options in module configuration are limited to a shell-side feed curtain module configuration. The curtain module allows for a low fibre packing density which creates minimal resistance. These findings are similar to a curtain-type module presented in a report by (Daal, et al., 2013). This report investigated water recovery from flue gas in an Israeli gas fire power station. From experience with the the Lab-scale curtain module, the spaces in between fibres was set to 2 mm to avoid resin creep as discussed in Section 4.2.5.

For a reasonable estimation of the feed channel pressure drop the project team consulted a professional with extensive knowledge of ANSYS (commercial available computational fluid dynamics (CFD) software). This was to guide another Masters student, Mr M Bihannic, working on the Water Research Commission project, with the required programming. The following steps were described in (Water Research Commission, 2019) where Mr M Bihannic was responsible for the work;

- Using the CAD (Computer Added Design) tool of the ANSYS software to design is created that represents the membrane module. Figure 3.7 shows how a narrow 2 dimensional slice of membrane module presents a fair representation of the entire module.
- The meshing step performed using the ANSYS MESHING software, is a process in which the designed object is divided into “finite elements” interconnected at discrete points called “nodes”. It is essential to have a good mesh in order for ANSYS to carry out meaningful calculations. There are two main types of finite elements to be created during the meshing; A) The square elements allow a regular and effective mesh with a good accuracy even if there are just few elements, B) The triangular element which makes it possible to adapt to complex shapes.
- Configuration of the parameters of analysis. This step is complex and requires a good knowledge of CFD studies. It will be used to inform the velocity, temperature and porosity of certain elements, the composition of the gas and the role of each part of the mesh.
- Finally the pressure drop as function of the following parameters were studied;
  - o The gas velocity at the entrance of the module
  - o The spacing between membranes fibres (windings)
  - o The spacing between membranes layers



**Figure 3.7: Intersect of a 8-layered hollow fibre membrane module; 1) Membrane intersect, 2) Membrane module frame, 3) Narrow slice of the membrane module which represents the system, 4) Distance between windings, 5) Distance between layers (Water Research Commission, 2019)**

Figure 3.8 shows how the pressure drop develops as exhaust flow rate increases for 4 different module configurations. The configurations change by either the spacing between windings and/or layers. Low exhaust flow rates result in low gas velocities and insignificant pressure drop. As expected, pressure drop increases when the windings are closer together (see C and D). However, when layers are packed closer together, the pressure drop decreases. Important to note is that the module pressure drop is still below 50 Pa, even at 500m<sup>3</sup>/h, which is equivalent to a gas velocity of 1.6m/s at the entrance of the module.

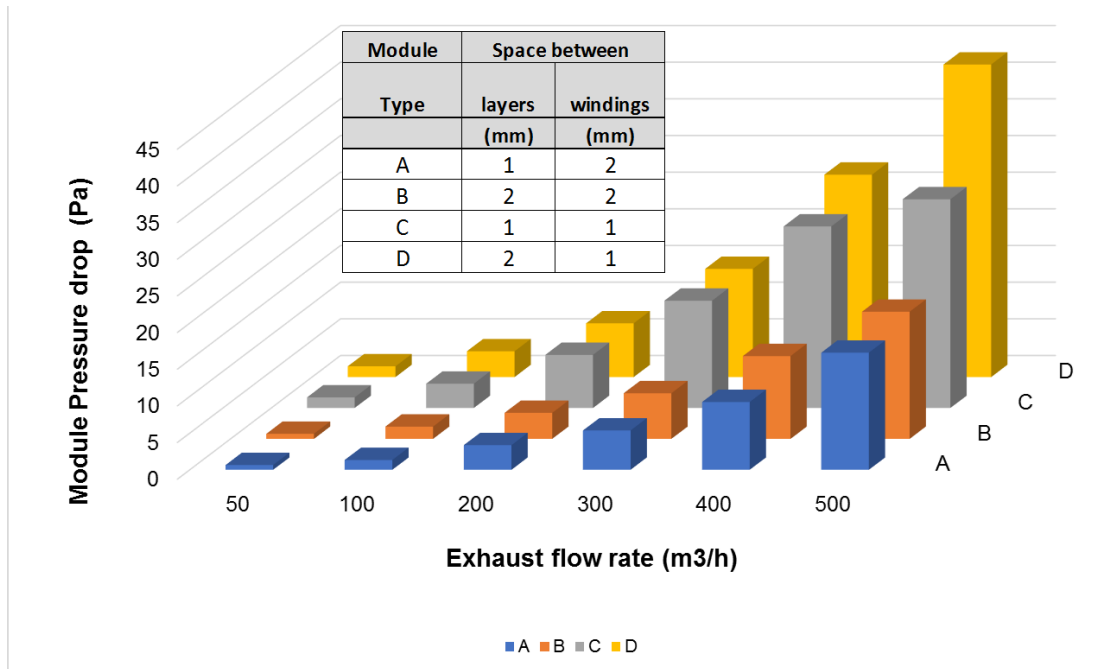
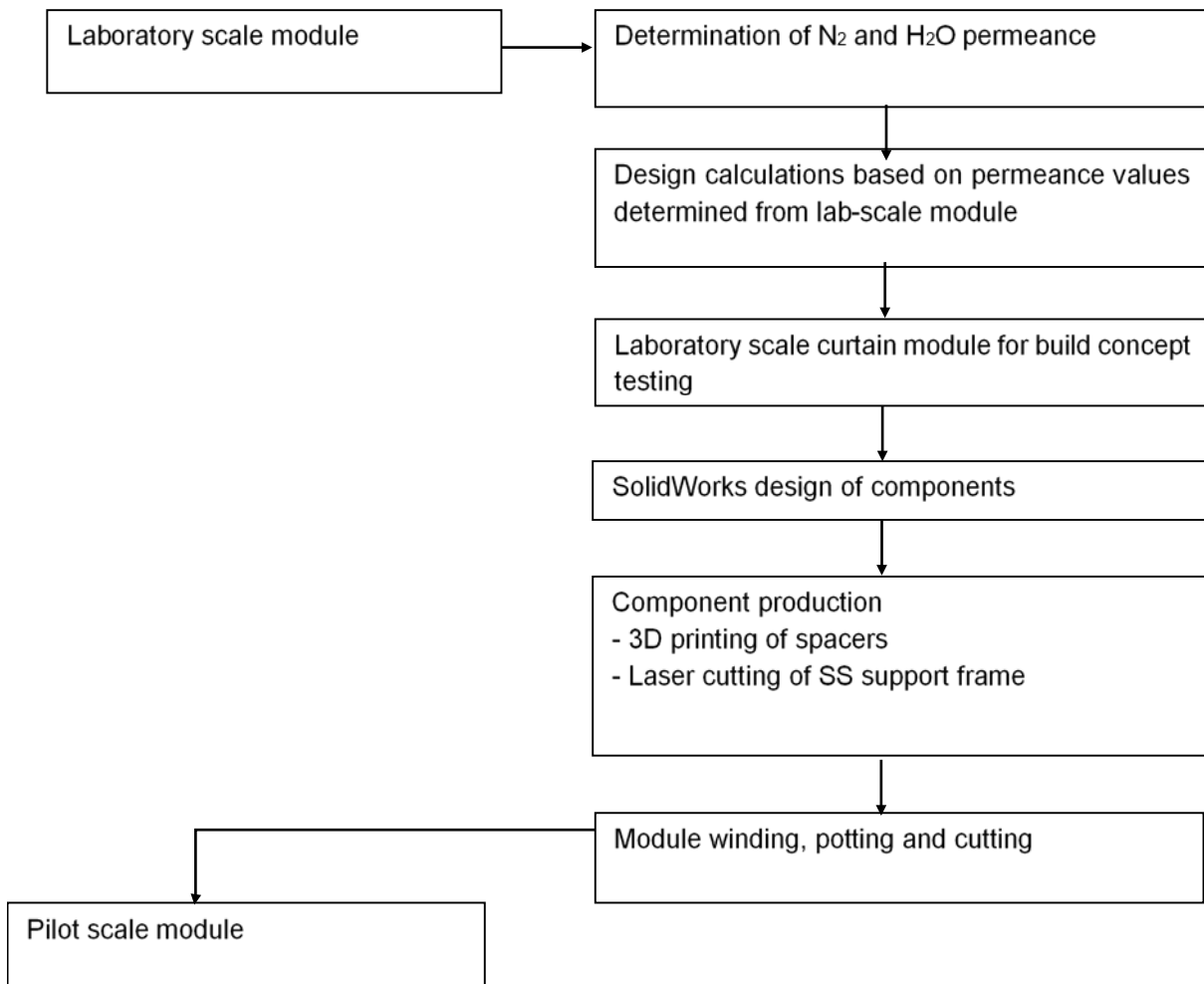


Figure 3.8: Pressure drop as function of module configuration and exhaust flow rate (Water Research Commission, 2019)



### 3.4 PILOT-SCALE MEMBRANE MODULE PRODUCTION

Figure 3.9 presents the process flow diagram for production of the pilot-scale membrane module.



**Figure 3.9: Process flow diagram for pilot-scale membrane module manufacture**

#### 3.4.1 Production of components

The solid works designed spacers were printed using a Zortrax M300 3D printer, giving a minimum print layer thickness of 90  $\mu\text{m}$ . The print material employed was Acrylonitrile Butadiene Styrene (ABS), a low cost thermoplastic which combines the properties of its three constituents to impart mechanical strength and heat resistance (Padzi *et al.* 2017). With a glass transition temperature of 92° - 105°C (depending on the measurement method) (Yadzi and Lee-Sullivan 2009), using the module at a maximum temperature of 80°C would not result in module failure. The module support frames were made of 2 mm thick stainless steel 304 panels that were laser cut into the design dimensions. Both Solid works® image designs for the spacers and module frame were produced by Bongibethu Hlabano-Moyo and can be found in Appendix C as Table C.1 and Table C.2 respectively.

### **3.4.2 Building of the module**

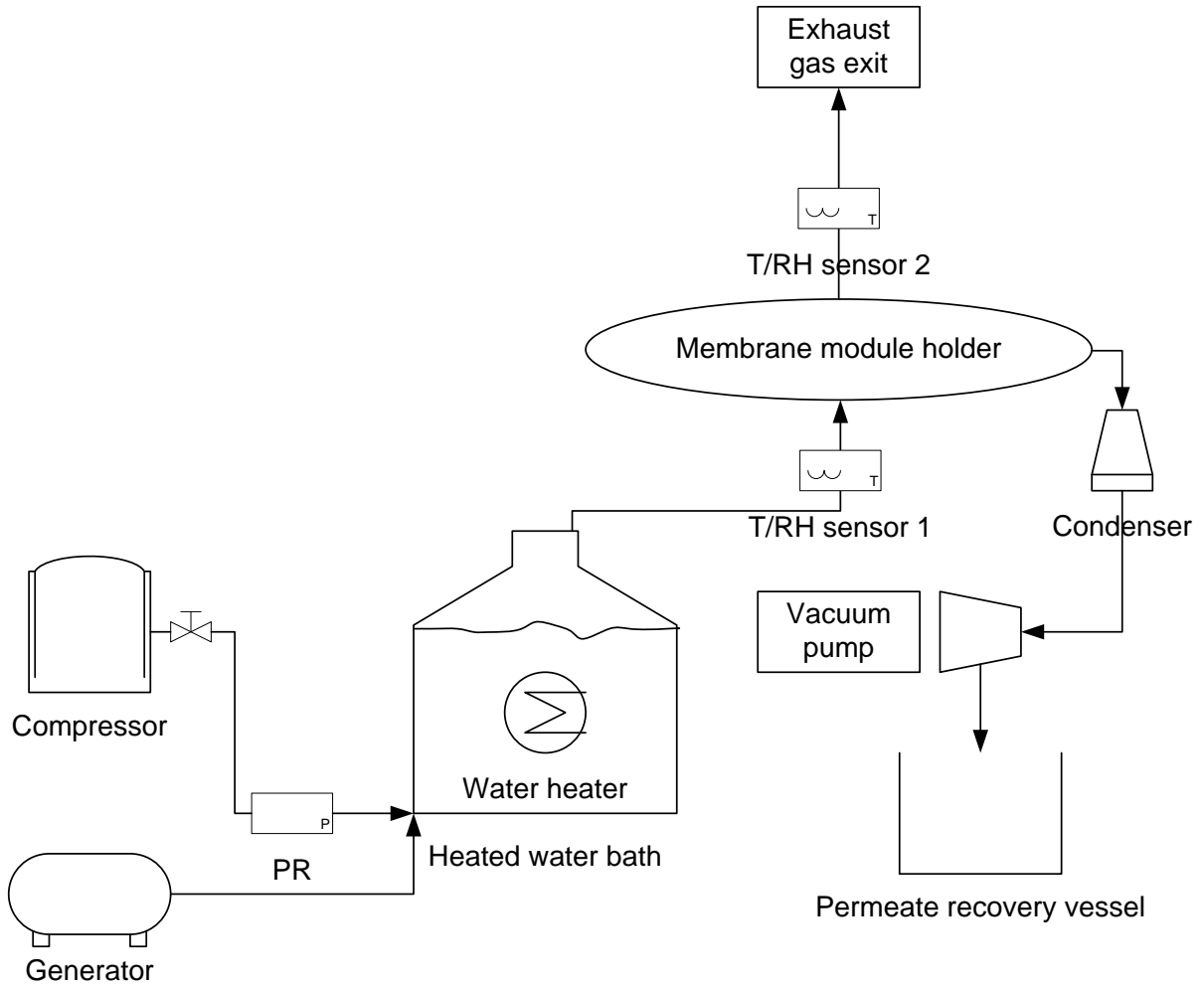
The printed spacers were slid onto the steel frame edges, i.e. starting off with spacer 1 which has a 2 mm groove (just as the thickness of the stainless steel frame). The hollow fibre was then wound over grooves in spacer 1, carefully aligning groove numbers from either edge. Once the first layer was complete, the second layer of spacers were clipped over the first layer and winding was repeated in the same fashion. This procedure was repeated with spacers 3 and 4. Ultimately spacer 5 was placed over the entire assembly and the module was ready for potting.

### **3.4.3 Potting and cutting of module**

The potting was conducted by adding the potting material (280 ml Epothin 2™ resin + 140 ml Epothin 2™ hardener) into a securely positioned pre-cast silicone mould. The silicon mould was cast from a template, designed and manufactured for this application. After potting material was added, the mould was left undisturbed for the curing duration. Once the edge of the assembly was completely submerged and bubbles expelled, it was left static for 16 hours at ambient temperatures to allow for complete curing of the resin. One edge of the assembly was initially inserted vertically and once cured, the module was removed and positioned for potting of the reverse side. After both sides of the module was potted, one side was cut to expose the open membrane lumens. This was for water recovery by the using the shell-side module configuration.

## **3.5 PROPOSED PILOT-SCALE FLUE GAS TREATMENT SYSTEM**

Figure 3.10 shows a process flow diagram for a possible pilot-scale system design. A petrol powered generator could provide the flue gas. This flue gas would be supplemented by a compressor to generate a high enough flow rate. The compressor flow rate would be controlled using a pressure regulator, denoted (PR). Combustion of petrol would yield a product gas similar to a coal combustion flue gas. Since a high relative humidity is required, the gas could be bubbled through a heated water bath. This would heat the gas to the required temperature range as stated in the parameters, as well as raise its relative humidity. Similar to the lab-scale testing system, RH and temperature sensors will be placed before and after the membrane module. A vacuum pump would be used to create a pressure difference between the feed and permeate side of the membrane, with a condenser cooling the permeate gas.







**Figure 3.10: Process flow diagram of proposed pilot-scale water recovery system**

## CHAPTER 4: RESULTS AND DISCUSSION

### 4.1 LAB-SCALE TESTING SYSTEM

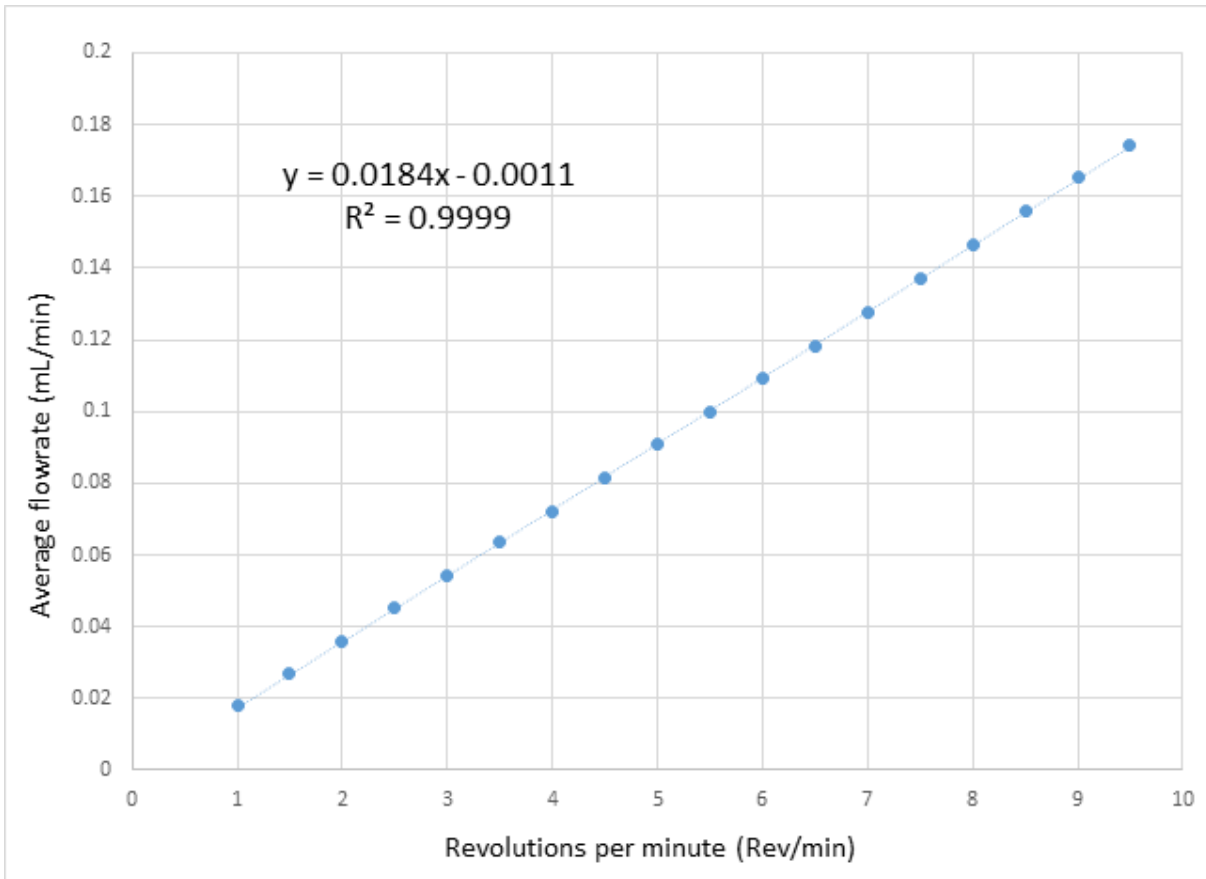
Table 4.1 presents the different controllers used in the lab-scale system. Temperature controllers were connected to the resistance heaters for thermal control. The Labview interface processed the signals from the temperature, mass and water-flow controllers in order to produce data of the measurements by the equipment.

**Table 4.1: Temperature and mass-flow controllers**

			
<p>Temperature controllers and resistance heaters</p>	<p>Mass Flow Controllers</p>	<p>Peristaltic pump for water-flow control</p>	

#### 4.1.1 Pump calibration

Since the RH value is completely reliant on the water provided by the peristaltic pump, the flow rate provided by the pump needs to be accurate and correlate with the RPM so as to produce a stable RH. Figure 4.1 presents the peristaltic pump's calibration curve, plotting the set-point of the pump and the average of the measured flow rate. A near perfect linear relationship between RPM and the resultant flow rate was found showing an  $R^2$  value of 0.9999.



**Figure 4.1: Watson Marlow 120U/DV calibration curve**

#### 4.1.2 Gas flow-rate control

Figure 4.2 presents the Nitrogen gas flow rate with time. With the Nitrogen flow rate set at 1000 ml.min<sup>-1</sup>, the average actual flow rate was calculated to be 1010 ml.min<sup>-1</sup>. This was done by using the flow rate data measured by the Bronkhorst © mass flow controllers and logged by the Labview system. Calculating the percentage error in flow rate:

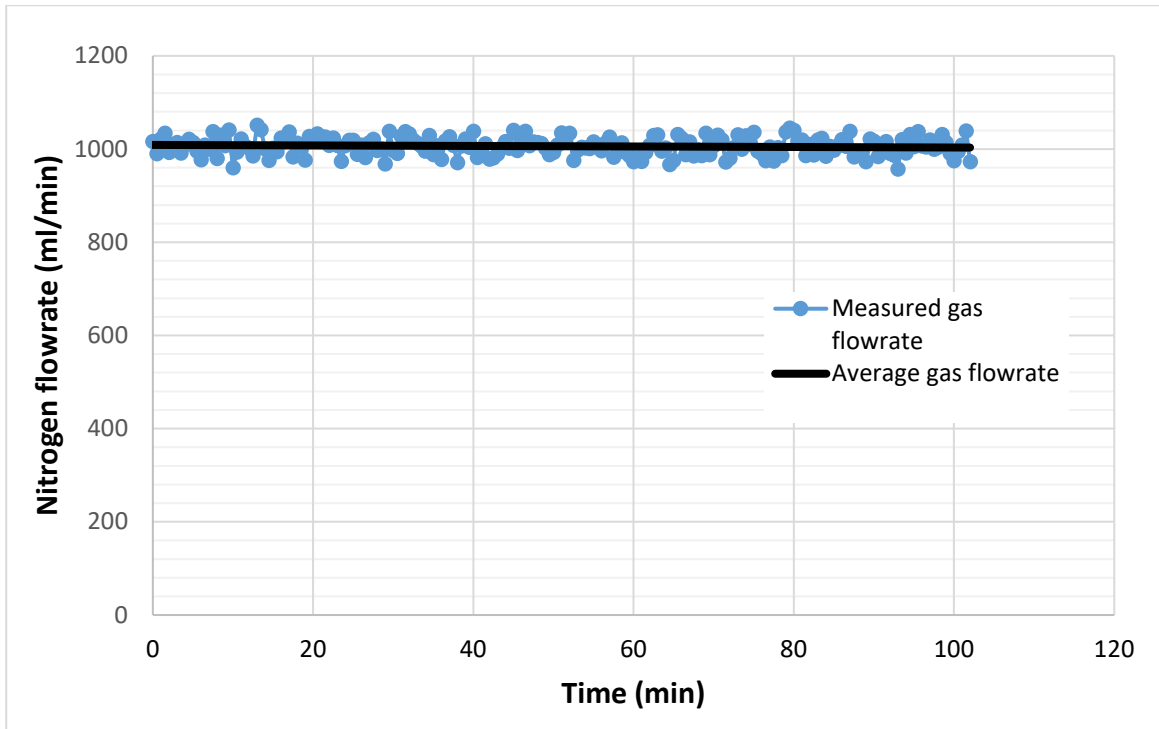
#### Equation 4.1

$$\% \text{ error in flow rate} = \frac{\text{measured flow rate} - \text{set flow rate}}{\text{set flow rate}} \times 100\%$$

$$\% \text{ error in flow rate} = \frac{1010[\text{mL}/\text{min}] - 1000[\text{mL}/\text{min}]}{1000[\text{mL}/\text{min}]} \times 100\%$$

$$\% \text{ error in flow rate} = 1\%$$

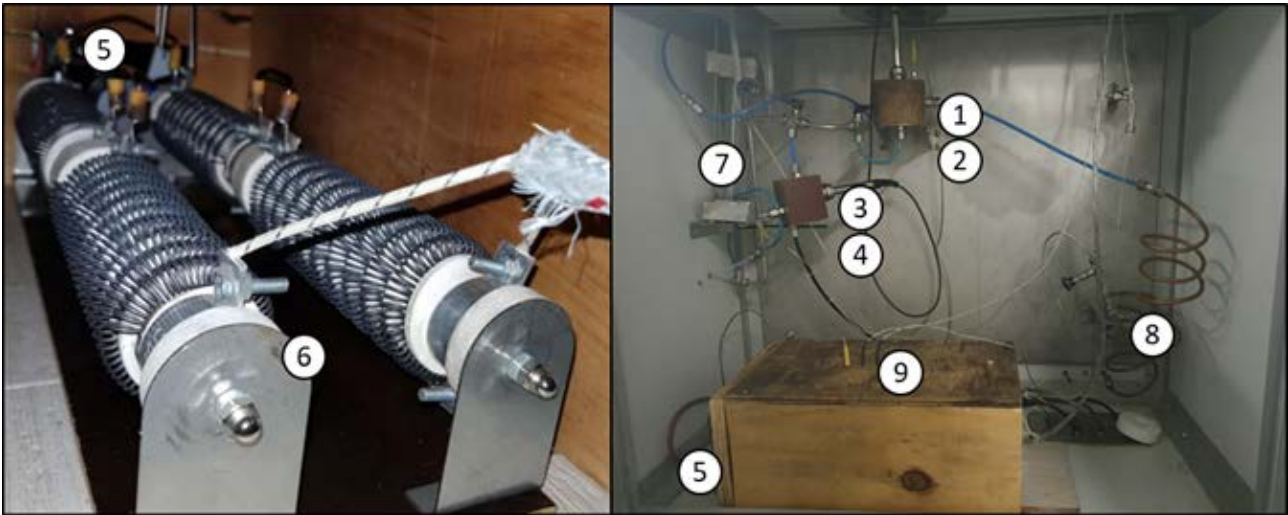
Such a low percentage error was considered insignificant in the synthesis of humid gas at lab scale. Figure 4.2 presents the N<sub>2</sub> flow rate over time as produced by the lab scale testing system.



**Figure 4.2: Nitrogen gas flow rate over time**

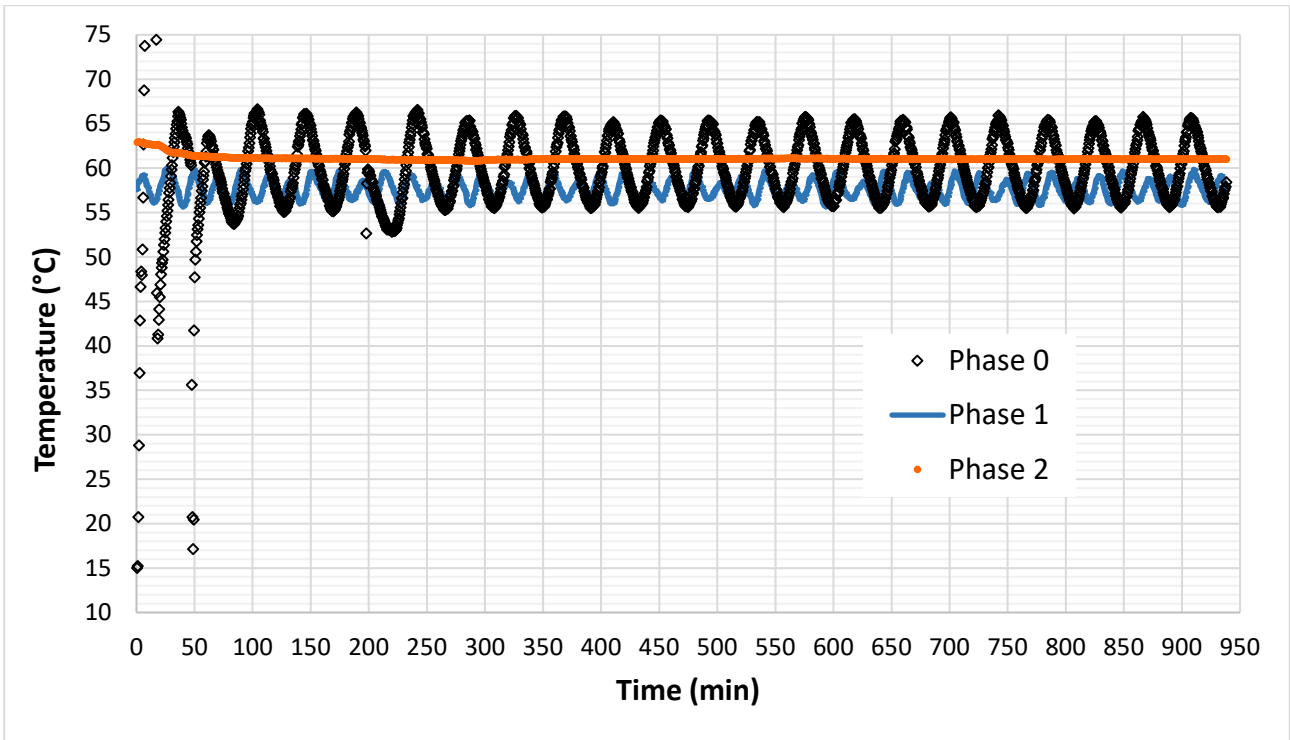
#### 4.1.3 Temperature control

Initially the system environment was heated with two tube heaters and a circulation fan placed so as to pass air over the heaters, this heating system was dubbed as modification phase 0. Since the thermal control of the environmental enclosure was not stable, the circulation fan was repositioned known as modification Phase 1. A wooden box was placed over the heaters in order to shield the thermocouples from direct radiation, causing an uneven heating of components such as the membrane module and the RH sensors. Despite some improved thermal control, a constant temperature oscillation was noted. It was concluded that the tube heaters were not designs for efficient heat transfer between heater and the air, which caused a delayed registration of the actual temperature of the heater, causing the heater temperature to overshoot the set-point value before the current was interrupted. During modification phase 2, the original tube heaters were replaced by 2 Lomacor Electric resistance elements, enclosed in the same wooden box. The resistance elements, shown in Figure 4.3, used a thin wire as the resistance element. This meant the heat transfer to air increased significantly due to higher exposed surface area. These resistance elements improved on the tube heaters in all aspects of the temperature control process. The electric fan was positioned on one side of the wooden box, ensuring an effective flow of air over the elements. The controlling thermocouple was placed at the exit of the wooden box in order for heated air to flow over it, before being released into the enclosure. The improved thermal modification for phase 2 is presented in Figure 4.3.



**Figure 4.3: Phase 2 enclosure modification: 1) RH1, 2) T1, 3) RH2, 4) T2, 5) Fan, 6) Lomacor resistance elements, 7) Membrane module, 8) Copper coil, 9) TE**

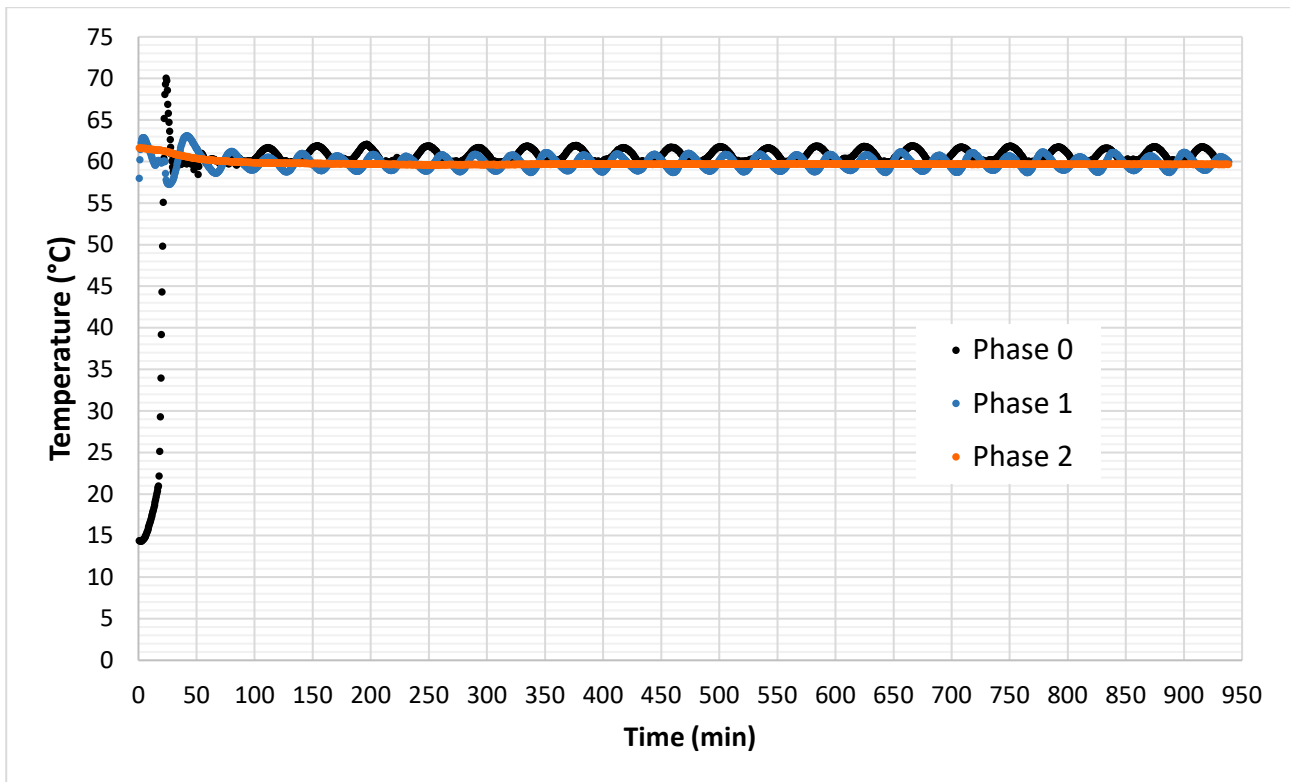
Temperature sensors located at the respective RH sensors, namely feed gas temperature (2) and retentate gas temperature (4), along with an environment temperature sensor (9) helped create a temperature profile for the system environment. Figure 4.4 illustrates the temperature as function of time for the different system modification phases. During Phase 0, temperature oscillations of up to 15 degrees C in amplitude were observed while using the SiC and tube heaters. Along with this, the equilibrium position of the T1 and TE oscillations seemed to be almost 5 °C higher than the set-point. Following this, the heating element was placed under a hand-made wooden box with two openings. The circulation fan was positioned at the front opening, with the back opening providing a means for the hot air to exit the wooden box and circulate through the system. In addition to this, it provided a means for shielding the temperature sensors from direct heat radiation exposure by the heating elements. The TE thermocouple was placed above the heaters at the wooden box exit, so as to indicate when TE reached the desired set-point. These changes in the system brought about a significant reduction in the temperature oscillation amplitude. The equilibrium position also being less than 2 °C different than set-point during Phase 1. Finally, after the installation of two Lomacor Electric resistance elements with a combined wattage of 1220W, an acceptable temperature profile with hardly any oscillations was produced in Phase 2. The temperature profiles for each phase in the development of the enclosure and feed gas temperature profiles are presented in Figure 4.4 and Figure 4.5.



**Figure 4.4: Enclosure Temperature profile as a function of time**

As seen in Figure 4.4, Phase 0 shows significant temperature oscillations. Phase 1 presents a substantial reduction in oscillation amplitude. Phase 2 presents readings with no visible oscillations and the temperature being within two degrees Celsius from its set-point.





**Figure 4.5: Feed gas temperature profile as function of time**

The feed gas temperature readings presented in Figure 4.5 also showed oscillatory readings. In Phase 0, the readings were oscillating and the equilibrium position was up to three degrees Celsius higher than its set-point. Phase 1 presented the same oscillatory readings, however, the equilibrium position matched the set-point temperature. Phase 2 showed a stable temperature profile with the same two degrees Celsius difference from its set-point. To counter-act the set-point difference from the actual temperature, the set-point was increased by two degrees Celsius which led to readings at the desired temperature and RH.

#### 4.1.4 Humidity control

The Antoine equation provides the relation between the amount of water vapour a gas can contain at any given temperature. In order to calculate the amount of water that needs to be added to a given amount of dry feed gas to obtain a desired relative humidity, an excel spreadsheet was created. Desired feed gas flow-rate, RH and temperature values are used as input values in cells Q1, Q2 and Q3 respectively. Using the Antoine equation, the required water vapour pressure is calculated in U4 from the input values. The spreadsheet then generated the required N<sub>2</sub> and water mass flow-rates, for producing this vapour pressure in the feed gas, in cells R6 and R7 respectively. Figure 4.6 presents the spreadsheet which shows that if one desires to use a feed gas flow-rate of 1000 ml.min<sup>-1</sup> at a temperature of 60 °C, one should add 0.16051 g/min water to obtain 90% RH.

Membrane Module Development For Water Recovery From Gas

	O	P	Q	R	S	T	U	V	W	
1		Desired flow rate	1000 ml dry gas/min							
2		Desired RH	90							
3		Desired Temp	60							
4						PH <sub>2</sub> O required	0.1765 bar			
5	Required mass/mol flow rates					moles of H <sub>2</sub> O obtained from $P_{H_2O}/P_{total} = [n_{H_2O}/(n_{H_2O}+n_{N_2})]$				
6	$n_{N_2} =$	0.042 moles/min		1.16462 (g/min)		$P_{H_2O} =$	0.1765 Bar			
7	$n_{H_2O}$	0.009 moles/min		0.16051 (g/min)		$P_{total} =$	1.0133 Bar			
8						$n_{N_2} =$	0.0416 moles/min			

Figure 4.6: Excel spreadsheet used to calculate the required water flow rate needed to humidify a desired gas flow rate to a desired RH at a desired temperature

Temperature, N<sub>2</sub> flow rate and water flow rate were all controlled and maintained at set values. Figure 4.7 presents the development of the relative humidity as function of time.

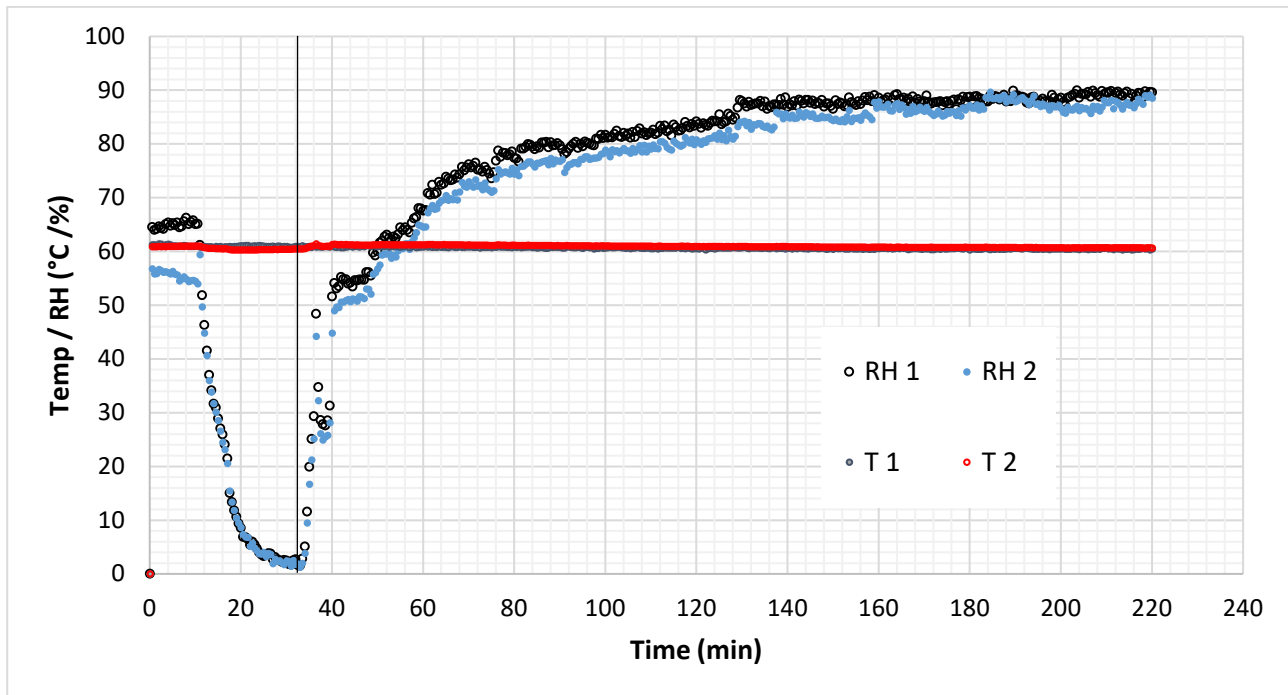


Figure 4.7: Relative Humidity measurement as function of time

At 12 minutes the peristaltic pump was activated. As a result, the RH steadily dropped to zero. At 32 minutes, the pump was deactivated and water flow rate was set at 0.16051 ml.min<sup>-1</sup>. The resistance heaters had a set-point of 62 °C in order to achieve a feed gas temperature of 60°C. Even though the response time is rather slow, the RH eventually stabilises at the desired relative humidity for both RH1 and RH2. This shows humidity control was achieved.

## 4.2 LAB-SCALE MEMBRANE MODULE DEVELOPMENT AND EVALUATION

### 4.2.1 Membrane fibre

Since the permeance of any specie for a particular membrane is dependent on the thickness of the membrane, a Scanning Electron Microscope (SEM) was used to obtain an image of the membrane film covering the fibre support. Several SEM images, each at different magnifications, were obtained and are presented below in Figure 4.8 - Figure 4.10. These images were used to measure the membrane thickness and calculate an average

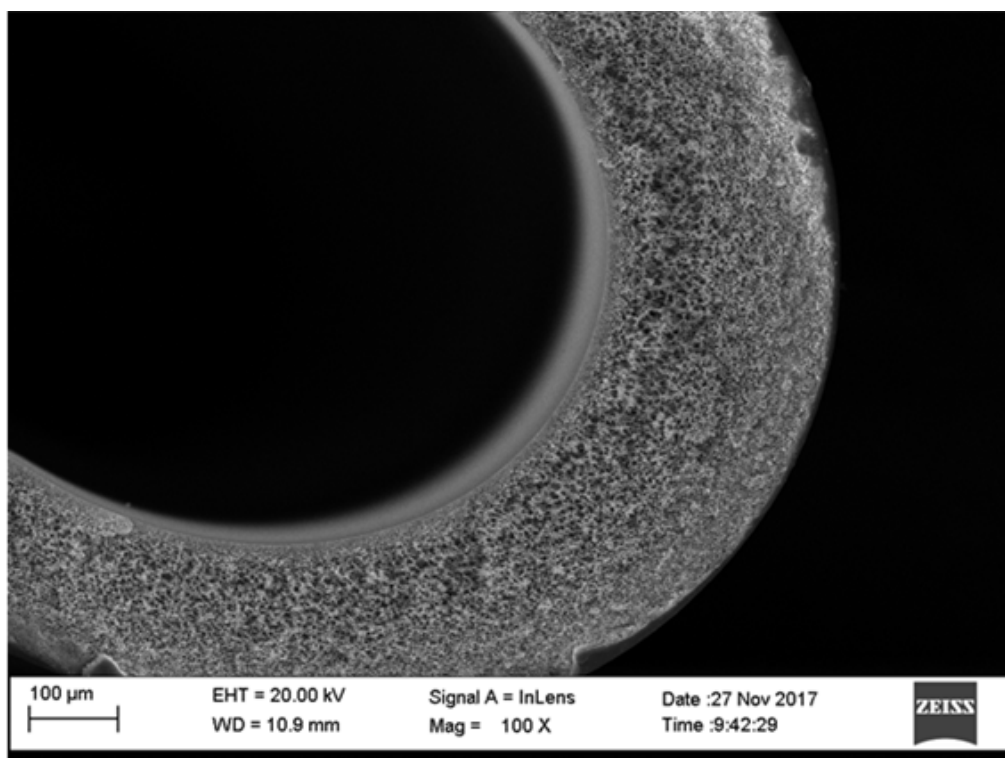


Figure 4.8: SEM image of hollow fibre membrane (100 μm scale)

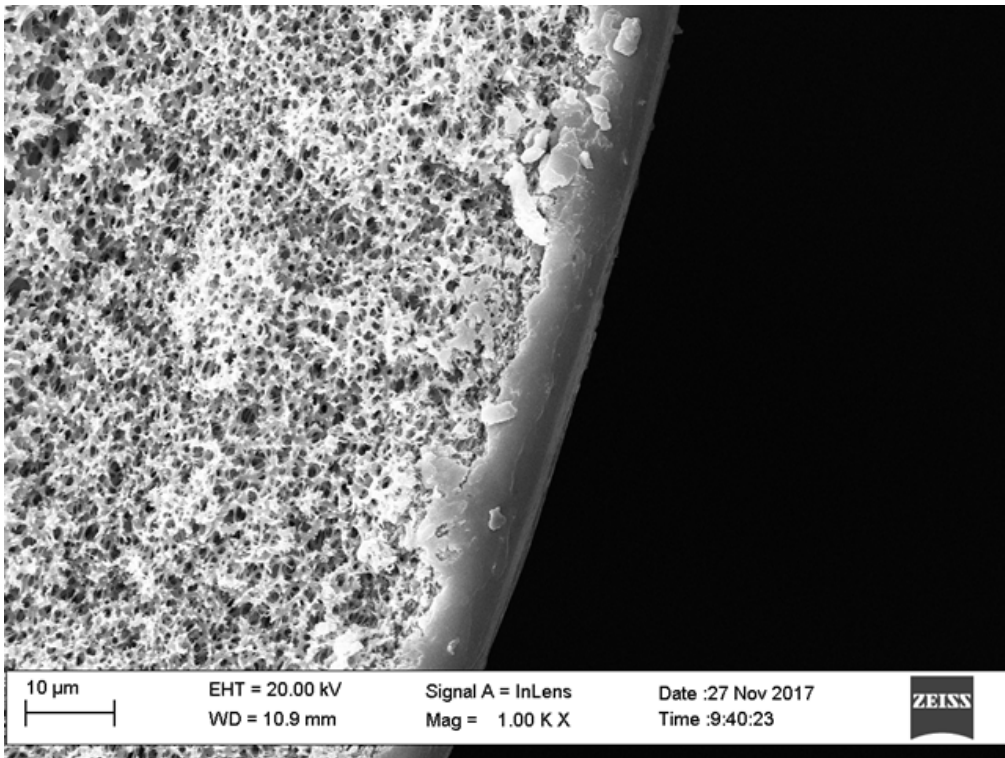


Figure 4.9: SEM image of hollow fibre membrane (10 µm scale)

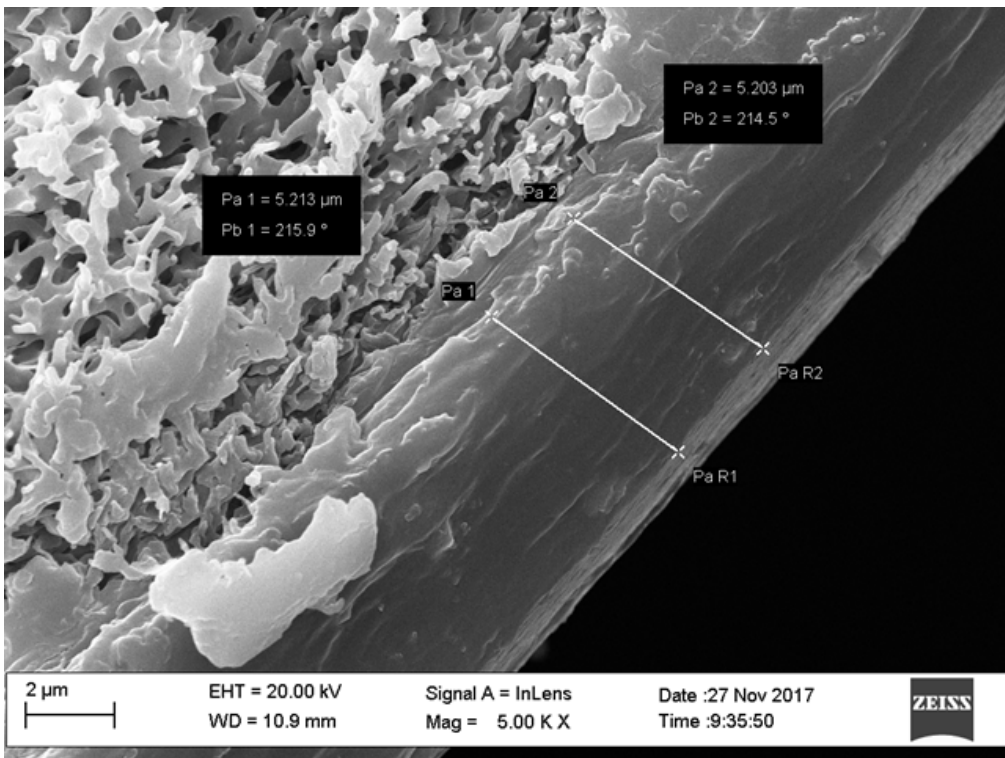


Figure 4.10: SEM image of hollow fibre membrane focused on the membrane layer thickness

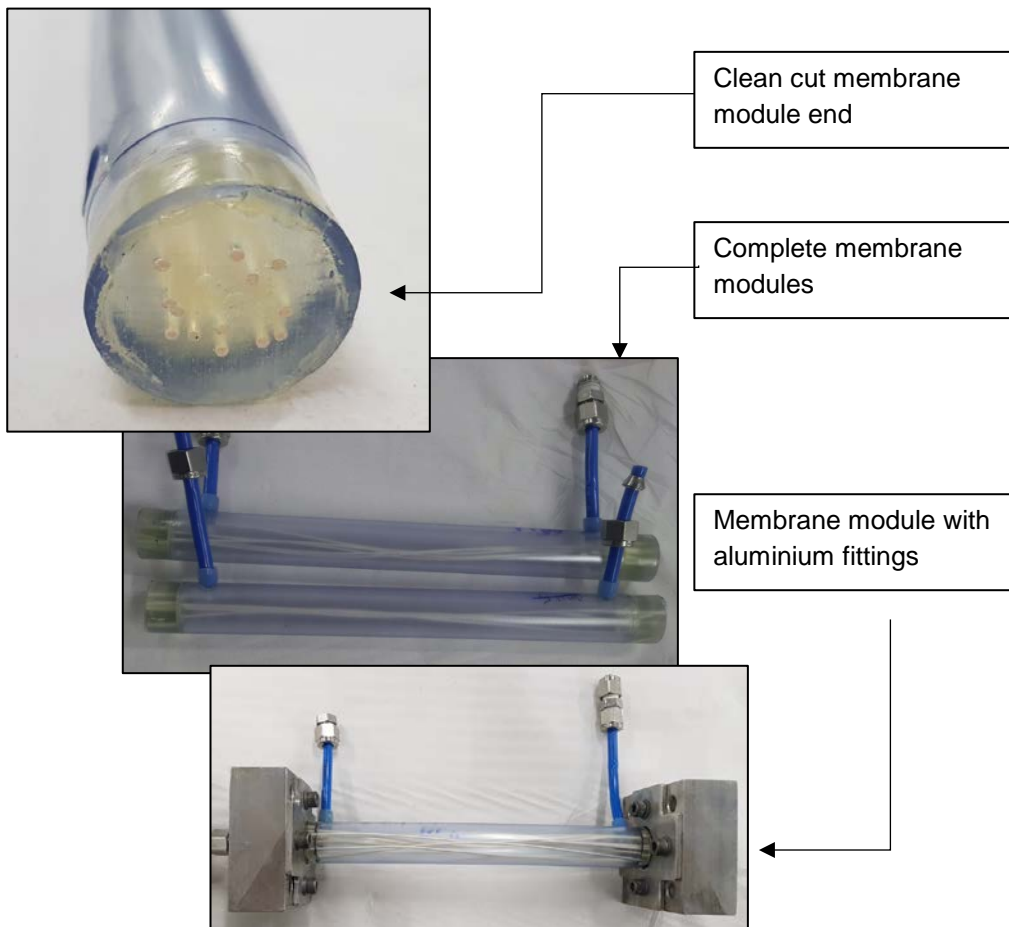
Measurements of the membrane thickness covering the support can be seen on Figure 4.10. All the membrane thickness measurements are shown below in Table 4.2.

**Table 4.2: Measurements for membrane thickness**

Measurement	Measured thickness ( $\mu\text{m}$ )
Pa 1	5.213
Pa 2	5.203
Pa 3	6.398
Pa 4	7.133
Average	6.0

**4.2.2 Tubular lab-scale membrane module production**

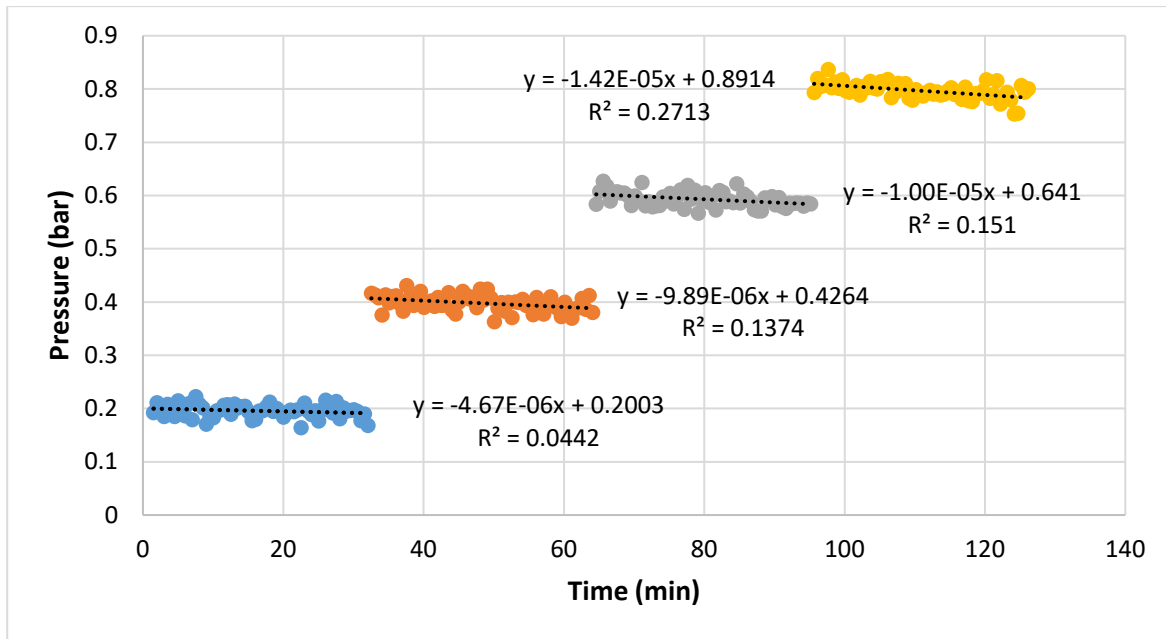
Lab-scale membrane modules were designed and produced to perform membrane characterization experiments using the lab-scale testing system. The lab-scale module development exercise formed a key part of the lab-scale curtain module development process. Figure 4.11 shows completed lab-scale membrane modules.



**Figure 4.11: Completed laboratory membrane modules**

### 4.2.3 Membrane module leak test

Figure 4.12 presents a leak test result of a developed membrane module at five different positive pressure values (0.2, 0.4, 0.6, 0.8 & 1.0 Bar). The purpose of the test was to establish leak-freeness of the module, which is a requirement for successful design. The configuration shown in Figure A.1 was used for the test. Apart from leaks due to a module design flaw, nitrogen permeance through the membrane could be attributed to a decrease in pressure. The rate of pressure loss would depend on the nitrogen permeability value for the membrane being used. If the rate of pressure loss exceeded the rate attributable to nitrogen permeance ( $3.35 \times 10^{-10} \text{ mol}\cdot\text{m}^{-2} \cdot\text{s}^{-1} \cdot\text{Pa}^{-1}$  as specified by supplier), a leak would be the cause.



**Figure 4.12: Membrane leak at increasing positive pressures**

Figure 4.12 shows that the tested module resisted a positive pressure of up to 0.8 Bar. The permeance of the module can be derived from the slope of the line segments. For example, the line formed by the measurements of pressure as function of time starting at 0.6 Bar, shows a slope of  $-1 \cdot 10^5 \text{ Bar/s}$ , which is the rate of pressure loss.

#### 4.2.3.1 Calculating nitrogen permeance

Since the volume of the feed section is known (module shell-side + tubing volume =69 ml) the observed pressure loss can be related to the number of permeating gas molecules. At constant temperature and volume, Equation 4.2 is a derivative of the ideal gas equation and can be used to calculate the permeance.

**Equation 4.2**

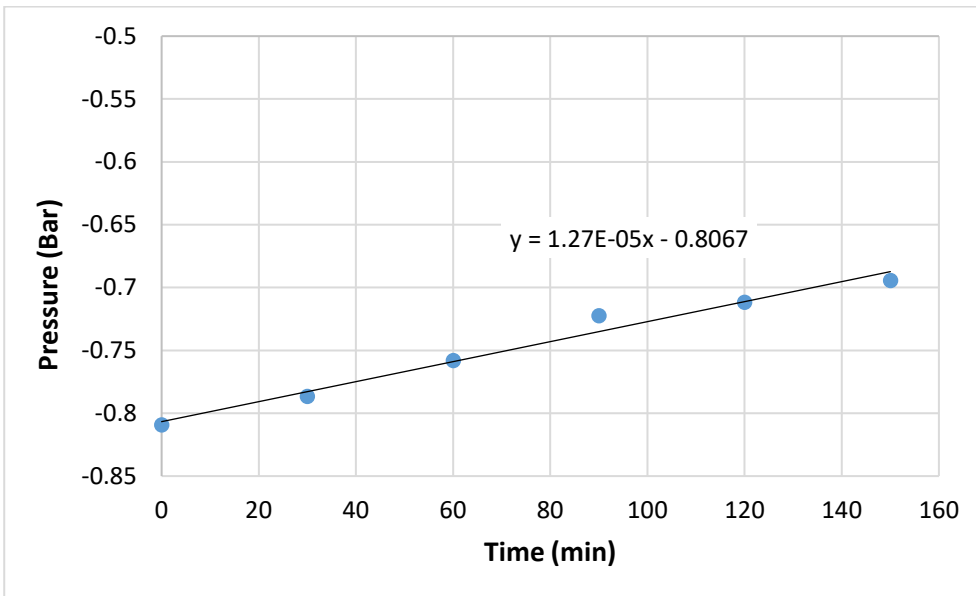
$$\frac{P_1}{n_1} = \frac{RT}{V} = \frac{P_2}{n_2}$$

$P_1$  and  $n_1$  represent the pressure and number of moles at the feed side at time 1 respectively.  $P_2$  represents the pressure and number of moles at the feed side at time 2 respectively.

**Table 4.3: Nitrogen permeance data obtained from leak test**

Applied Pressure (bar)	Permeance (mol.s <sup>-1</sup> .m <sup>-2</sup> Pa <sup>-1</sup> )	
	Provided by the supplier	Calculated
0.2	<3.35 10 <sup>-10</sup>	1.30 x 10 <sup>-10</sup>
0.4		1.38 x 10 <sup>-10</sup>
0.6		1.82 x 10 <sup>-10</sup>
0.8		1.93 x 10 <sup>-10</sup>

Since the water recovery experiments will involve a negative pressure being applied on the permeate side, Figure 4.13 presents a negative pressure leak test of the membrane module. By comparing the gradient values for 0.8 Bar in Figure 4.13 and Figure 4.12, the correspondence in results become apparent.



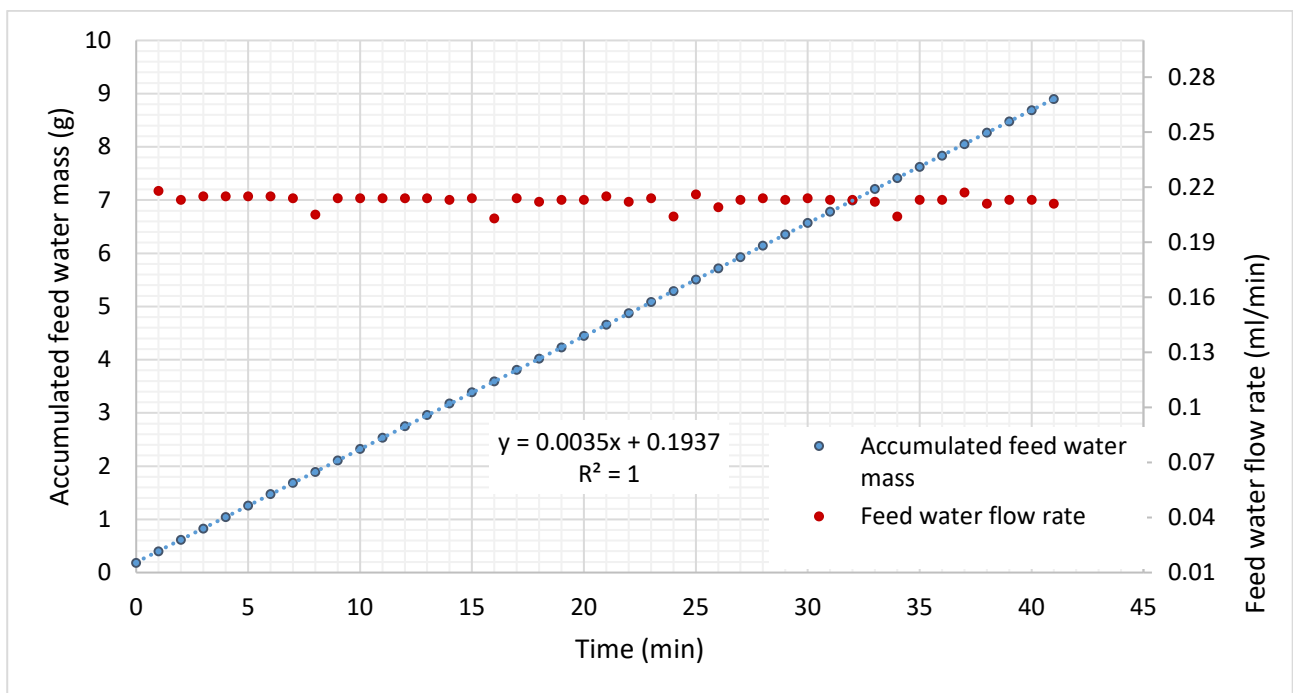
**Figure 4.13: Membrane module leak testing at negative pressure**

#### 4.2.4 Water recovery experiments

Before a water recovery experiment could be conducted, any possible errors in system performance need to be eliminated or accounted for. These errors could be caused by a temperature difference between different points in the flow-line. Another possibility is a build-up of water, since there are various twists, turns, bends and corners in the gas flow-line. Any water built up in this way would not reach the sensors or retentate collection point and cause an error in the results. A solution to this was to run the system, exactly as it would during the experiment, for at least 5 hours prior to starting the experiment. This would result in a fully heated system at all points, and any possible build-up of water to occur. This was referred to as steady-state conditions. In this way, any errors caused by water not reaching the intended locations, would be eliminated. To prove that steady state had truly been reached, a mass balance of the feed was needed.

##### 4.2.4.1 Mass balance of water in feed gas

Figure 4.14 presents a graph for the mass of water continuously fed into the lab-scale system over a period of 41 minutes.



**Figure 4.14: Mass of accumulated feed water and feed water flow rate**

The flow of gas in this experiment was configured to bypass the membrane module. The water fed into the system was collected by condensing the effluent gas. By using the Antoine equation, the amount of water not condensed at the condenser temperature of 6.7 °C could be calculated. Summing this value, with the mass of condensed water, the mass of water exiting in the effluent is known. When compared with the mass of water fed into the system, a percentage error can be calculated. Table 4.4 presents the results of four different mass balance experiments that were conducted. Figure 4.14 is represented by experiment 1.



**Table 4.4: Percentage error obtained from mass balance (membrane is bypassed)**

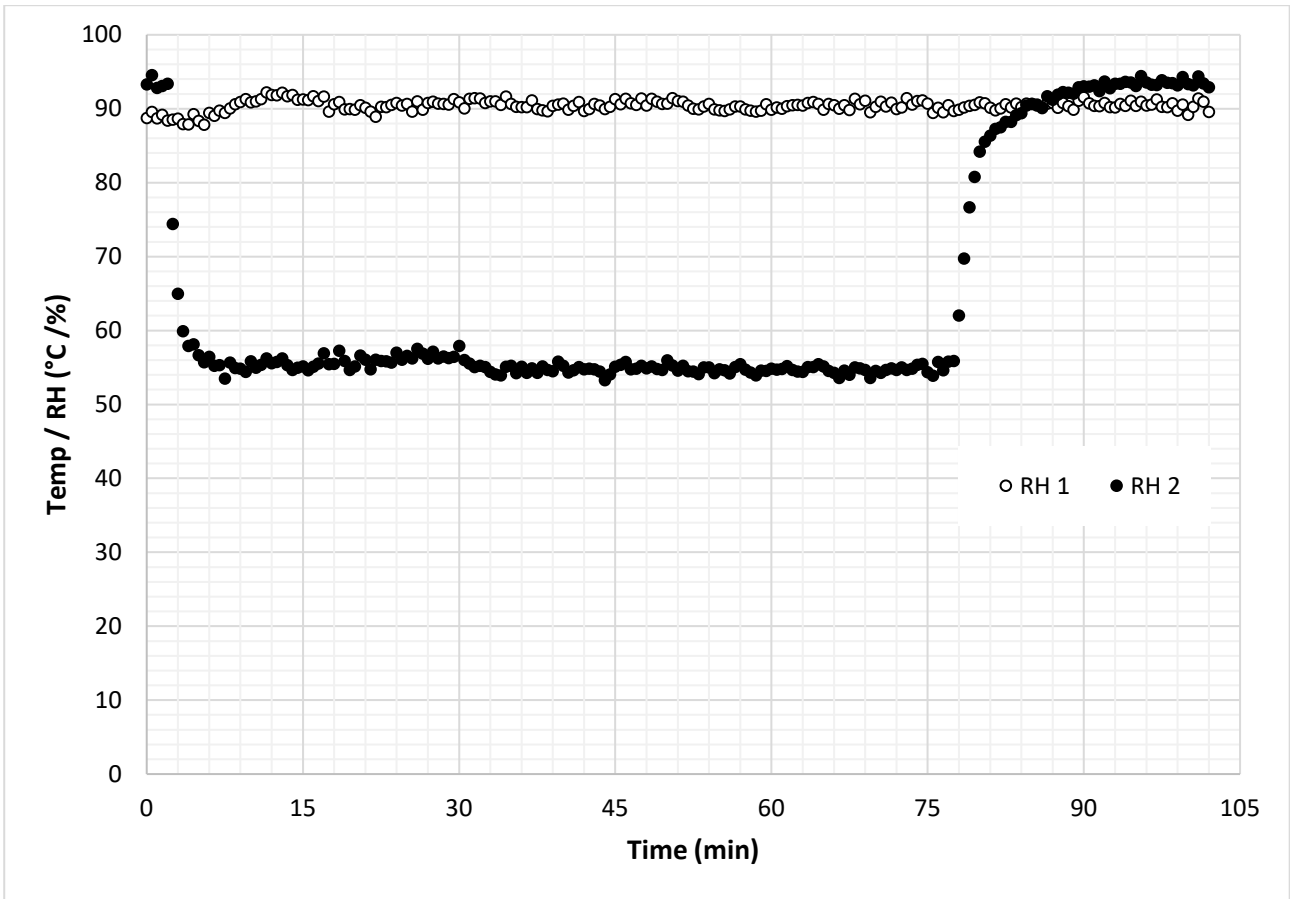
Experiment	WATER IN (Water injected into the feed stream)	WATER OUT (Exiting the condenser as vapour in the reject stream in ml/min)	WATER OUT (Recovered as condensate from reject stream)	WATER OUT (combined in ml/min)	Error
No	(g)	(g)	(g)	(g)	%
1	8.72	0.32	8.29	8.61	0.98
2	7.29	0.29	6.64	7.10	0.97
3	7.10	0.46	6.55	7.01	0.98
4	11.13	0.65	10.39	11.05	0.99

The average percentage error can be considered to be 1 % in Table 4.4 which was low enough to consider the mass balance successful. This also confirmed that the system is stable enough to start water recovery experiments.

As mentioned in Section 2.3 there are two different configurations for recovery. To see which configuration delivered the highest recovery percentage, both the shell-side and tube-side configurations needed to be tested and results compared.

#### **4.2.4.2 Shell-side water recovery**

Whilst the shell-side configuration (Figure 2.4) exposed the outside of the membrane fibre to the feed gas, a negative pressure is applied inside the hollow fibre to create a pressure difference. As a consequence, water permeates through the membrane from the shell side to the lumen. The lumen side is connected to the condenser where the water vapour condenses. At about 200 seconds a constant negative pressure is applied to the permeate side of the membrane. As seen below in Figure 4.15, relative humidity of the retentate gas exiting the membrane module (RH 2), dropped to 55% for the duration of the experiment. At around 78 minutes, the vacuum pump inducing the negative pressure, was switched off. Following this, RH 2 was restored to 90%. This indicated water vapour permeation through the membrane fibre, which was confirmed by droplets forming in the permeate collection vessel.



**Figure 4.15: Water recovery experiment with a shell-side configuration**

When calculating the amount of water recovered in the experiment, another mass balance is created. This mass balance differs in that the water recovery in the reject stream, both condensed and non-condensed water vapour, is subtracted from the mass fed into the system to calculate the amount of water recovered. Due to the error calculation in Table 4.4, these values were considered precise to within 1%. Results of two different experiments with the shell-side configuration are shown in below Table 4.5.

**Table 4.5: Summary of shell-side water recovery**

Experiment	WATER IN (Water fed into the system)	WATER OUT (Exiting the condenser as vapour in the reject stream)	WATER OUT (Recovered as condensate from reject stream)	WATER OUT (Permeated water ( $W_p$ ) *)	Recovery
No	(g)	(g)	(g)	(g)	%
1	15.84	0.59	7.34	7.91	49.93
2	8.72	0.32	3.95	4.45	51.03

4.2.4.3 Tube-side water recovery

When the tube-side configuration (Figure 2.3) was used, the feed gas flowed through the hollow fibre membranes. A negative pressure was applied on the outside of the membrane wall inside the module housing (or inside the module shell). This configuration has the same driving force for recovery (a pressure difference between feed and permeate), but water vapour permeates from the inside of the membrane fibre towards the outside. Figure 4.16 presents a water recovery experiment with a tube-side flow configuration. As with Figure 4.15, it is clear the RH 2 value dropped significantly once the vacuum was switched on. This indicated water vapour permeating through the membrane. Once the vacuum was switched off, the RH 2 value started increasing towards the RH 1 value.

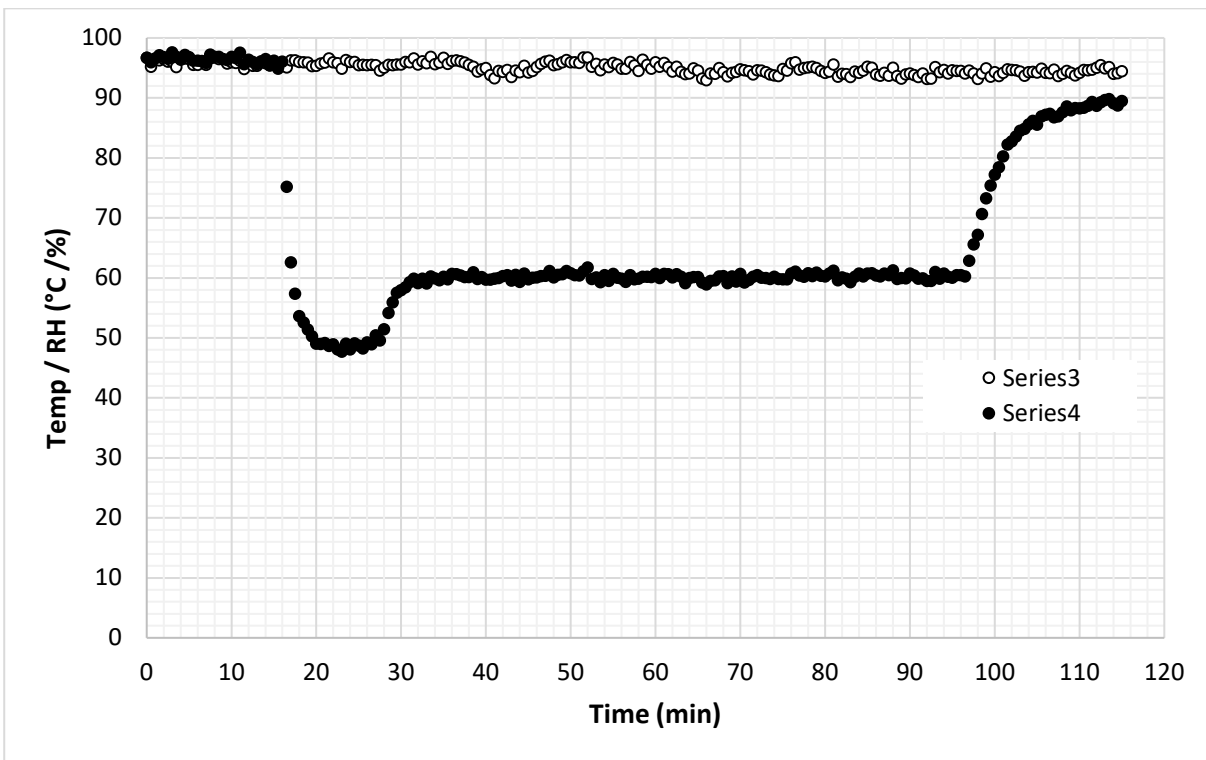


Figure 4.16: Water recovery experiment with a tube-side configuration

The value of RH2 shows a peculiar hump shortly after the vacuum was applied at 15 minutes where the RH initially establishes itself at about 50% but then slowly adjusts to 60%. Even though the cause of this anomaly is not entirely clear, it needs to be noted that since the membrane layer is positioned on the shell side, the support structure may provide a significant resistance to water transfer. Meaning that when the water permeates through the membrane, the remaining feed gas with reduced RH is “trapped” in the microporous support structure forming an additional barrier for water molecules to diffuse through. This may be the reason why the RH first drops to 50% but increases to 60% a moment later. The mass balance results of two water recovery experiments, utilising a tube-side configuration, are presented in Table 4.6. It was assumed that these results had the same precision as the shell-side feed results, since they were measured in the same system at similar conditions.

**Table 4.6: Summary of tube-side water recovery**

Experiment	WATER IN (Water injected into the feed stream)	WATER OUT (Exiting the condenser as vapour in the reject stream)	WATER OUT (Recovered as condensate from reject stream)	WATER OUT (Permeated water ( $W_p$ ) *)	Recovery
No	(g)	(g)	(g)	(g)	%
3	8.43	0.37	4.25	3.81	45.19
4	3.80	0.18	2.07	1.55	40.78

From the obtained results and Figure 4.15, it can be noted that the shell-side configuration consistently presented superior water recovery performance over the tube-side configuration. This can be attributed to the fact that the membrane layer is at the shell side as explained above. In addition the velocity of the feed gas in the shell side configuration is lower than the velocity of the gas in the tube side configuration. This means that the feed gas spends a longer time in contact with the membrane surface, allowing for a more effective vapour transport through the membrane.

#### 4.2.4.4 Water vapour permeance calculation

The following exercise was performed to determine the water permeance value for the membranes. Numbers 1, 2, 3, 4, 9, 11 and 12 in Table 4.7 are measured values obtained from the equipment in the lab-scale testing system. The partial pressure of the feed water vapour was calculated using the Antoine equation as the normalised  $N_2$  flow rate was converted to the actual  $N_2$  flow rate. The partial pressure of the  $N_2$  feed was calculated as well as the flow rate of water in the feed. The flow rate of water at the entrance of the module was calculated based on the values of RH and temperature (0.175g/min), while the mass loss rate of water pumped out of the feed water reservoir was found to be 0.178g/min (see value 8 and 9 in Table 4.7). These results were considered to be within the analytical error of measurements since the error resembles the mass balance error in Table 4.4. Knowing the  $N_2$  flow rate, as well as water vapour flow rate into the system, the total flow rate of the feed was calculated. After the permeate pressure was reduced to 0.3 Bara, and the permeate was exposed to the actively cooled condenser surface. The temperature of the reject stream remained 61°C throughout the experiment while the reject RH stabilized at 81% after 5 minutes. Since the reject/retentate RH is known, the partial pressure of water in the reject was calculated to be 12000 Pa. The temperature of the cooling element (4°C) was used to calculate the partial pressure of the water vapour in the permeate. Knowing the partial pressure of both  $N_2$  and  $H_2O$  in the feed, reject and permeate led to the calculation of the average trans-membrane pressure ( $TMP_{ave}$ ). Finally, the membrane permeance was found to be  $1.63 \mu\text{mol}\cdot\text{m}^{-2}\cdot\text{s}^{-1}\cdot\text{Pa}^{-1}$ , very much in line with (Sijbesma, et al., 2008).

**Table 4.7: Establishment of the membrane permeance using experimental lab-scale testing process parameters and the calculations as explained in 3.2.1.3**

No	Parameter	Value	Type of value
1	$\Phi_{\text{Normalized N}_2}$	0.001 ( $\text{Nm}^3 \cdot \text{min}^{-1}$ )	Measured using MFC feedback signal
2	$P_{\text{atmospheric}} = P_{\text{feed}}$	101224 Pa	Measured using S8 Samsung
3	$T_{\text{feed}}$	61 °C	Measured using thermocouple
4	$\text{RH}_{\text{feed}}$	92%	Measured using RH sensor 1
5	$P_{\text{H}_2\text{O feed}}$	19143 Pa	Calculated
6	$\Phi_{\text{N}_2}$	0.001141 ( $\text{m}^3 \cdot \text{min}^{-1}$ )	Calculated
7	$P_{\text{N}_2 \text{ feed}}$	82080 Pa	Calculated
8	$\Phi_{\text{H}_2\text{O feed}}$	0.000266 ( $\text{m}^3 \cdot \text{min}^{-1}$ )	Calculated
		0.0096916 ( $\text{mol} \cdot \text{min}^{-1}$ )	Calculated
		0.175 ( $\text{g} \cdot \text{min}^{-1}$ )	Calculated
9	$\Phi_{\text{H}_2\text{O feed}}$	0.178 ( $\text{g} \cdot \text{min}^{-1}$ )	Measured
10	$\Phi_{\text{feed}}$	0.001407 ( $\text{m}^3 \cdot \text{min}^{-1}$ )	Calculated
11	$T_{\text{element}}$	4 °C	Measured using thermocouple
12	$\text{RH}_{\text{reject}}$	81%	Measured using RH sensor 2
13	$P_{\text{H}_2\text{O reject}} = P_{\text{H}_2\text{O exit}}$	11999.98 Pa	Calculated
14	$\Phi_{\text{Permeate H}_2\text{O}}$	$2.11 \cdot 10^{-5} \text{ mol} \cdot \text{s}^{-1}$	Calculated
15	$\text{TMP}_{\text{ave}}$	15607 Pa	Calculated
16	$\text{SA}_{\text{laboratory mini module}}$	0.00075 $\text{m}^2$	Calculated
17	Membrane permeance	1.63 $\mu\text{mol} \cdot \text{m}^{-2} \cdot \text{s}^{-1} \cdot \text{Pa}^{-1}$	Calculated

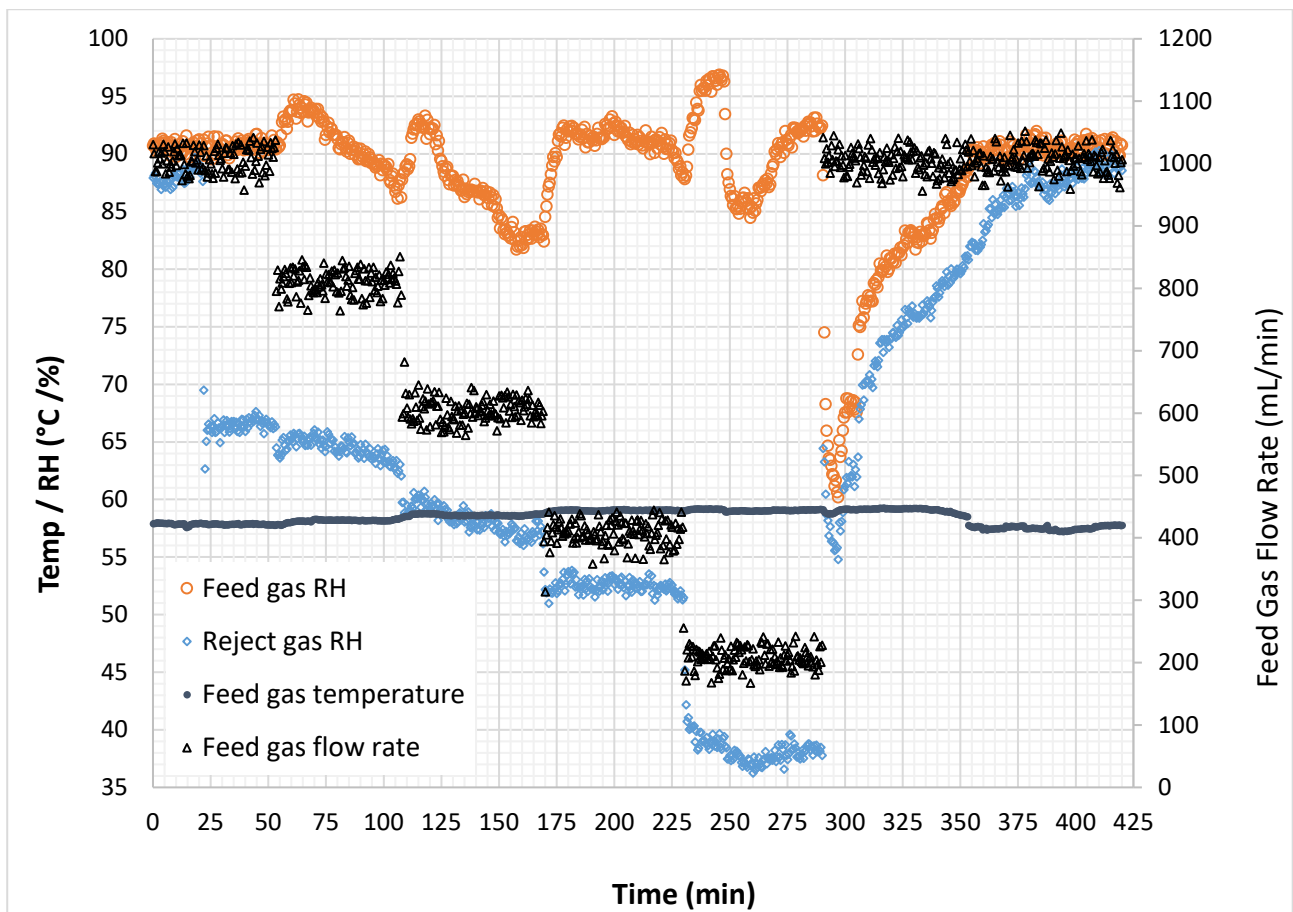
#### 4.2.4.5 Water recovery as function of feed gas flow rate

In order to investigate the effect flow rate has on the percentage recovery, the feed gas flow rate was reduced with time. Initially a flow rate of 1000 ml/min was used to stabilize the system. When both RH 1 and RH 2 reached constant values (within a 4% difference of the set-point of 90%), a negative pressure was applied to reduce permeate pressure to 0.3 Bara and start water recovery. The relative humidity of the permeate gas dropped from 90% to 68% and remained stable. After 30 minutes the gas flow rate was reduced by 20%, from 1000 to 800ml/min. Subsequent to the gas flow rate reduction, the water flow rate was also reduced with 20% in order to keep the RH of the feed gas constant. Every 30min both the gas flow rate and the water flow rate were reduced. Despite the fact that these changes in feed gas flow rate did not render a stable reading, a consistent increase in percentage water recovery was observed with each reduction in feed gas flow rate. With a feed gas flow rate dropped to 200 ml/min an impressive reduction in the relative humidity was noticed, as seen in Figure 4.17. As the RH does not represent a linear relation with water content, the percentage water recovery is calculated as the ratio of the partial pressure of water at the reject side over the partial pressure of water and the feed side. The water recovery as function of feed flow rate is shown in Table 4.8.

**Table 4.8: Water recovery at different feed flow rates**

Feed side					Reject			Permeate	H <sub>2</sub> O recovery
No	flow rate	Ave RH	Temp	PH <sub>2</sub> O	Ave RH	Temp	PH <sub>2</sub> O	PH <sub>2</sub> O =P permeate	
	(ml/min)	(%)	(°C)	(Pa)	(%)	(°C)	(Pa)	(Pa)	(%)
1	200	91	59	16982	38	59	7188	9794	58
2	400	91	59	17022	52	59	9826	7196	42
3	600	87	59	16271	58	59	10897	5373	33
4	800	91	59	17054	64	59	12058	4996	29
5	1000	91	59	16973	66	59	12438	4536	27

Table 4.8 confirmed that an adjustment of the feed flow rate can significantly increase water recovery. With the reduction in gas flow rate from 1000ml/min to 200ml/min, the water flow rate was reduced from 0.17 ml/min to 0.03 ml/min.



**Figure 4.17: Percentage water recovery at decreasing feed gas flow rates**

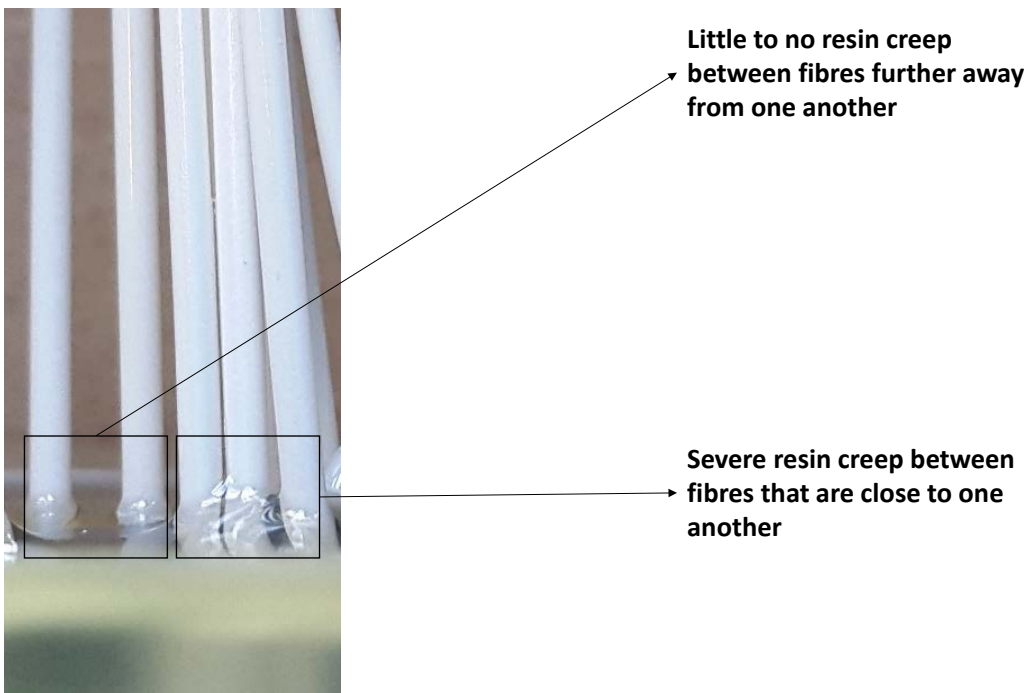
From the values in Figure 4.17, it became clear that the peristaltic pump showed a significant upward deviation at low set-points. This in turn caused the amount of water supplied to the system to be higher than desired. As a result, the stability of the RH 1 reading was affected. However, this exercise provided valuable insight into

the water recovery process. As the feed gas flow rate decreased, a substantial increase in recovery was observed. This is due to the higher residence time of the feed gas giving the water more contact time with the membrane. Another important observation was the significant increase in module permeance. This particular module was kept saturated with water throughout the module making process. By keeping the membrane moisturized, optimal permeance is expected.

#### 4.2.5 Lab-scale curtain-type membrane module production

A curtain type lab-scale membrane module was produced as a trial in order to identify possible complications that could arise with the design and development of the pilot-scale module. This trial module gave valuable information on design challenges to be solved prior to development of pilot-scale membrane modules. Figure 4.18 shows that resin creep occurs when the space between two adjacent fibres is less than approximately 1 mm.

Creep of resin increases the chances of fibre damage specifically when the fibres start resonating with the passing gas flow. The ridged resin edges may cut the fragile skin of the membrane, causing leaks and thus rendering a module with reduced selective properties.




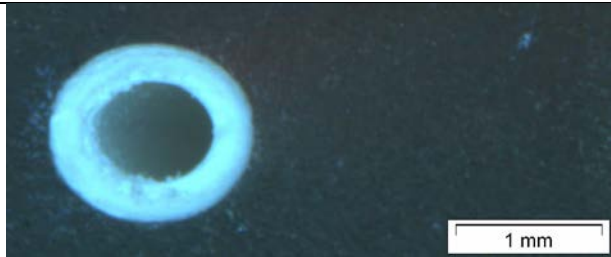



**Figure 4.18: Lab-scale curtain-type membrane module showing creep effects of resin on membranes**

##### 4.2.5.1 Cutting of the lab-scale curtain-type membrane module

Valuable information was also obtained with regards to the appropriate cutting method for curtain type modules. The guillotine method effectively produced clean cuts on the lab-scale membrane modules, however, applying the guillotine method on the pilot-scale membrane is far more challenging. The curtain

module is cast with the aid of a mould which needs to be removed before the module can be cut. Premature removal of the mould will however result in the deformation of the potting, compromising the sealability of the module. This means that the mould can only be removed when the resin is fully cured and subsequently too hard for the guillotine to be cut. Alternative cutting methods had to be evaluated. The results presented in Table 4.9 show that a router as a cutting tool rendered a module with almost entirely closed fibres. Employing a plane did show some improvement but the fibre ends appear only partially open. Reasonable results were obtained with the Altendorf C90 panel wood saw yielding reproducible cuts with clear open fibres. Interesting to note are fibres that showed 100% of the lumen exposed when the router “ripped” a portion of the module to pieces. Unfortunately, the ripping action is not reproducible, causes unstable movements and should be avoided from a safety point of view. Cutting the module using a water jet was effective, however light microscope images revealed that the water jet method leave an undesired residue inside the pores. Going forward, modules were cut using the wood panel saw.

**Table 4.9: Module cutting attempts using various cutting techniques**

Cutting method	Details	Image	Lumen exposure
Router	Cut at 28000 RPM		0-10%
Wood panel saw	Cut with Altendorf C90 wood panel saw		90%
Plane	Shaved with a planer		10-30%
Guillotine	Guillotine	As soon as the mould is ready to be removed, the resin is too hard to be cut.	
Ripped	Ripped with router at 28000 RPM		100%
Water jet cut			90%



### 4.3 PILOT CURTAIN-TYPE MEMBRANE MODULE DESIGN AND DEVELOPMENT

#### 4.3.1 Required membrane area based on fixed process parameters

With reference to Table 4.10, numbers 1, 2, 3, 4 and 5 are the process parameters that were selected in Section 3.2.1 as the requirements for the pilot-scale membrane module. The Antoine equation was used to calculate the partial pressure of water in mmHg which was then converted to Pa. Application of the ideal gas law ( $PV = nRT$ ) combined with the water recovery requirement gives the permeating water vapour flow rate in mol/h. Using the ideal gas law once again and converting the total normalised flow rate to actual flow rate, the total feed gas flow rate is calculated in mol/h. The permeating water vapour flow rate was subtracted from the total feed gas flow rate to yield the total exit flow rate. Using the Antoine equation once more, and converting from mmHg to Pa, the partial pressure of the permeate water vapour was calculated. The partial pressure of water vapour at the exit of the module was found to be 33.3% lower than the inlet, in line with the water recovery target. Knowing the values of the water vapour feed, reject and permeate, the average Trans-membrane pressure (TMP) was calculated.

**Table 4.10: Calculated values for selected process parameters**

No		Value	Type of value	Equation used
1	$T_{\text{feed}}$	60 °C	Variable process parameter	
2	$T_{\text{element}}$	30 °C	Variable process parameter	
3	$\varphi_{\text{Normalized Feed}}$	30 Nm <sup>3</sup> h. <sup>-1</sup>	Variable process parameter	
4	RH <sub>feed</sub>	95 %	Variable process parameter	
5	Water recovery requirement (WRR)	33.3%	Process requirement	
6	$P_{\text{H}_2\text{O feed}}$	18857.83 Pa	Calculated value	2.1
7	$\varphi_{\text{permeate H}_2\text{O}}$	73.58 mol.h <sup>-1</sup>	Calculated value	3.10
8	$\varphi_{\text{Feed}}$	34.13 m <sup>3</sup> h. <sup>-1</sup> 1247.21 mol.h <sup>-1</sup>	Calculated value	3.1
9	$\varphi_{\text{exit H}_2\text{O}}$	147.16 mol.h <sup>-1</sup>	Calculated value	3.14
10	$\varphi_{\text{exit total}}$	1173.63 mol.h <sup>-1</sup>	Calculated value	3.16
11	$P_{\text{H}_2\text{O permeate}}$	4231.67 Pa	Calculated value	2.2
12	$P_{\text{H}_2\text{O exit}}$	12692.05 Pa	Calculated value	3.3
13	TMP <sub>ave</sub>	15774.94 Pa	Calculated value	2.3 /3.08

The TMP<sub>AVE</sub>, permeating water vapour flow rate and the value of the membrane permeance were calculated employing Equation 3.17, Equation 3.8 and Equation 3.9 respectively and used to determine the required membrane module surface area ( $SA_{\text{module}}$ );

**Equation 4.3**

$$SA_{module} = \frac{\varphi_{permeate H_2O}}{Permeance \cdot TMP} = \frac{\frac{73.58 \left[ \frac{mol}{h} \right]}{3600 \left[ \frac{s}{h} \right]}}{1.63 \cdot 10^{-6} \left[ \frac{mol}{m^2 s Pa} \right] \cdot 15774.94 [Pa]} = 0.8 m^2$$

**4.3.2 Amount of fibre per module**

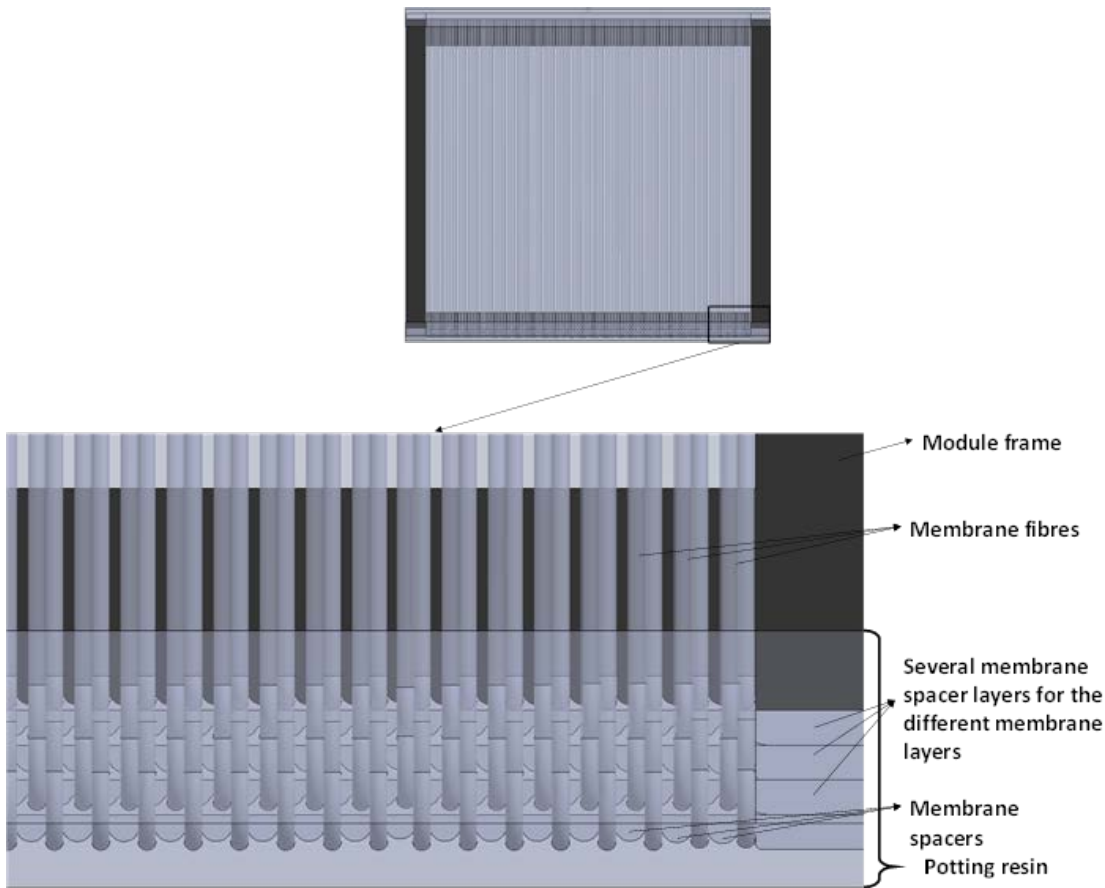
As the shell-side feed configuration was selected as the configuration of choice, the feed gas would be exposed to the outside of the fibre. As such the outer diameter of the fibre (1.2 mm) was used to calculate the required fibre length from the required membrane module surface area. The total exposed length of fibre per module needed was found to be:

**Equation 4.4**

$$Exposed\ Fibre\ length_{module} = \frac{SA_{module}}{Circumference_{fibre}} = \frac{0.8[m^2]}{\pi D_{fibre}[m]} = \frac{0.8[m^2]}{3.14159 \cdot 0.0012[m]} = 212m$$

Using the knowledge gathered from the lab-scale curtain-type module design, a design for the pilot-scale module was developed in Solid works®.

Figure 4.19 shows the design of the pilot-scale membrane module as well as a zoomed in piece of the membrane module which identifies the different components in the module. Solid works® designs are compatible with most 3D printers. Since machining of the spacer component would be tedious and time consuming, these parts were produced using a 3D printer.



**Figure 4.19: Design for pilot plant curtain-type membrane module**

The design included a stainless steel frame with a thickness of 2mm. Spacer strips were added onto the top and bottom of the frame. These spacers ensured a fixed gap of 2 mm between each fibre was maintained, large enough to prevent resin creep. After the first 99 windings onto the frame, two more spacers were placed at either side of the module before a second 99 windings were applied onto the frame. Another two layers of 99 windings each were added to give a total of 4 membrane fibre layers. After a fourth layer was wound, the potting process followed. Each module would have 396 fibre windings which constitutes 216 meter of fibre exposed to the feed gas (not covered by resin). The active membrane areas per module was 0.8 m<sup>2</sup> per module.

### 4.3.3 Potting of pilot-scale membrane module

Epothin™ 2 Epoxy Resin 20-3440-128, which was used for the lab-scale membrane modules was also used in production of the pilot-scale membrane module. From the production of the lab-scale membrane modules it was noted that when the potting material (Epothin™ 2 Epoxy Resin 20-3440-128 and Epothin™ 2 Epoxy Hardner 20-3442-064) had a hardness of below 30 shore D, the resin would not be hard enough to yield a satisfactory cut. However, with hardness above 55 shore D, the resin would be too hard to cut through by a guillotine. However, due to the exothermic reaction of the resin mixed with the hardener in quantities above 50 ml, controlling the speed of curing proved problematic. Therefore, diverse ratios of resin to hardener were investigated. Table 4.11 shows the hardness of the potting material with different ratios and curing times.

**Table 4.11: Hardness of potting material with different ratios (per unit volume) of resin compared to hardener at different curing times**

Ratio ( Per unit volume )		Average Hardness (Shore D)		
Resin	Hardener	17 hours	22 hours	48 hours
2	1	65	65	65
2.3	1	34.6	43.3	43.3
2.4	1	32.5	41.0	41.0
2.5	1	27.6	33.8	33.7
2.6	1	16.3	22.0	22.1
2.7	1	11.8	16.1	16.3

From the tables above it was concluded that a mixing ratio of 2.3 : 1 resin to hardener should be used when conducting potting of the pilot-scale membrane module.

#### **4.3.4 Completed pilot-scale membrane module**

The fully developed pilot-scale membrane module, and its assembly, is shown in Appendix D.

## CHAPTER 5: CONCLUSIONS, RECOMMENDATIONS AND OUTPUTS

---

### 5.1 LAB-SCALE MEMBRANE MODULE TESTING STATION

- During the course of this MSc study, the gas mixing station was successfully converted into a water vapour permeance measurement system. Using the system, the water vapour permeance and nitrogen permeance was measured. These values correspond with those reported in literature and provided by the supplier. This indicates success of the measurement system.
- Complete thermal stability of the measurement system was achieved. An accurate and constant temperature was maintained within the system while conducting experiments. Due to the importance of a constant temperature with regards to RH, complete thermal stability proved instrumental to success of the research.
- A feed water mass balance was created and confirmed excellent control over the mass of water supplied to and recovered from the system. The feed and reject water masses agreed to within a 1% difference. This exceptionally small error percentage means that that a difference between RH1 and RH2 is a mainly a consequence of water permeation through a membrane rather than an error in the system (control of temperature, water- or N<sub>2</sub> flow).

### 5.2 LAB-SCALE MEMBRANE MODULE

- A completely leak free lab-scale membrane module was successfully designed and produced. The leak freeness was confirmed by leak tests conducted on the produced modules.
- Results of the permeance tests coincided with the permeance figures given by literature as well as the suppliers of the membrane. This indicates that the permeance tests were successfully and accurately conducted.
- A relationship between gas flow rate and water recovery was established, revealing a key element to water recovery using membrane modules. It was established that the percentage water recovery significantly increased as feed flow rate decreased.
- The shell-side configuration was identified as a more effective configuration for water recovery than the tube-side. The shell-side consistently yielded a higher percentage water recovery, making it the preferred configuration in membrane module design and development.
- The most effective cutting method was discovered to be a guillotine method, which was specifically built for cutting the module. The optimal thermal treatment in terms of temperature and time was established. The guillotine method yielded a smooth cut with a completely open membrane lumen.

### 5.3 PILOT-SCALE MEMBRANE MODULE

- The pilot-scale membrane module was designed and produced. The length of fibre necessary for the design was calculated and aided in the design.
- The pilot-scale module potting was longer and thicker than the lab-scale module potting. In turn, these different geometries caused the potting material to harden at different rates throughout the potting, yielding both hard and soft areas which appeared to be challenging for the guillotine. It was concluded that a wood panel saw was the most effective cutting method for a completely cured pilot-scale module.
- Resin creep between the fibres was identified and addressed during the pilot-scale module design. A solution to the creep was to space the membranes 2 mm apart, which solved the resin creep problem. To achieve such equal spacing, a membrane spacer, was successfully designed and 3D printed. The spaces between membranes are controlled by the spacer design and can be reduced or increased when the feed gas pressure loss over the module is too high or too low receptivity.

### 5.4 RECOMMENDATIONS

- Secure a membrane supplier that readily produces hollow-fibre membranes and will be able to provide the project with a constant supply.
- Decide on a potting material which can be easily cut by pre-determined means in order to optimise the cutting process and not experiment until a suitable method is found.
- Design a pilot-scale testing system. This can be used to test a pilot-scale membrane module which would give more insight on whether the use of membrane modules are viable at industrial scale.

## REFERENCES

---

- Anon., 2018. *STERLITECH Corporation*. [Online]  
Available at: <https://www.sterlitech.com/membrane-modules.html>  
[Accessed 02 03 2018].
- Anon., n.d. *Separation Processes*. [Online]  
Available at: [http://www.separationprocesses.com/Membrane/MT\\_Chp03b2.htm](http://www.separationprocesses.com/Membrane/MT_Chp03b2.htm)  
[Accessed 03 04 2018].
- Asatekin, A. & Mayes, A., 2009. Oil Industry Wastewater Treatment with Fouling Resistant Membranes Containing Amphiphilic Comb Copolymers. *Environmental Science and Technology*, 43(12), pp. 4487-4492.
- Baker, R., 2002. Future Directions of Membrane Gas Separation Technology. *Industrial and Engineering Chemistry Research*, 41(6), pp. 1393-1411.
- Baker, R., 2004. *Membrane Technology and Applications*. 2nd ed. Chichester: John Wiley and Sons Ltd.
- Burtraw, D. et al., 1998. COSTS AND BENEFITS OF REDUCING AIR POLLUTANTS RELATED TO ACID RAIN. *Contemporary Economic Policy*, 16(4), pp. 379-518.
- Chen, N., 1979. An Explicit Equation for Friction Factor in Pipe. *Industrial & Engineering Chemistry Fundamentals*, 18(3), pp. 296-297.
- Choi, J.-H., Dockko, S., Fukushi, K. & Yamamoto, K., 2002. A novel application of a submerged nanofiltration membrane bioreactor (NF MBR) for wastewater treatment. *Desalination*, 146(1-3), pp. 413-420.
- Coulson, J., Richardson, J., Harker, J. & Backhurst, J., 1999. *Coulson and Richardson's Chemical Engineering Volume 1*. 6th ed. Oxford: s.n.
- Croopnick, G. A., Michaels, J. M. & Paul, D. G., 1977. *Gasket arrangement for purification apparatus*. United States of America, Patent No. US05781761.
- Daal, L., de Vos, F. & van Daele, P., 2013. *A new source of water that saves energy*, Rutenburg: s.n.
- Department of Mineral Resources, 2014. *South Africa's coal industry Overview, 2014*, Pretoria: Mineral Economics Directorate.
- Dew Point , 2017. *Dew Point*. [Online]  
Available at: <http://www.dewpointmfg.com/>  
[Accessed 13 04 2018].
- Dictionary, C. E., 2018. *Definition of 'plasticization'*, s.l.: HarperCollins Publishers.
- Dindore, V., Versteeg, G., Brillman, D. & Feron, P., 2004. CO<sub>2</sub> absorption at elevated pressures using a hollow fiber membrane contactor. *Journal of Membrane Science*, 235(1-2), pp. 99-109.
- Drioli, E., Criscuoli, A. & Curcio, E., 2002. Integrated membrane operations for seawater desalination. *Desalination*, 147(1-3), pp. 77-81.
- Epotek, 2012. *Tg - Glass Transition Temperature for Epoxies*, Billerica : Epoxy Technology Inc..
- Forwardosmosistech, 2014. *ForwardOsmosisTech*. [Online]  
Available at: <http://www.forwardosmosistech.com/plate-and-frame-forward-osmosis-modules/>  
[Accessed 09 02 2018].
- Franklin, C., Burnett, R., Paolini, R. & Raizenne, M., 1985. Health risks from acid rain: a Canadian perspective. *Environmental Health Perspectives*, Volume 63, pp. 155-168.
- Geng, X., Wu, H. & He, Q., 2014. Study on a new air-gap membrane distillation module for desalination. *Desalination*, 334(1), pp. 29-38.
- Günther, R., Perschall, B. & Hapke, J., 1996. Engineering for high pressure reverse osmosis. *Journal of Membrane Science*, 121(1), pp. 95-107.
- He, X. & Hägg, M.-B., 2012. *Membranes for Environmentally Friendly Energy Processes*. [Online]  
Available at: <https://www.ncbi.nlm.nih.gov/pmc/articles/PMC4021925/>  
[Accessed 28 02 2018].
- Hoffman, M., Carrick, P., Gillson, L. & West, A., 2009. Drought, climate change and vegetation response. *South African Journal of Science*, Volume 105, pp. 54-60.

- Houde, A. et al., 1995. Field tests of membrane modules for the separation of carbon dioxide from low-quality natural gas. *Gas Separation & Purification*, 9(1), pp. 35-43.
- Isetti, C., Nannei, E. & Magrini, A., 1997. On the application of a membrane air-liquid contactor for. *Energy and Buildings*, 25(3), pp. 185-193 .
- Ismail, A. & Kumari, S., 2004. Potential effect of potting resin on the performance of hollow fibre membrane modules in a CO<sub>2</sub>/CH<sub>4</sub> gas separation system. *Journal of Membrane Science*, 236(1-2), p. 183–191.
- Jensen, O., 2012. A method for high accuracy determination of equilibrium relative humidity. *Sensors and Actuators A: Physical*, Volume 181, pp. 13-19.
- Judd, S. & Jefferson, B., 2003. *Membranes for Industrial Wastewater Recovery and Re-use*. Oxford: Elsevier Advanced Technology.
- Koros, W. & Mahajan, R., 2000. Pushing the limits on possibilities for large scale gas separation: which strategies?. *Journal of Membrane Science* , 175(2), pp. 181-196.
- Koros, W. & Pinnau, I., 1994. Membrane Formation for Gas Separation Processes. In: *Polymeric Gas Separation Membranes* . Florida: CRC Press, pp. 209-272.
- Koros, W. & Vu, D., 2002. High Pressure CO<sub>2</sub>/CH<sub>4</sub> Separation Using Carbon Molecular Sieve Hollow Fiber Membranes. *Industrial and Engineering Chemistry Research*, 41(3), p. 367–380.
- Levy, E. et al., 2008. *Recovery of water from boiler flue gas*, United States of America: U.S. Department of Energy.
- Levy, E. et al., 2008. *Recovery of Water from Boiler Flue Gas*. [Online]  
Available at: <https://www.osti.gov/biblio/952467>  
[Accessed 21 01 2019].
- Li, D. & Chung, T.-S., 2004. Fabrication of lab-scale hollow fiber membrane modules with high packing density. *Separation and Purification Technology*, 40(1), pp. 15-30.
- Li, D., Chung, T.-S. & Wang, R., 2004. Fabrication of lab-scale hollow fiber membrane. *Separation and Purification Technology*, Volume 40, pp. 15-30.
- Liu, S., Li, K. & Hughes, R., 2003. Preparation of porous aluminium oxide (Al<sub>2</sub>O<sub>3</sub>) hollow fibre membranes by a combined phase-inversion and sintering method. *Ceramics International*, Volume 29, p. 875–881.
- Macedonio, F., Brunetti, A., Barbieri, G. & Drioli, E., 2012. ) Membrane condenser as a new technology for water recovery from humidified “waste” gaseous streams. *Industrial and Engineering Chemistry Research*, Volume 52, pp. 1160-1167.
- Mc Keon, B. J. et al., 2004. Friction factors for smooth pipe flow. *Journal of Fluid Mechanics*, Volume 511, pp. 41-44.
- Mc Nemar, A., 2006. *National Energy Technology Laboratory*. [Online]  
Available at: <https://www.netl.doe.gov/research/coal/crosscutting/environmental-control/water-and-energy-interface/power-plant-water-management/water-reuse--recovery/reduction-of-water-use-in-wet-fgd-systems>  
[Accessed 03 03 2018].
- Molewa, B., 2012. *List of activities which result in atmospheric emissions which have or may have a significant detrimental effect on the environment, including health, social conditions, economic conditions, ecological conditions or cultural heritage*, Pretoria: Department of Environmental affairs.
- Mottern, M., Shi, J., Shqau, K. & Verweij, H., 2008. Microstrutural Optimisation Of Thin Supported Inorganic Membranes for Gas and Water Purification. In: N. Li, A. Fane, W. Ho & T. Matsuura, eds. *Advanced Membrane Technology and Applications*. Hoboken: John Wiley and Sons, Inc, pp. 899-928.
- National Physical Laboratory (Great Britain), I. o. M. a. C., 1996. *A Guide to the Measurement of Humidity*. s.l.:Institute of Measurement and Control.
- Pandey, P., Chauhan, R. S. & Shrivastava, R. H., 2002. Carbon-Dioxide-Induced Plasticization Effects in Solvent-Cast Polyethylene Membranes. *JOURNAL OF APPLIED POLYMER SCIENCE*, Volume 83, pp. 2727-2731.
- Pankhania, M., Stephenson, T. & Summens, M., 1994. Hollow fibre bioreactor for wastewater treatment using bubbleless membrane aeration. *Water Research*, 28(10), pp. 2233-2236.
- Parker Hannifin Corp, 2018. *Parker*. [Online]  
Available at:  
<http://www.parker.com/portal/site/PARKER/menuitem.223a4a3cce02eb6315731910237ad1ca/?vg>



[nextoid=03334f9d37a5e210VgnVCM10000048021dacRCRD&vgnnextfmt=EN](#)

[Accessed 13 04 2018].

Parker Hannifin Corporation, 2009. *Parker*. [Online]

Available at:

[http://www.parker.com/Literature/Hiross%20Zander%20Division/PDF%20Files/PIS/K3.1.333\\_Tech\\_nology\\_overview\\_membrane\\_modules\\_for\\_nitrogen\\_and\\_oxygen\\_systems\\_EN.pdf](http://www.parker.com/Literature/Hiross%20Zander%20Division/PDF%20Files/PIS/K3.1.333_Tech_nology_overview_membrane_modules_for_nitrogen_and_oxygen_systems_EN.pdf)

[Accessed 15 03 2018].

Park, Y., Shafiq, M., Hur, S. & Ashraf, I., 2019. Floor Identification Using Magnetic Field Data with Smartphone Sensors. *Sensors (Basel)*, Volume 19.

Peng, C. & Howell, J., 1984. The performance of various types of regenerators for liquid desiccants. *Journal of Solar Energy Engineering*, 106(5), pp. 133-141.

PermSelect - MedArray Inc., n.d. *PermSelect*. [Online]

Available at: <https://www.permselect.com/files/Data%20Sheet%207500%20Rev-17-09.pdf>

[Accessed 13 04 2018].

PermSelect, 2017. *PermSelect*. [Online]

Available at: <https://www.permselect.com/>

[Accessed 13 04 2018].

Ritchie, H. & Roser, M., 2019. *Energy Production & Changing Energy Sources*. [Online]

Available at: <https://ourworldindata.org/energy-production-and-changing-energy-sources>

[Accessed 28 07 2019].

Rosenberg, M., 1995. Current and future applications for membrane processes in the dairy industry. *Trends in Food Science & Technology*, 6(1), pp. 12-19.

Schwinge, J., Neal, P., Wiley, D. & Fane, A., 2004. Spiral wound modules and spacers: Review and analysis. *Journal of Membrane Science*, 242(1-2), pp. 129-153.

Sijbesma, H., Nymeijer, K., Potreck, J. & Wessling, M., 2008. Flue gas dehydration using polymer membranes. *Journal of Membrane Science*, Volume 313, pp. 263-276.

Sonjica, B., 2010. <https://www.environment.gov.za>. [Online]

Available at:

[https://www.environment.gov.za/sites/default/files/legislations/listofactivities\\_atmospheric\\_emissions.pdf](https://www.environment.gov.za/sites/default/files/legislations/listofactivities_atmospheric_emissions.pdf)

[Accessed 28 02 2018].

Strathman, H., 1988. *Synthetic Membranes and their Preparation*. New Jersey: Noyes Publications.

Wan, C. et al., 2017. Design and fabrication of hollow fiber membrane modules. *Journal of Membrane Science*, Volume 538, pp. 96-107.

Wang, D., Bao, A., Kunc, W. & Liss, W., 2012. Coal power plant flue gas waste heat and water recovery. *Applied Energy*, 91(1), pp. 341-348.

Water Research Commission, 2019. *WRC Project K5/2571//3 Water Recovery From Flue Gas Evaluation*, Pretoria: WRC.

Way, J. P. C. D., 1993. *Hydrogen-selective membrane*. United States of America, Patent No. US08064513.

Winter, D., 2011. Desalination using membrane distillation: Experimental studies on full scale spiral wound modules. *Journal of Membrane Science*, 375(1-2), pp. 104-112.

Wood, J. & Gifford, J., n.d. *Evoqua Water Technologies*. [Online]

Available at: <http://www.evoqua.com/en/brands/IonPure/productinformationlibrary/ion-cedi-process-system-design-wp.pdf>

[Accessed 23 03 2018].

World Wildlife Fund, 2018. *WWF South Africa*. [Online]

Available at: [http://awsassets.wwf.org.za/downloads/wwfwaterfiles\\_19july2018.pdf](http://awsassets.wwf.org.za/downloads/wwfwaterfiles_19july2018.pdf)

[Accessed 26 09 2019].

Yacou, C., Smarta, S. & da Costa, J., 2012. Long term performance cobalt oxide silica membrane module for high temperature H<sub>2</sub> separation. *Energy and Environmental Science*, 5(2), pp. 5820-5832.

Yang, Q., Wang, K. & Chung, T.-S., 2009. Dual-Layer Hollow Fibers with Enhanced Flux As Novel Forward Osmosis Membranes for Water Production. *Environmental Science and Technology*, 43(8), pp. 2800-2805.

Zakrzewska-Trznadel, G. et al., n.d. *International Atomic Energy Agency*. [Online]  
Available at: [http://www.iaea.org/inis/collection/NCLCollectionStore/\\_Public/38/083/38083054.pdf](http://www.iaea.org/inis/collection/NCLCollectionStore/_Public/38/083/38083054.pdf)  
[Accessed 13 03 2018].  
Zhao, S., Wei, Y., Feron, P. & Yan, S., 2017. Simultaneous heat and water recovery from flue gas by membrane condensation: Experimental investigation. *Applied Thermal Engineering*, Volume 113, pp. 843-850.




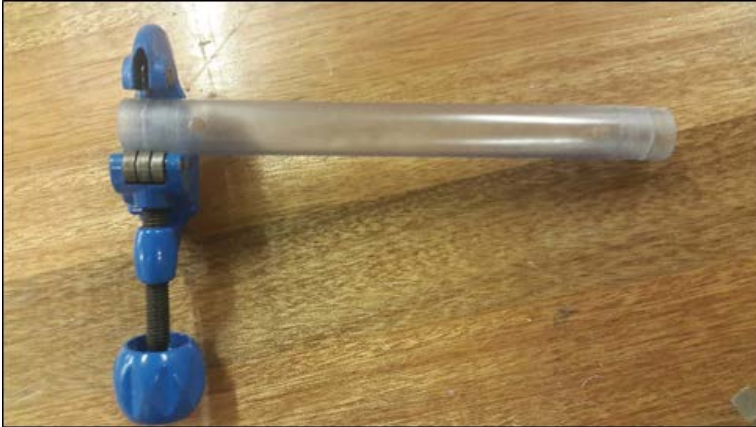
## APPENDIX A

**Table A.1: Equipment and materials needed for production of a laboratory-scale membrane module**

Equipment/Material	Specifications	Purpose	Supplier
Guillotine/cutter		Module end cutting	Thermodynamics Fluid Design (SA)
Polyvinylchloride clear tubing	Outer diameter = 25 mm Inner diameter = 21 mm	Module housing	Maizey (SA)
Polyurethane tubing	Outer diameter = 6 mm Inner diameter = 4 mm	Influent and effluent module tubing	Festo (SA)
NPT Swagelok fittings	¼"	Connection from aluminium fitting to water recovery condenser	Swagelok
NPT quick connect Swagelok fittings	¼"	Connection for influent and effluent Festo piping to module	Swagelok
Epothin 2™ Epoxy Resin 20-3440-128	N/A	Membrane module potting	Buehler (UK)
Epothin™ 2 Epoxy Hardner 20-3442-064	N/A	Membrane module potting	Buehler (UK)
Self-Adhesive Tape	Insulation tape	Sealing sides of module	Parow Bolt & Tool
Membrane hollow fibres	PEBAX® 1074 N <sub>2</sub> permeability 0.1 GPU CO <sub>2</sub> permeability 5.45 GPU Thickness 1200 µm	Separation medium for water recovery	Membrana (D)
Plastic syringes	20 ml volume	Resin filling upon potting	Laborem (SA)
Aluminium fittings	L x W x H = 77 x 74 x 31 mm	Membrane housing holder	CFW Industries (SA)
Thread bar	M8 Length = 900 mm	Holding fittings and housing	Parow Bolt & tool (SA)
“O” rings	Inner diameter = 26 mm Outer diameter = 30 mm	Sealant to curb leakages	Bearing Man Group (SA)
Oven	Song-Ling	Acceleration of resin curing	Song-Ling
LRP-1/4-0.7 Festo pressure regulator	P1 max: 12 bar P2 max: 0.7 bar	Leak testing of module	Festo (SA)
Fragram Impact drill	500 W (MCOP1573)	Drilling of influent and effluent holes on module housing	Parow Bolt & Tool
Taper	5 mm	Adding thread to influent and effluent holes on module housing	Parow Bolt & Tool
Glue gun	Stanley GR 35K	Sealing of potting grid holes	Parow Bolt & Tool
Glue stick	Topline mini 7.5 x 100 mm	Sealing of potting grid holes	Parow Bolt & Tool

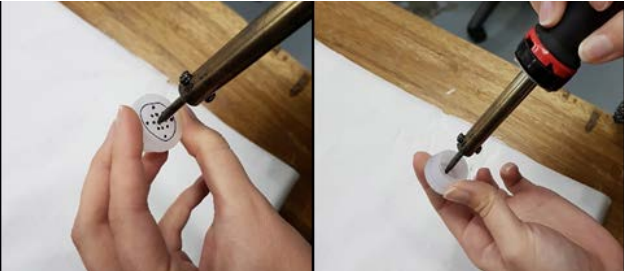



Potting grid	PVC	Potting	Maizey Plastics
--------------	-----	---------	-----------------

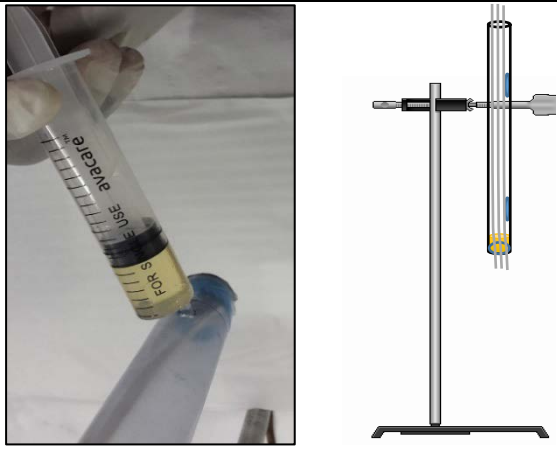
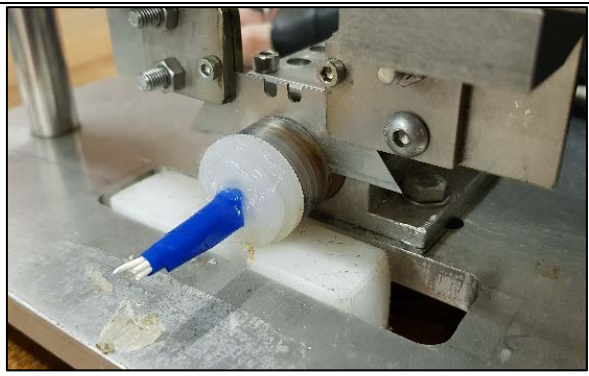
**Table A.2: Preparation of the membrane module housing**

Step No	Description	Image
1	Cut a length of 250mm of a cylindrical PVC clear tube, the openings on the tube edges would form the liquid outlets with a diameter of 16.5mm	
2	Measure and mark, on each side of the tube, 10 mm, 25 mm and 35 mm. This will also be referred to as mark 1, 2 and 3 respectively.	
3	Drill a hole on each side of the tube (with diameter of 6.5 mm each) on the 3 <sup>rd</sup> mark, by first piloting with a 5 mm drill bit followed by the 6.5mm. These holes will be drilled on either side of the module. One of the drilled holes will become the gas inlet and the other, the gas outlet.	
4	Use the cylindrical clamp cutter in order to make slight cuts around the module on the 10mm and 25 mm marks. Next, use the cylindrical cutter to almost completely cut through the PVC piping at the first mark (10 mm). Do this for both ends of the module.	

When the membrane module housing has been prepared, the potting procedure as explained in Table A.3 is followed to embed the fibres in the membrane module housing.

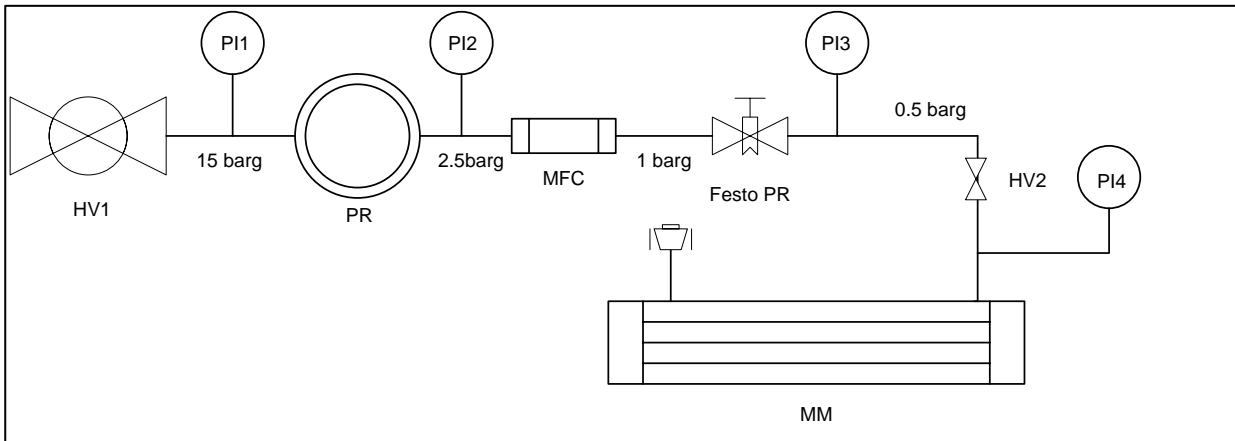
**Table A.3: Membrane fibre cutting and potting procedure**

Step No	Description	Image
1	<p>On the plastic cap, use a hot soldering iron with a fine point to make enough holes that would allow penetration of the given number of fibres to be used.</p>	
2	<p>Place the membrane fibres into the tube (membrane housing). On one side, place one of the plastic caps and allow the fibres to penetrate through the cap holes. Repeat this for the other side. Use insulation tape to secure the membranes outside of the module on both sides in order for the membranes to be fully extended in the module. Use sellotape to seal the module at the first mark to avoid external leaks of resin.</p>	
3	<p>Use the glue gun to glue in between the holes where the fibres go through in order to close the holes. Allow 10 minutes for the glue to set. Then repeat for the other side of the module.</p>	
4	<p>Make a mixture of resin (2 parts Resin and 1 part Hardener by volume). After the resin and hardener has been added together, mix thoroughly with any tool for 2 minutes.</p>	

5	<p>Use a clamp to hold the membrane housing and place it on a stand. Using a plastic syringe, carefully add the resin through the gas inlet hole.</p>	
6	<p>Place the module inside an oven at 35 degrees C for 1 hour. Once the resin is set, remove the module from the oven. Remove the sellotape and use the guillotine to cut the end of the module at the 1<sup>st</sup> mark (10mm).</p>	
7	<p>Once the end of the module has been cut off, reverse the side and repeat steps 4 – 6.</p>	

**Table A.4: Manual for conducting a leak test on a laboratory-scale membrane module**

Step	Description
1	Turn the Nitrogen feed valve on and set the downstream pressure of the Tescom pressure regulator to 1 barg.
2	Set the Nitrogen gas flow rate to moderate flow using the Labview program (100-400 ml.min <sup>-1</sup> ).
3	Set the LRP-1/4-0.7 Festo pressure regulator to 0.5 Barg
4	Block either the influent or effluent tube with a Swagelok stopper and connect the alternate tube to Nitrogen gas feed line extending from the LRP-1/4-0.7 Festo pressure regulator.
5	Once the pressure build-up into the module reaches the set 0.5 Barg, close the valve downstream of the Festo pressure regulator so as to isolate the module from further gas supply as the online digital pressure meter records pressure values throughout the duration of the test.
6	Subject the module to the 0.5 Barg for a minimum duration of 1 hour.



**Figure A.1: Piping and instrumentation diagram for leak testing of a membrane module (P = Pressure, I= Indicator, R= Regulator, MFC= Mass flow controller, MM=Membrane Module, HV = Hand Valve)**

**Table A.5: Production and potting procedure for a mini curtain-type membrane module.**

Step	Description
1	Take a pre-cut PVC frame and glue the start of the membrane fibre tot the corner of the frame.
2	Wind the membrane fibre around the PVC frame, leaving approximately 1 mm gap between each fibre.
3	Once the fibre has been wound around the frame 30 times, cut the fibre and glue the fibre end to corner of the frame.
4	Make a mixture of resin (2 parts Resin and 1 part Hardener by volume). After the resin and hardener has been added together, mix thoroughly with any tool for 2 minutes.
5	Place the PVC frame into the Teflon mould. Using a plastic syringe, fill the Teflon mould with the resin mixture until the base of the PVC frame has been covered with resin.
6	Place the Teflon mould with the PVC frame and resin into an oven that has been pre-heated to 35 degrees Celcius. Leave it in the oven for 3 hours, or until resin has completely hardened.
7	Remove the Teflon mould from the oven and let it rest for 5 minutes to cool down. Afterwards, remove the curtain-type module from the Teflon mould.
8	Repeat steps 4-7 for the other side
9	Once the membrane module has been potted, use an Altendorf C90 industrial panel saw to cut through the resin and frame in order to open the fibres on one side of the membrane module.

## APPENDIX B

---

### DESIGN AND DEVELOPMENT OF THE LABORATORY-SCALE TESTING SYSTEM

Figure B.1 and Figure B.2, produced by (TFD), presents a Solid works® schematic diagram of the Lab-scale testing system (Front view) and (Interior view). Figure B.3 shows the Piping and Instrumentation diagram of the testing system along with Table B.1 providing the list of equipment and components in the system.

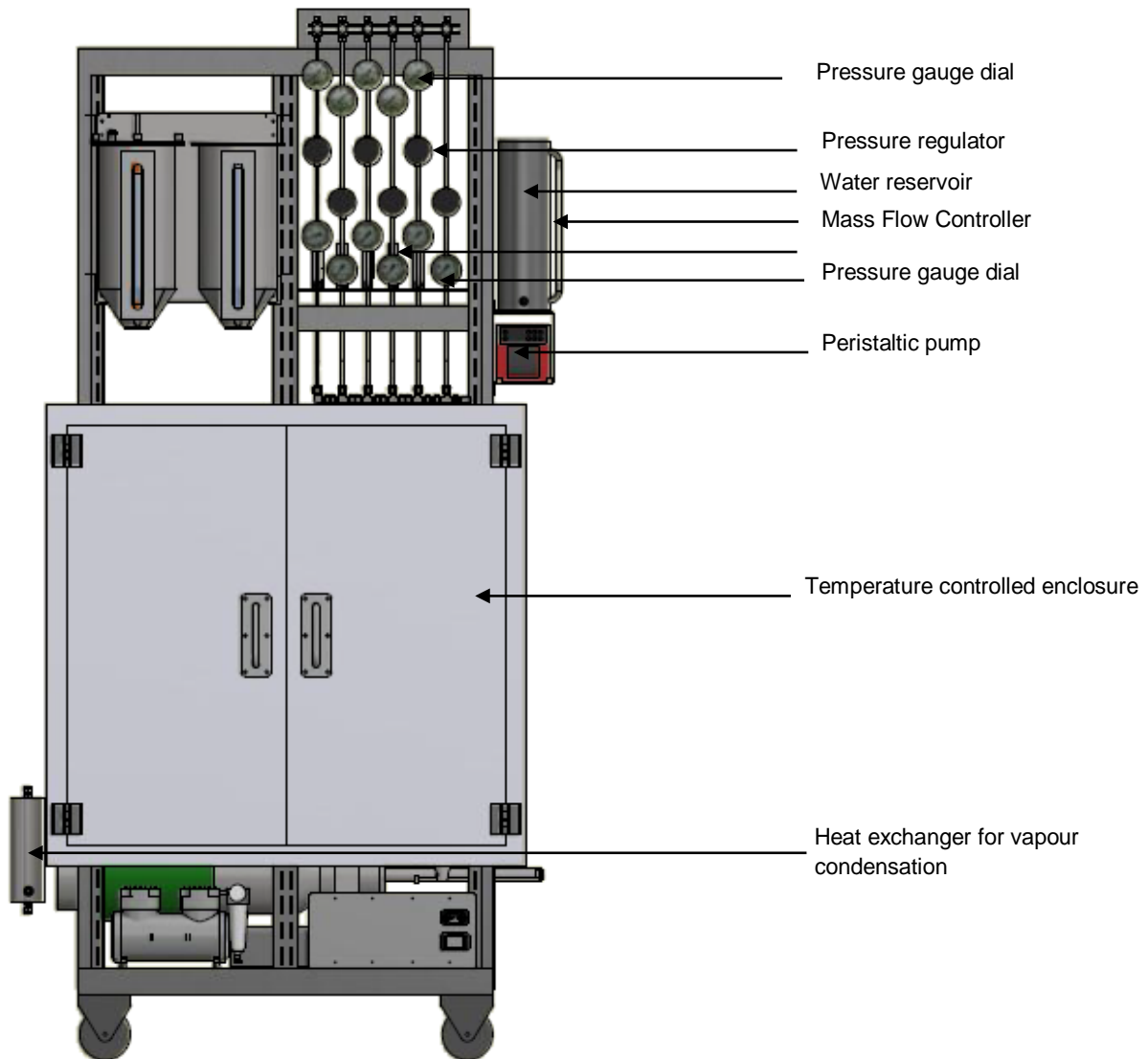


Figure B.1: Solid works® drawing, provided by TFD, illustrating the humidity controlled laboratory-scale testing system (Front view)



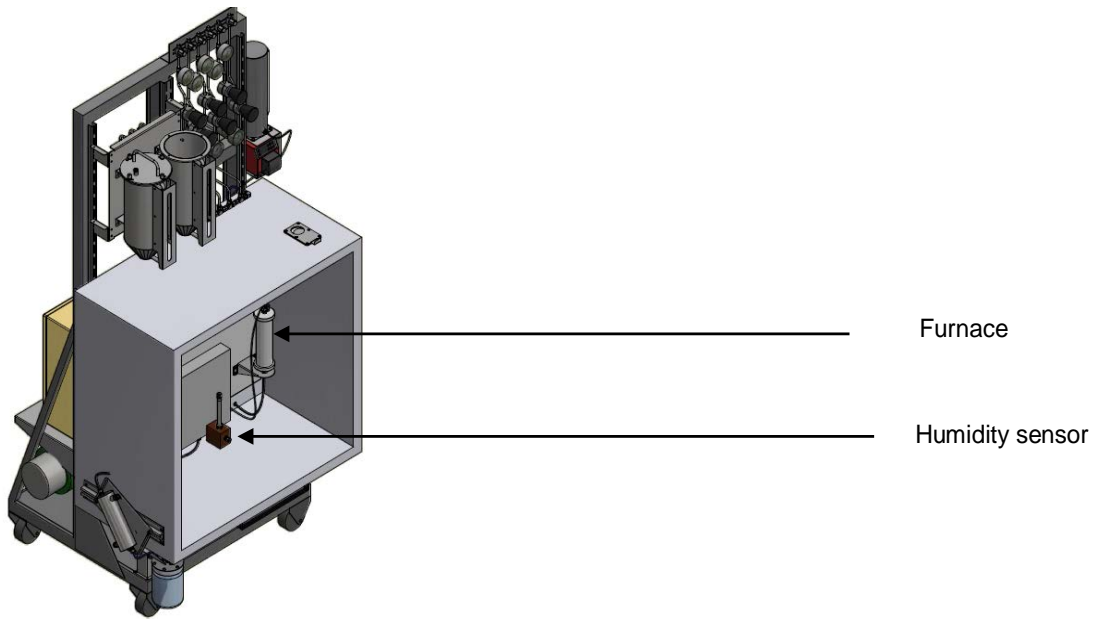


Figure B.2: Solid works® drawing, provided by TFD, illustrating the humidity controlled laboratory-scale testing system (Interior view)

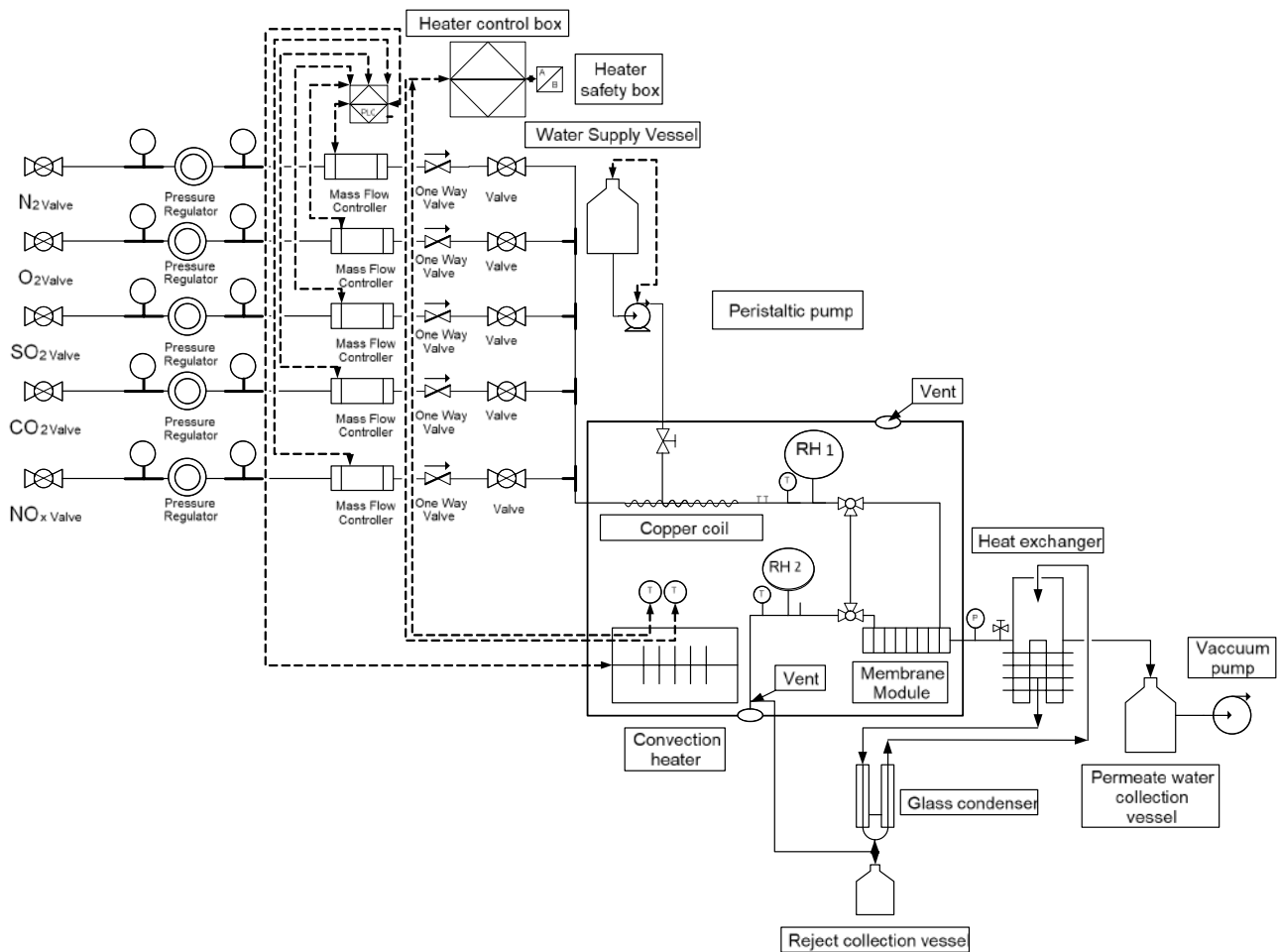


Figure B.3: Piping and instrumentation diagram for the laboratory-scale testing system

**Table B.1: List of equipment and components used in development of the lab scale testing system**

Equipment/Material	Specifications	Purpose	General
5 x Mass Flow Controllers	Bronkhorst ® High Tech EL-Flow ® Select	Flow control of gaseous components & flue gas synthesis	Mecosa
Peristaltic pump	Watson Marlow 120 U/DV analogue control.	Injection of water into system	Watson-Marlow
Pump Tubing	Marprene 602.0008.016	Medium of water transport from the reservoir	Watson-Marlow
Thermocouples	Type K (Nickel-Chromium/Nickel-Alumel)	Flue gas temperature measurement	TF Design
Stainless steel tubing	¼" diameter	Gas flow channel	Swagelok
N <sub>2</sub> pressure regulator	Inlet 20 Bar, Outlet 2.5 Bar minimum	Stepping down N <sub>2</sub> (g) pressure	Tescom
2 x Relative Humidity sensors and Transmitters	2-Wire current loop transmitter for HVAC HD4901ET Relative humidity 0- 100 % RH	Humidity measurement	Delta OHM
Pressure dials	Pressure range = 0-100 Bar. & 0 – 2.5 Bar.	Pressure readings at inlet/outlet of pressure regulator.	Wika Instruments
Internal fan	125 x 125 mm	Temperature control	Papst
Support frame	Stainless steel	Support of system components	TF Design
Two way valve	Stainless steel 316 ¼" fitting connection. SS-42GS4-A	Directing flow streams	Swagelok
One-way valve	Stainless steel 316 ¼ "SS-4C-1.	Directing flow streams	Swagelok
Fittings	Stainless steel 316 ¼" Union tee	Pipe joining	Swagelok
Programing software	Labview 11.0 Development system	Process Control Software	National Instruments
2 x Relays	Coil voltage = 24 V	Power supply/ temperature control	Omron Industrial automation
Grant refrigeration system	Grant R1 refrigerator, GD 120 pump	Condensation of retentate and permeate streams.	Grant Industries, England
Retentate condenser	Glass, height = 0.65 m	Condensation of retentate	Laborem
TRED30-7R Logtag recorder	TRED30-7R, Temperature range (-30°C to 60°C)	Retentate condenser temperature measurement	Logtag Recorders
Dry Vac 400 vacuum pump	Max Capacity = 650mmHg	Supply of vacuum on permeate side of module	Dry Vac
SPCD data collection software	Version 2.01	Water flow data logging	Ohaus corporation, USA
PA413 Ohaus Scale	Maximum Capacity=410g, Readability=0.001g	Water flow measurement	Ohaus corporation, USA
Air Heating System	Heater [220V 1220 Watts], Control Box = 400°C	Heating up the temperature controlled cabinet	Lomacor Electric, SA, Thermon
Soap flow meter	100 ml, BS 846, Ex 20°C	Measurement of retentate gas flow rate	Laborem
Vacuum gauge	-100 to 0 Kpa	Measurement of vacuum pressure on permeate side	Wika Instruments

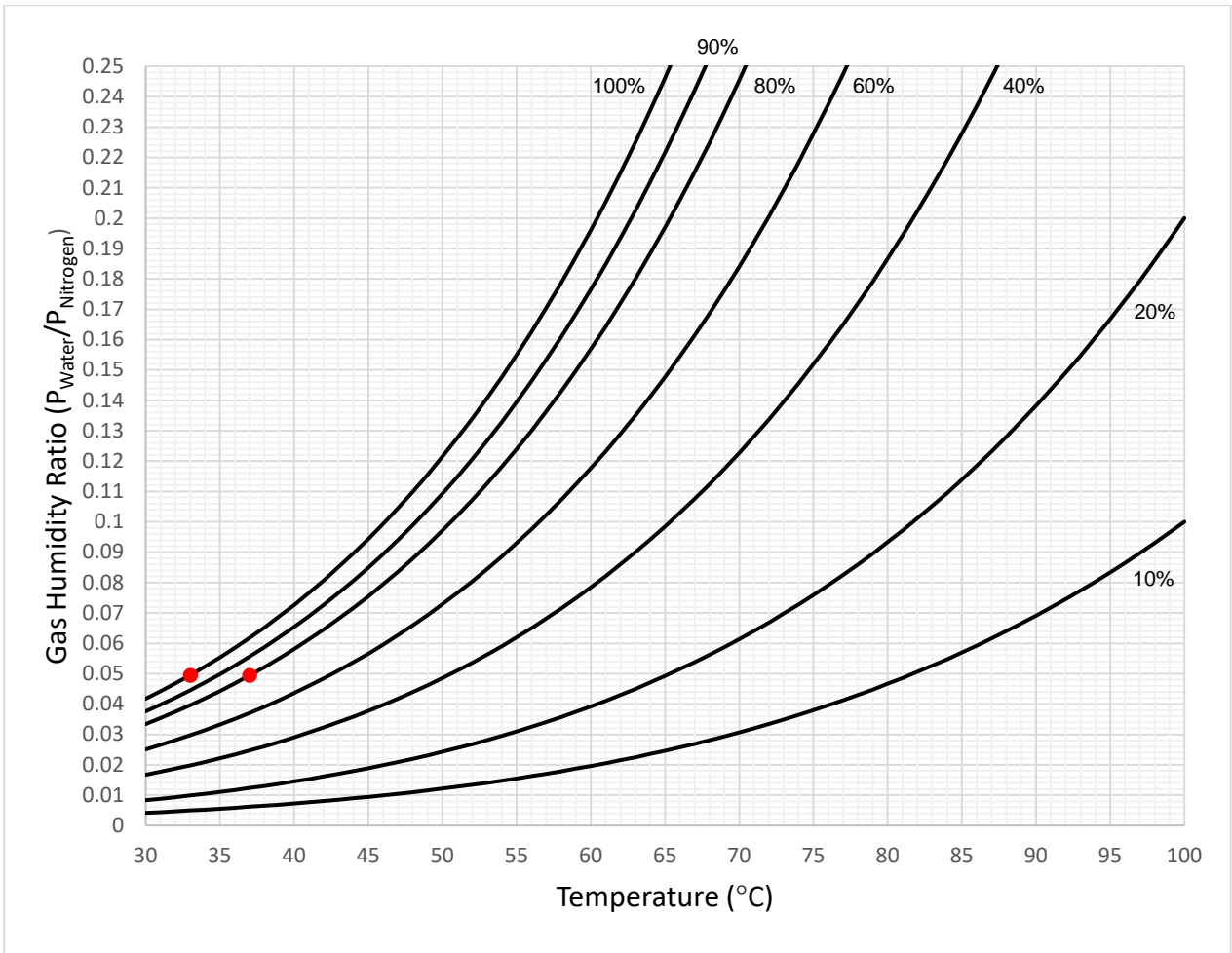
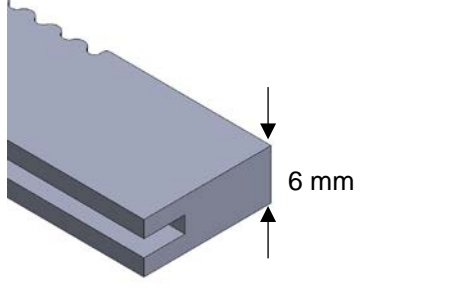
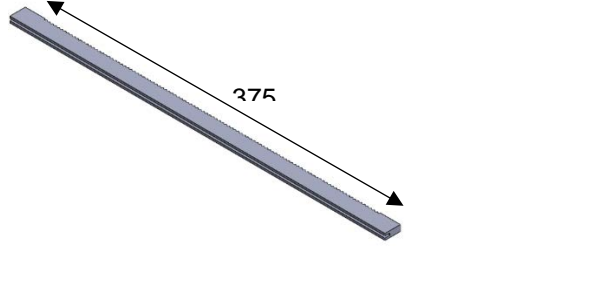
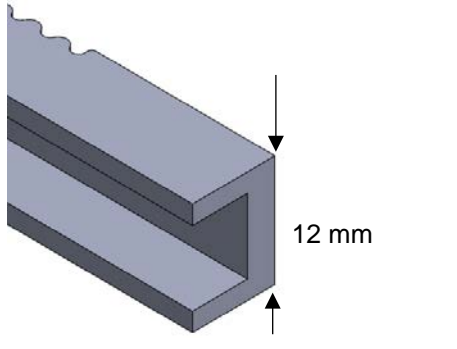
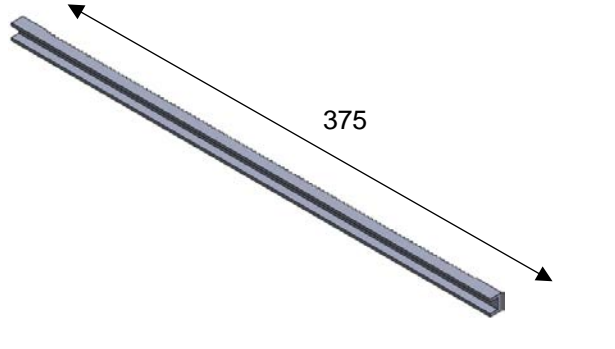
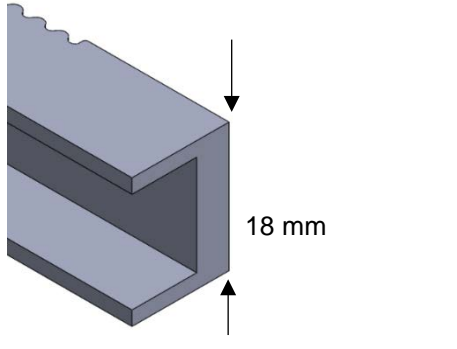
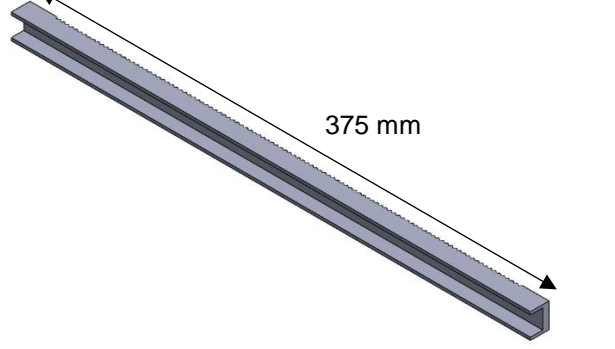
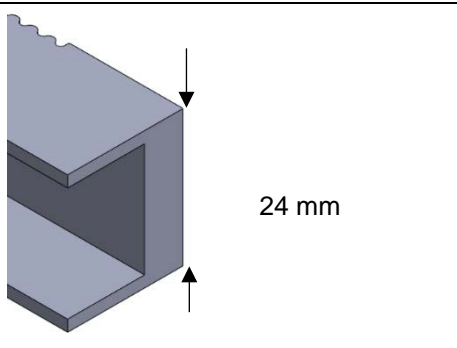
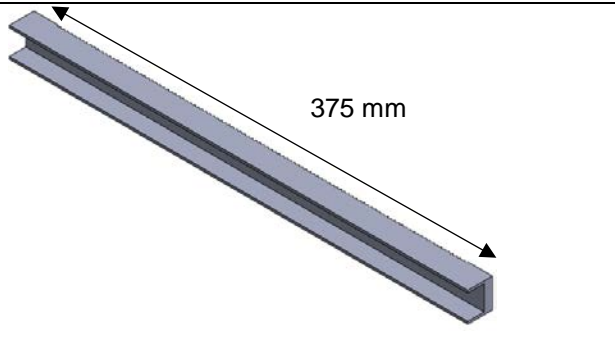


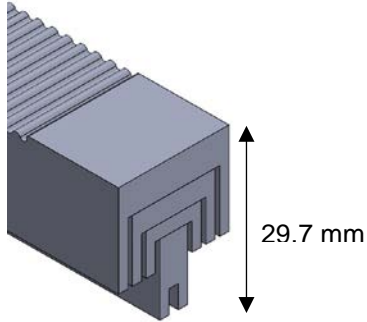
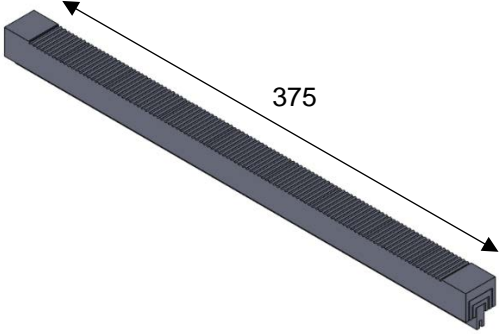
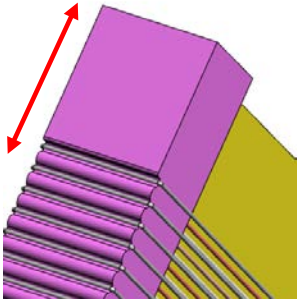
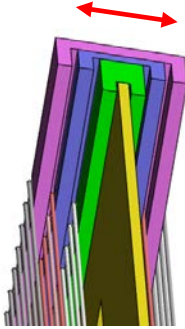
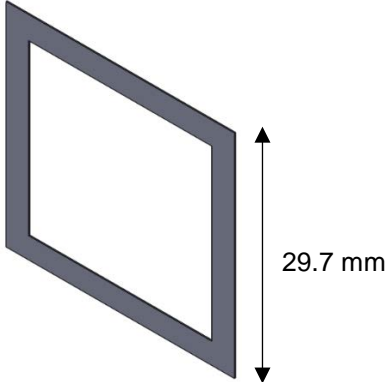
Figure B.4: Humidity-Temperature-Relative Humidity relation of the H<sub>2</sub>O-N<sub>2</sub> system

## APPENDIX C

Table C.1: Design of the 3D printed module spacers for every different layer of membrane

SPACERS		
Spacer 1	 <p>6 mm</p>	 <p>375</p>
Spacer 2	 <p>12 mm</p>	 <p>375</p>
Spacer 3	 <p>18 mm</p>	 <p>375 mm</p>
Spacer 4	 <p>24 mm</p>	 <p>375 mm</p>

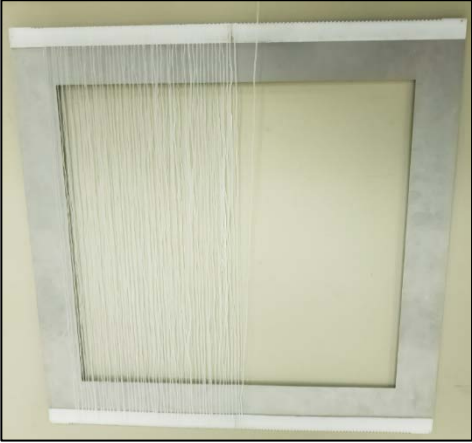

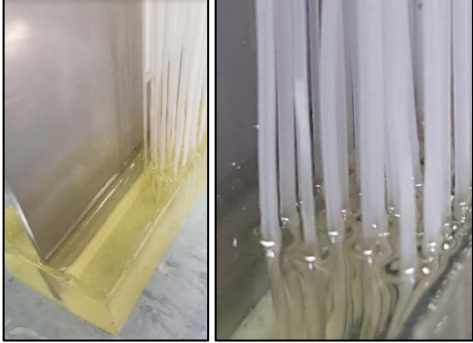

**Table C.2: Module spacer assembly and frame**

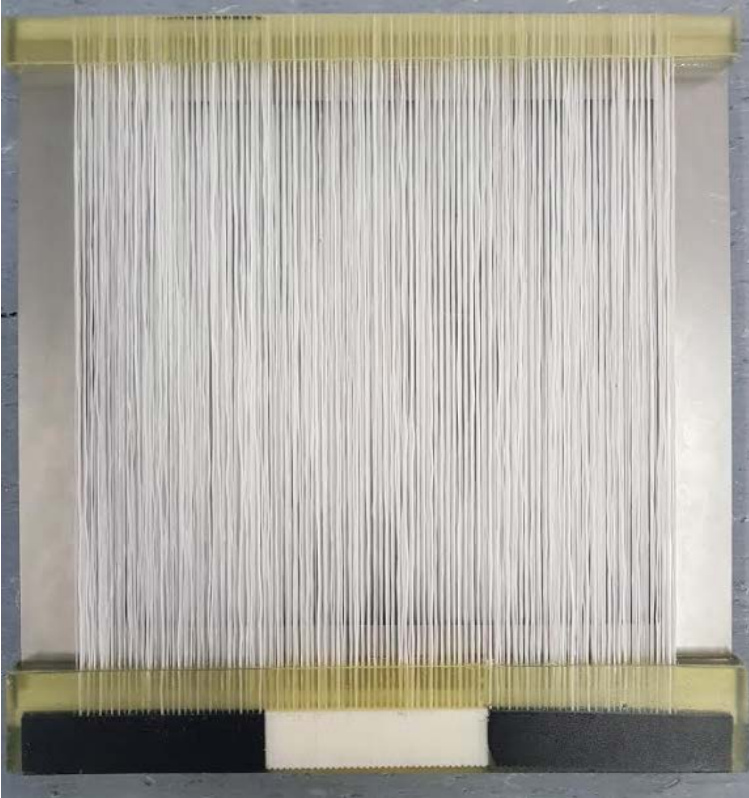
SPACER ASSEMBLY AND FRAME		
Assembly		
Assembly with fibres wound	 Longitudinal	 Lateral
Stainless steel frame		

## APPENDIX D

The images presented in the Table D.1 illustrate photos of the progressive development of the pilot-module. Figure D.1 shows the pilot-scale curtain membrane module in its potted form.

**Table D.1: Produced Pilot-scale membrane module**

	
<p>Module in the process of winding</p>	<p>Completely wound module assembly placed vertical in silicone mould</p>
	
<p>Module assembly with resin in the silicon mould</p>	<p>Potted module edge, no signs of creep as a result of adequate spacing between fibres</p>
	
<p>Cut module edge with open lumens</p>	



**Figure D.1: Complete Pilot-scale membrane module**